Study of Heat Balance and Aeration Strategies in the Solar Greenhouse Biodrying System

温室内バイオドライングシステムにおける熱収支とエアレーション方法に関する研究

By

Katitep Ngamket

A dissertation submitted in partial fulfillment of the requirements for the degree of Doctor of Philosophy

Division of Environmental Engineering

Graduate School of Engineering

Hokkaido University

JAPAN

March 2026

Abstract

The high moisture content of municipal solid waste (MSW) significantly reduces the efficiency of mechanical separation and thermal conversion processes in waste management practices. Biodrying, as a pre-treatment method to reduce moisture content (MC) in MSW, offers a sustainable solution by utilizing metabolic heat to evaporate water together with the aid of the aeration system. After the biodrying process, refuse-derived fuel (RDF) can be produced. Biodrying under a greenhouse condition or a solar greenhouse biodrying system is a practical option for reducing moisture in MSW, especially in developing countries with high solar radiation intensity. Although this method has good potential, only a few studies have explored how it performs in various environmental conditions. A clear understanding of how different energy sources contribute to biodrying in a greenhouse system is still lacking. To fill this research gap, a detailed heat balance analysis is needed to quantify the role of each energy source in water removal and to clarify the thermodynamic behavior of the solar greenhouse biodrying process. This study investigated heat transfer behavior through a proposed heat balance model and conducted a comprehensive comparison of solar greenhouse biodrying performance under different aeration patterns and environmental conditions. The background and objectives of this study were summarized in Chapter 1. In Chapter 2, the literature review was organized.

In Chapter 3, a new heat balance model was proposed to predict temperatures of waste and air (headspace) in greenhouse, offering higher accuracy than conventional heat balance models. The pilot-scale solar greenhouse biodrying system was used as a test case to evaluate the newly proposed heat balance model. Heat balance analysis indicated that metabolic heat (66%) was the primary energy input, followed by the enthalpy of inlet air (27%) and solar radiation (7%). Additionally, a primary proportion of the total heat use was associated with latent heat for water evaporation, which accounted for 59%. In the greenhouse headspace, most heat was transferred as sensible and latent heat to the air, representing 88% of the heat supplied to this zone. Heat losses occurred through the greenhouse structure (19%) and through the exhaust air (81%) in the headspace zone. Comparative simulations between greenhouse and non-greenhouse conditions were conducted, and the result found that the use of a greenhouse system provides several benefits for the biodrying process. First, it increased heat input by allowing solar radiation into the waste pile, which enhances daytime water evaporation. Second, simulation results indicated that the solar greenhouse biodrying system can reach the target moisture content (<30%) for RDF production within 7 days. Third, the greenhouse roof minimized heat loss from wind-driven convection and thermal radiation from MSW surface to the surroundings. Finally, the enclosed structure prevents rainwater intrusion, helping maintain the quality of the biodried waste materials.

In Chapter 4, the effects of positive, negative, and passive aeration patterns at varying airflow rates (4–15 L/min or 0.45–1.7 m^3/kg waste/day) on the laboratory-scale biodrying under the greenhouse system were evaluated to investigate aeration strategies. The results showed that the air direction controlled how heat moves inside the biodrying pile. Positive aeration transfered heat to the upper layers, negative aeration spread heat more evenly, and passive aeration trapped heat in the middle layer of the waste pile. For mass changes in each aeration pattern, positive aeration mainly dried the waste with minimized organic loss, especially in the case of positive aeration at 8 L/min (0.9 m^3/kg waste/day). Meanwhile, negative and passive aeration caused more organic solid

decomposition and leachate generation. Positive aeration, airflow rate at 0.9 m^3/kg waste/day, had no leachate generation, suggesting that upward airflow promotes water removal primarily through evaporation. This finding highlighted a practical advantage of using positive aeration with a greenhouse system, offering effective moisture removal while preventing leachate production despite variation of surrounding air temperature. In contrast, negative aeration and passive aeration led to higher leachate production. Negative aeration at 8 L/min (0.9 m^3/kg waste/day) and passive aeration generated 16 and 35–70 ml leachate per kg waste input, respectively. Furthermore, environmental conditions played a critical role on this system. Trials conducted during periods of higher solar radiation and ambient temperature exhibited evaporation rates 1.75 to 3.65 times higher than the trial conducted in cooler weather conditions.

A comprehensive assessment of biodrying performance was conducted to understand how operational conditions influence the biodrying process efficiency in Chapter 5. At first, biodrying performance evaluation through a key indicator as biodrying index (BI). BI refers to the ratio of water loss to organic solid loss during the biodrying process. Consequently, positive aeration at 0.9 m^3/kg waste/day yielded the highest BI values (from 8 to 12), indicating effective water removal with high solid mass retention. In contrast, passive aeration resulted in the lowest BI (0.23), indicating limited drying capacity without forced convection. While the traditional biodrying index (or the mass-based biodrying index) provides a simple ratio of mass reduction between water and organic solid, it fails to reflect the exact concept of biodrying performance. The proposed energy-based biodrying index (BI_{EB}) offers suitable evaluation of biodrying process efficiency by quantifying the ratio of metabolic heat into latent heat for water evaporation. From the results, the energy-based biodrying index showed significant variation across the experimental trials, ranging from a low of 0.03 to a high of 1.57 kJ of latent heat for evaporation per kJ of metabolic heat. The highest efficiency was achieved in the positive aeration trials at 0.9 m^3/kg waste/day, with index values more than 1.0 across winter and summer seasons. In contrast, the negative and passive aeration trials exhibited low BI_{EB} of 0.05 and 0.03, respectively. Despite high microbial heat generation in the negative aeration at 0.9 m^3/kg waste/day, this heat was not effectively used for evaporation. This was because the saturated air in the headspace together with the air direction, causing heat to build up (sensible heat) instead of being used to remove moisture (latent heat) within the waste. Furthermore, by accounting for both metabolic energy and energy input for aeration, positive aeration at 0.9 m^3/kg waste/day was the most effective pattern for maximizing water loss with high energy efficiency in this study. Additionally, the heat balance model was shown to be applicable to both positive and negative aeration patterns, providing a more understanding of heat contributions within the waste pile in the solar greenhouse biodrying system.

In Chapter 6, conclusion was described. This study revealed that the solar greenhouse biodrying system, combined with optimized aeration pattern, effectively enhanced waste drying while minimizing organic loss and leachate generation. The proposed heat balance model quantified heat distribution within the system to understand heat transfer behavior. Positive aeration at 0.9 m^3/kg waste/day consistently maximized moisture removal efficiency, as confirmed by both the traditional and the newly proposed energy-based biodrying index, effectively converting metabolic and solar energy into water evaporation. Lastly, this study provided scientific evidence for the application of the solar greenhouse biodrying system under different operational and environmental conditions, establishing a foundation for future research in this field.

Table of Contents

List of Figures

List of Tables

Chapter 1
Introduction

1.1 Background of the Study

Many countries have been concerned about waste management issues, and they try to improve their strategies to convert linear economy to circular economy. The recycling and prolonged use of existing materials represent a key approach aligned with the principles of the circular economy. The high moisture content (MC) of municipal solid waste (MSW), particularly in developing countries, contributes to inefficient waste separation for resource recovery, operational burdens in waste transportation and low performance of thermal conversion processes. According to those challenges in practical waste management, Mechanical–biological treatment (MBT) could potentially be the suitable system as a waste management tool to improve effective waste management in many areas. The operational units in MBT facilities can be flexible, depending on the goals of the waste management strategy. Additionally, the advantages of MBT are not only in terms of suitable mixed MSW management but also in terms of resource recovery, such as RDF production or metal recovery via the mechanical separation process [1]. Given the high MC of MSW, drying can play a crucial role in the waste treatment process by improving the physicochemical properties of the waste, thereby facilitating its subsequent utilization.

Biodrying is an optional method that removes moisture from solid waste through heat generated by microbial activity, assisted by forced aeration [2, 3]. Additionally, biodrying is a cost-effective and environmentally beneficial technology, as it utilizes the heat generated from the biological decomposition of organic matter in MSW [3]. Hence, biodrying is a sustainable option for treating MSW, as it operates without the need for external heat [4]. However, some studies have discussed the limitations of biodrying applications. For instance, the energy consumption of the air supply system can result in a lower net energy output compared to mass-burn incineration without the biodrying process (by less than 3%) [5]. With merits and demerits of biodrying technology, biodrying under greenhouse system is appropriate for developing countries, where high intensity of solar radiation is available, and this system seems to be inexpensive since it can be operated by local accessible technologies [6]. Also, it is possible to enhance the drying process to accelerate the reduction of MC in MSW.

The solar greenhouse biodrying system (or biodrying under a greenhouse condition) could potentially be the sustainable solution for moisture reduction in MSW, but there are a few studies, conducting experiments on this method. According to the study by Robles-Martínez et al. [7], indicated that the biodrying process conducted within a greenhouse cover benefited from the combined effects of solar heat capture and the metabolic heat generated by microbial activity in market food waste. As a result, the trials conducted with a greenhouse cover demonstrated a faster reduction in MC compared to open drying (non-greenhouse cover). The solar greenhouse biodrying system offers several advantages, including enhanced heat capture, improved water removal efficiency, and sustained drying performance even after the decline of microbial activity during the biodrying process [7–9].

Although the general advantages of the solar biodrying system are well recognized, a comprehensive understanding of their thermodynamic behavior (heat transfer), particularly within this specific system, remains unclear. The quantitative heat balance of the solar greenhouse biodrying system requires further investigation to clarify how these systems effectively reduce moisture content. Therefore, the development of mass and heat balance models for this system is necessary.

Given that aeration is important for declining the weight of MSW and its MC, the aeration system is an indispensable component of the biodrying process, whether it operates in conventional biodrying systems or solar greenhouse biodrying systems [3, 10]. According to the literature, both positive aeration (upward air movement) and passive aeration (natural ventilation) have been investigated in greenhouse biodrying systems [7, 9–12]. An alternative air supply method, such as air suction or negative aeration, needs further investigation in the case of the biodrying process under a greenhouse system.

Altogether, Given the existing gaps in the literature, this thesis addresses the need for a comprehensive understanding of the thermodynamic behavior and moisture reduction mechanisms in the solar greenhouse biodrying system. Although the advantages of this system have been acknowledged, the quantitative model that explains heat and mass transfer performance remains undeveloped. Moreover, previous research has overlooked the comprehensive comparison of various aeration patterns within this system. Hence, this thesis contributes to addressing the research gap in the development of solar greenhouse biodrying systems. The outcomes of this study are intended to provide a scientific foundation for optimizing both system design and operational practices. Ultimately, the solar greenhouse biodrying systems could be widely applied to support sustainable waste management systems and circular economy.

1.2 Objectives of the Study

1. To develop a mathematical model of mass and heat balance for the solar greenhouse biodrying system
2. To quantify the advantages of the solar greenhouse biodrying system under tropical climate conditions
3. To investigate the effect of aeration patterns and external environmental conditions on the solar greenhouse biodrying system
4. To evaluate the biodrying performance under different aeration patterns and external environmental conditions in the solar greenhouse biodrying system

1.3 Study Overview

This thesis provides a comprehensive investigation into the development and optimization of the solar greenhouse biodrying system for treating MSW. The thesis structure began with Chapter 2 associated with a foundational literature review before introducing the modelling framework in Chapter 3, which focused on developing the model to analyze the mass and heat balance in the solar greenhouse biodrying system and simulated its performance under various scenarios by considering non-greenhouse condition as well as rainfall availability. After that, experimental studies in Chapter 4 were conducted, to investigate the effects of different aeration patterns and external environmental conditions (winter and summer seasons). The results in Chapter 4 were shown as outputs, such as temperature profiles, mass changes, leachate quantities and qualities. Next, in Chapter 5, the findings from Chapters 4 are integrated using experimental data to assess the biodrying performance of the greenhouse system under varying operational conditions. Additionally, the model developed in Chapter 3 is further applied to different aeration patterns, and this developed model also provides supporting evidence for the evaluation of biodrying performance. Lastly, Chapter 6 presents the conclusions of the thesis, offering recommendations for system optimization and identifying areas for further research to improve the efficiency of solar greenhouse biodrying in MSW treatment. Figure 1.1 Thesis Structurepresents thesis structure.

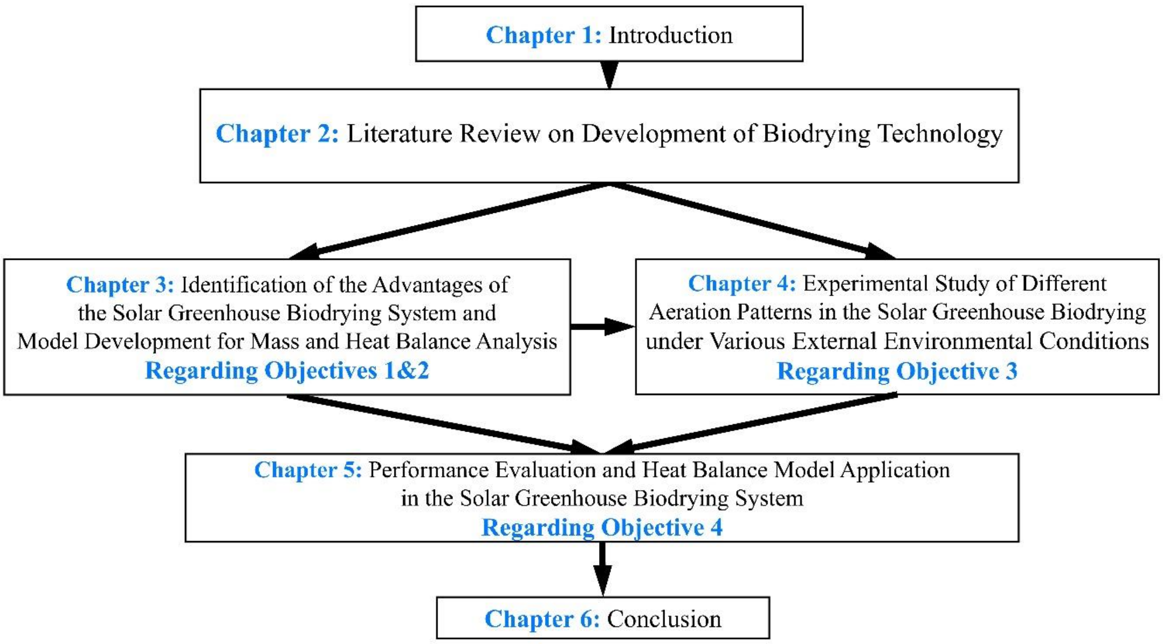

Figure 1.1 Thesis Structure

1.4 Terminology

To ensure clarity and consistency throughout this thesis, key terms and concepts related to the solar greenhouse biodrying system are defined in this section. The definitions include commonly used synonyms and technical explanations to provide readers with a precise understanding of the terminology used in the study.

Aeration Pattern

Definition: The manner in which air is supplied to a system, including the direction of the air movement, timing, and airflow rate.

External environmental conditions

Definition: Ambient climatic factors surrounding the biodrying system, including air temperature, relative humidity, solar radiation, which influence microbial activity, heat balance, and moisture removal efficiency.

Negative Aeration

Other words: Air suction

Definition: the aeration pattern in which air is drawn downward through the waste materials.

Passive Aeration

Other Words: Natural ventilation

Definition: A method of aeration in which air moves naturally through the waste materials without the use of mechanical devices, relying on convection and diffusion.

Positive Aeration

Definition: The aeration pattern in which air is introduced into waste materials using fans or blowers in an upward direction to enhance oxygen supply for microbial activity.

Solar Greenhouse Biodrying

Other words: Greenhouse-type biodrying; Biodrying under greenhouse conditions

Definition: The use of a greenhouse structure to capture heat from solar energy together with the use of metabolic energy from biodegradation to accelerate a drying process for reducing moisture in solid waste or organic substrates prior to further treatment.

References

[1] National Institute for Environmental Studies (NIES) (2020) Mechanical Biological Treatment (MBT) guideline. Tsukuba

[2] Velis CA, Longhurst PJ, Drew GH, et al (2009) Biodrying for mechanical–biological treatment of wastes: A review of process science and engineering. Bioresour Technol 100:2747–2761. https://doi.org/10.1016/j.biortech.2008.12.026

[3] Jalil NA, Ahmad IK, Basri H, et al (2022) Biodrying of Municipal Solid Waste: A Case Study in Malaysia. Springer, pp 375–434

[4] He P, Zhao L, Zheng W, et al (2013) Energy balance of a biodrying process for organic wastes of high moisture content: A review. Drying Technology 31:132–145. https://doi.org/10.1080/07373937.2012.693143

[5] Psaltis P, Komilis D (2019) Environmental and economic assessment of the use of biodrying before thermal treatment of municipal solid waste. Waste Management 83:95–103. https://doi.org/10.1016/j.wasman.2018.11.007

[6] Tun MM, Juchelková D (2018) Drying methods for municipal solid waste quality improvement in the developed and developing countries: A review. Environmental Engineering Research 24:529–542. https://doi.org/10.4491/eer.2018.327

[7] Robles-Martínez F, Silva-Rodríguez EM, Espinosa-Solares T, et al (2012) Biodrying under Greenhouse Conditions as Pretreatment for Horticultural Waste. J Environ Prot (Irvine, Calif) 03:298–303. https://doi.org/10.4236/jep.2012.34038

[8] Ngamket K, Wangyao K, Towprayoon S (2021) Comparative Biodrying Performance of Municipal Solid Waste in the Reactor under Greenhouse and Non-greenhouse Conditions. Journal of Environmental Treatment Techniques 9:211–217. https://doi.org/10.47277/jett/9(1)217

[9] Contreras-Cisneros RM, Orozco-Álvarez C, Piña-Guzmán AB, et al (2021) The Relationship of Moisture and Temperature to the Concentration of O2 and CO2 during Biodrying in Semi-Static Piles. Processes 9:520. https://doi.org/10.3390/pr9030520

[10] Ngamket K, Wangyao K, Patumsawad S, et al (2021) Quality improvement of mixed MSW drying using a pilot-scale solar greenhouse biodrying system. J Mater Cycles Waste Manag 23:436–448. https://doi.org/10.1007/s10163-020-01152-w

[11] Widyarsana IMW, Sevina R (2024) Study on the Quality Improvement of Mixed Municipal Solid Waste by Greenhouse Blackout Tarp with Biodrying System. Journal of Ecological Engineering 25:200–209. https://doi.org/10.12911/22998993/192673

[12] Colomer-Mendoza FJ, Robles-Martinez F, Herrera-Prats L, et al (2012) Biodrying as a biological process to diminish moisture in gardening and harvest wastes. Environ Dev Sustain 14:1013–1026. https://doi.org/10.1007/s10668-012-9369-1

Chapter 2
Literature Review on Development of Biodrying Technology

This chapter introduces the background of biodrying technology for solid waste, and the first part of this chapter elaborate on mechanical-biological treatment (MBT). Since biodrying is an optional biological unit in MBT system. Additionally, this chapter presents the principle of biodrying technology as well as the application of biodrying within MBT system. This chapter will also present research studies focused on enhancing biodrying performance. Various techniques aimed at improving biodrying efficiency will be listed, including solar greenhouse biodrying systems, hot-air aeration, and negative aeration application. The biodrying under greenhouse condition as the primary focus of this study will be discussed. The objective is to highlight the importance of biodrying technology and to provide a comprehensive reference of operational aspects of this technology. Moreover, it is feasible to outline directions for developing the technique of solar greenhouse biodrying

2.1 Introduction to Mechanical-Biological Treatment (MBT)

Mechanical Biological Treatment (MBT) essentially involves the integration of mechanical crushing and sorting processes with biological treatment, such as aerobic and anaerobic decomposition [1]. Germany is the origin of MBT and stands as a significant market for well-established MBT plants. The development of MBT in Europe was driven by regulatory restrictions on landfill space, as evidenced by the Landfill Directive in Europe (1999/31/EC), focusing on the reduction of biodegradable waste disposal in landfills, together with the searching opportunity for incineration application and the high costs of landfill disposal [2].

Figure 2.1 presents the typical flow chart of MBT processes. It can be seen that MBT implementation with mixed solid waste contributes to variety of objectives, like recyclable material recovery, Refuse Derived Fuel (RDF)/Solid Recovered Fuel (SRF) production, and compost-like output (CLO) generation. The operational units in MBT facilities can be flexible, depending on the goals of the waste management strategy. Therefore, the advantages of MBT are not only in terms of suitable mixed municipal solid waste (MSW) management but also in terms of resource recovery, such as RDF production or metal recovery via the sorting processes [1]. Despite MBT appearing as a promising technology with potential advantages for energy and the environment, it is important to acknowledge certain limitations. MBT is unsuitable for handling hazardous waste, bulky waste, or large-size waste and it requires an economic support policy [3]. Moreover, the potential for odor issues from MSW should also be taken into consideration. To present a comprehensive overview of the pros and cons of MBT, Table 2.1 illustrates the advantages and disadvantages of MBT along with its requirements through various dimensions, including waste management, potentials of technology, economic implications, and public health & environment.

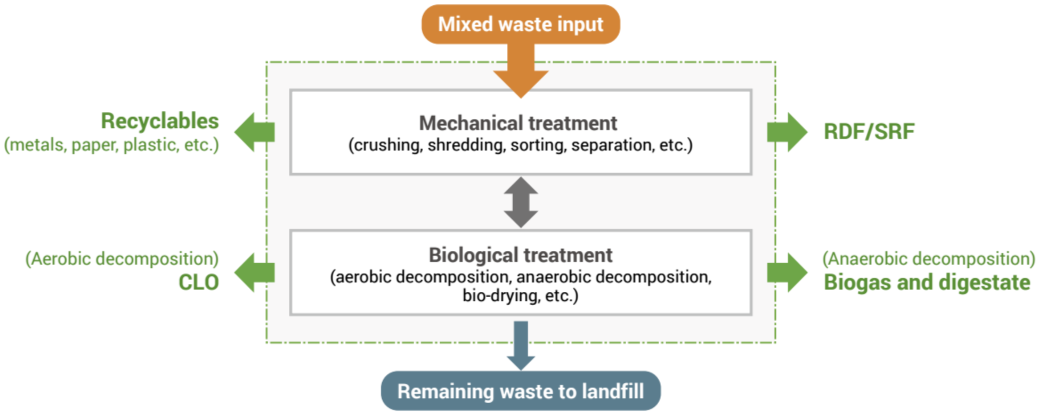

Figure 2.1 Typical Flow Chart of MBT Processes

Source: [1]

Table 2.1 Advantages and Disadvantages of MBT along with Its Requirements

Noted: Refuse Derived Fuel (RDF), Solid Recovered Fuel (SRF) production, compost-like output (CLO)

Dimensions	Advantages	Disadvantages	Requirements
Waste management	- Reduction in the volume of waste destined for landfills	- Low quality of dry recyclables separated during the MBT process	- Necessity for managing debris, including rejected solid fuels or compost-like product
Potentials of technology	- Integration with existing technology or local technology is highly feasible. - No requirements of advanced technology or high-end machines - Suitability for moist MSW with anaerobic digestion or biodrying before separation	- Incompatibility with bulky waste, liquid waste, and night soil	- Necessity to adapt drying and separation processes for waste with high moisture content, as well as for organic waste, in Asia. - The requirement for an initial waste sorting process to eliminate foreign objects and enhance efficiency.
Economic implications	- Intensive, low-energy method - Savings in fuel costs for users of RDF/SRF - Potential use of CLO as soil conditioners or back filling materials - Adaptability to markets for recyclables, RDF/SRF, CLO, and biogas.	- RDF/SRF consumption relies on fuel prices and industrial situations. - Necessity to consider the limited pool of industrial consumers of RDF/SRF in Asian markets, along with the risk of overstocking rejected RDF/SRF or an increase in the volume of waste for disposal. - Fewer benefits in the utilization of CLO.	- Crucial need to secure multiple sales channels for RDF/SRF. - Anticipation of profits from sales of valuable metals and CLO for income rather than treatment costs. Conversely, the cost for the disposal of solid waste should be taken into account, even though it has potential for use as CLO.
Public health & environment	- Reduced infectiousness and toxicity compared to dumpsites. - Reduction in environmental pollution from landfills - Efficiency in resource and energy recovery, contributing to the conservation of natural resources such as soils, metals, and fuels.	- Ineffectiveness in waste sanitization when compared to thermal treatment or composting. - Projections for noise, - vibration, dust and waste - volume - Potential emissions of atmospheric pollutants by RDF/SRF consumers.	- Important concerns for the regulation and screening of feedstock for non-hazardous waste

Modified from [1]

The implementation of MBT technology is prevalent in many regions, and there are many types of MBT facilities, such as MBT with biodrying, MBT with biogas production unit. The important factor for selection of suitable MBT types depends on MSW characteristics [2]. The rationale for the adoption of MBT technology varies, for instance, in European countries, it is compulsory to implement MSW pretreatment in compliance with EU directives [2]. Meanwhile, in Asia, there is the need to address organic waste treatment and the utilization of byproducts (e.g., RDF, SRF, biogas, and CLO) [1].

In summary, MBT technology offers a sustainable solution for waste management, serving diverse functions such as organic waste treatment and byproduct utilization. MBT can be adaptable based on the size of city, industrial concentration, and the objectives of waste management strategies in both developing and developed countries.

2.2 Biodrying Technology

The terminology of "Biodrying" started by Jewell et al. [4] in 1984. They reported the operational parameters associated with drying of daily manure, and it is possible to distinguish it from composting. Biodrying is often used for removing excessive moisture from MSW, and contributes to increasing the heating content in MSW, while composting is commonly used for organic MSW bio-stabilization to produce compost for soil quality improvement [5].

Literally, "Biodrying" is an aerobic process that utilizes the metabolic heat generated from biodegradation to evaporate water in MSW or organic substrates. According to [6], the term of biodrying is combination between two words, including "bio" (related to living organisms) and "drying", indicating that this approach is a biological process that utilizes organic waste from MSW. Scientifically, drying is hydration, involving the removal of water from a material through evaporation, where heat is applied to facilitate water loss. Also, biodrying is a pre-treatment that uses passive and forced aeration together with the heat generated by aerobic bioconversion of organic matters to dry the waste [7]. There are two main steps in biodrying for reducing moisture content from the waste, including (1^{st}) evaporation of water molecules, transitioning from a liquid state to a gaseous state at the surface of waste fragments into the surrounding air; and (2^{nd}) the evaporated water is conveyed through the waste matrix by airflow and subsequently eliminated with the exhaust gases [8].

The principle of biodrying aligns with the same concept as the aerobic digestion reaction (Equation 2.1). Biodegradable waste materials in MSW are primarily degraded, generating energy as bioheat (or metabolic heat), carbon dioxide (CO_2), and water (H_2O). The evaporation of moisture is facilitated by natural air movement or forced aeration; thus, this process enhances the calorific value of MSW by reducing moisture content. Figure 2.2 presents the general principle of MSW biodrying.

$$\text{(Organic materials) } C_xH_yO_zN + O_2 \rightarrow CO_2 + H_2O + NH_3 + \textbf{Metabolic heat} \quad \textit{Eq. 2.1}$$

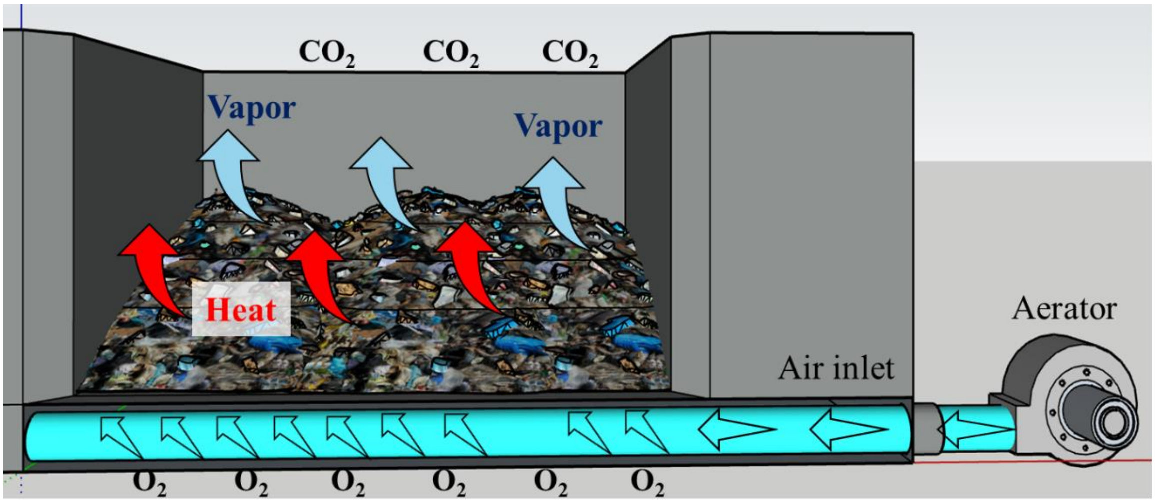

Figure 2.2 The Principle of General MSW Biodrying

The original figure

The first commercial biodrying plants became operational in the late 1990s. An Italian company (Eco-deco) that developed biodrying in the mid-1990s and they operate plants in Italy, the UK, and Spain [8]. Based on the literature review from Velis et al. [8], the initiation of practical biodrying within MBT processes can be outlined as follows.

- The Eco-deco plant in Italy started in 1996, utilizing the "BioCubi" aerobic drying process.
- The Herhof process in Asslar, Germany, began in 1997, employing the "Rotte-boxes" as a bioreactor.
- In 2000s, despite that there were commercial applications, biodrying remained a relatively new technology, and research publication on this field was limited.

2.3 Comparison of Biodrying with Other Drying Methods

According to the study by Tun et al. [7], they conducted a systematic review on comparing drying methods for MSW. Among 40 studies, the general characteristics of each drying method can be summarized. The thermal drying relies on external energy source to heat waste, operating at the drying temperature of 115±40 °C for a short duration of 0.11±0.06 days, resulting in moisture reduction of 63±32%. Meanwhile, solar-assisted drying has a drying temperature of 59±37 °C, this method also takes a short drying period of 0.38±0.04 days, achieving a high moisture reduction of 85±17%. In case of biodrying method, it takes place at a drying temperature 55±15 °C for a more extended drying period of 16±7 days, resulting in a moisture reduction of 61±24%. Biostabilization, with a drying temperature of 58±11 °C and a substantial duration of 52±40 days, achieves a moisture reduction of 54±32%. Each method offers different advantages. Thermal and solar-assisted drying provide faster drying time, while biostabilization has a long-term drying period for moisture reduction. Biodrying is a method that uses organic matter in MSW for evaporating water, so that energy consumption, particularly electricity, in this method will be lower than thermal drying. Nevertheless, biodrying requires a longer duration compared to thermal and solar-assisted drying methods. It is remarkable that solar-assisted drying and biodrying can reach a similar level of drying temperatures. However, each method has its limitations. Solar-assisted drying is appropriate for regions or countries with sufficient solar radiation. Meanwhile, biodrying is well-suited for countries with high moisture and organic content in their MSW, essentially those with lower levels of waste separation. Table 2.2 provides the details about comparison among different drying methods.

Table 2.2 Comparison among Different Drying Methods

Method	Description	Drying Temperature (°C)	Moisture Reduction (%)	Drying Time (days)
Thermal Drying	Thermal drying is the method that uses an external energy source to heat waste materials. This method removes moisture by transferring thermal energy, leading to the evaporation of water content and heating of the waste materials.	115 ± 40	63 ± 32	0.11± 0.06
Solar-assisted Drying	Solar-assisted drying involves utilizing a modular solar dryer with forced air convection, designed to facilitate heating and air circulation during the drying process. This method uses solar heat and air movement to efficiently dry waste. The solar collector might be used for raising temperature of the air inlet.	59 ± 37	85 ± 17	0.38 ± 0.04
Biodrying	Biodrying is an aerobic process using metabolic heat from biodegradation to vaporize water in MSW or organic substrates, facilitating moisture reduction and waste stabilization.	55 ± 15	61 ± 24	16 ± 7
Biostabilization	Biostabilization is the method that enhances the biological degradation of organic matter in MSW. This results in a reduction in both weight and volume of waste, contributing to decreased environmental pollution such as leachate and landfill gas. The microbial metabolism involved is similar to biodrying, but key differences lie in process duration and management criteria. Notably, it requires a longer time for an effective process compared to biodrying.	58 ± 11	54 ± 32	52 ± 40

Modified from [7]

Noted that the values were derived from the research papers collected up to the year 2018. The distribution of research papers on drying methods is as follows: From total 40 papers, there were 5 papers on thermal drying, another 2 papers on solar-assisted drying, a significant 28 papers focused on biodrying, and 5 papers addressing biostabilization.

2.4 Applications and Configuration Types of Biodrying in MBT System

There are many cases (in both Asia and Europe regions) where biodrying technology is applied in MBT. It is worth noting that biodrying can be key component for reducing moisture content in MSW to increase the efficiency of mechanical separation process and produce RDF/SRF. The satisfactory qualities of RDF/SRF depend on the specific conditions of each country, including practical waste management and the utilization of RDF/SRF. RDF/SRF is able to feed into various industries, such as cement and paper industries.

There are various biodrying configurations for MSW treatment, and despite their differences, the primary objective remains similar. According to Chiemchaisri [9], MBT with biodrying can be classified into three types: 1) biodrying thin-layer type, 2) biodrying windrow type, and 3) biodrying bunker type (or in-vessel type). Figure 2.3 shows the classification of MBT with biodrying based on configurations.

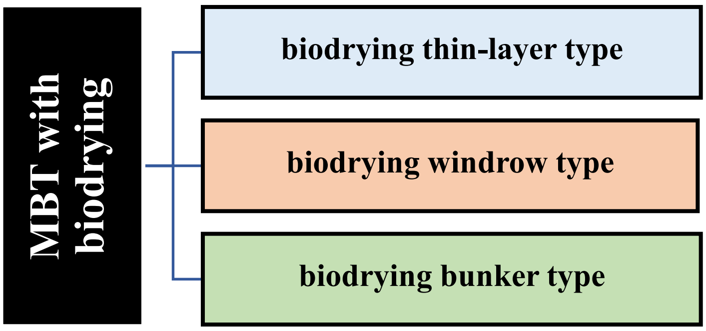

Figure 2.3 Classification of MBT with Biodrying

Biodrying thin-layer type refers to a specific method that involves spreading the waste material into thin layers or shallow windrow piles. This approach is operated by arranging waste in elongated rows with heights ranging from 0.5 to 1.0 meters and this method presents a cost-effective solution for biostabilizing MSW in developing countries with availability of land [9]. By this approach, it can enhance aeration and microbial activity for facilitating the evaporation of moisture from the waste, leading to a reduction in overall moisture content. The process maintains the waste piles for a period of 12 to 18 months before taking into the mechanical separation processes [9]. Because the long retention time is required for reducing moisture content, this approach could be classified as a fully biostabilization method, as indicated in the study by Tun et al. [7]

Biodrying windrow type is a method that builds windrows (the waste piles are long and narrow). The windrow pile maintains the same shape as that used in composting. Figure 2.4 exhibits the example components in biodrying windrow. This type can be operated under active aeration or passive aeration. Windrow pile is covered with cover material such as, vinyl sheet or polypropylene filament cover sheet. A rim weight can be used for preventing air leakage from the system.

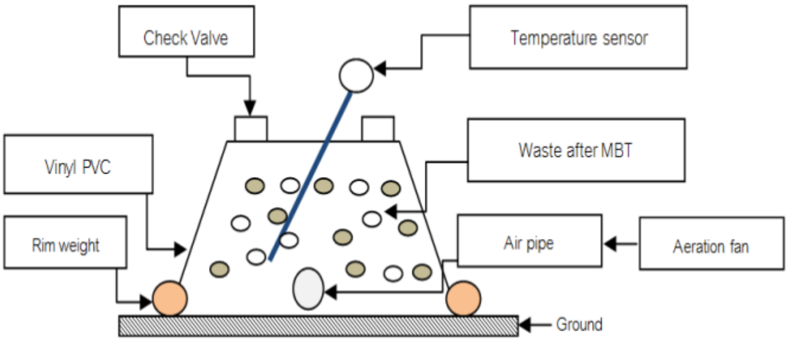

Figure 2.4 Components in Biodrying Windrow

Source: [10]

Noted: The study by Raksanau and Maneechot [10] applied a biodrying windrow type with MSW after MBT process. The MSW was collected after MBT had been left in the landfill for 9 months, and this biodrying process took 20 days of drying time. The moisture content decreased from 53% to 2.67%.

Biodrying bunker type or in-vessel type is a method, operating the aerobic degradation process in bioreactors, or in concrete tunnels, or enclosed containers. This type is usually seen in commercial biodrying systems, such as Eco-deco, Hernof. The configurations of bioreactors are diverse, depending on the unique expertise and knowledge within each company. Figure 2.5 shows the Hernof biocell and its relative processes for biodrying and biostabilization.

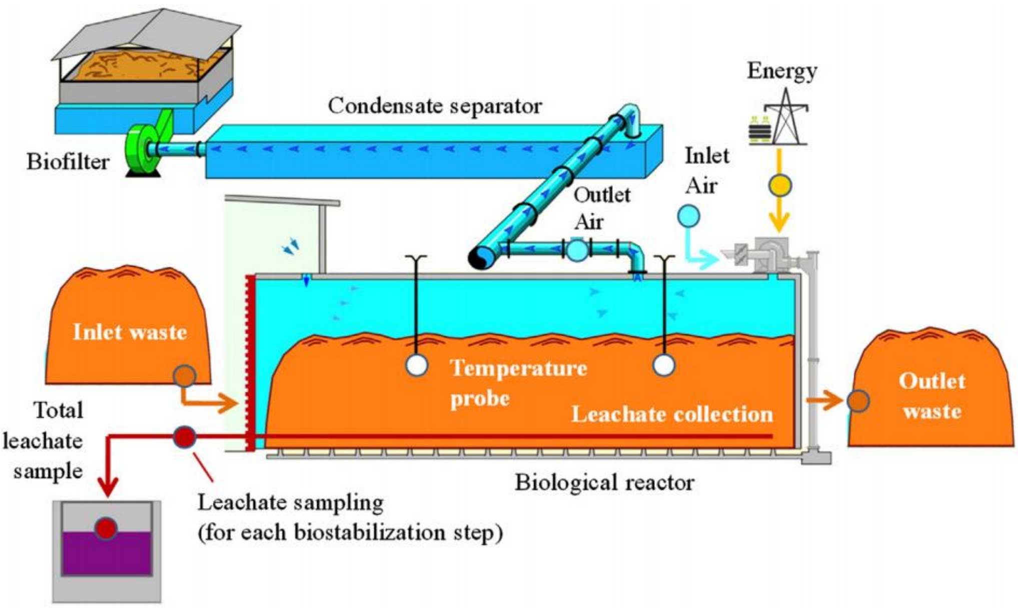

Figure 2.5 The Hernof Biocell and Its Relative Processes in Taranto, Italy

Source: [11]

Noted: this process mainly used for biostabilization of MSW, because the initial moisture content of MSW was around 23.9±1.9%. The primary function of this process (Figure 2.5) was to reduce dynamic respirometric index (DRI), as the indicator for evaluating levels of waste reactivity. The result found that the process declined DRI value from 3,965±1,965 $mgO_2/kgVS/hour$ to 750±375 $mgO_2/kgVS/hour$

Ther are many cases, representing practices of MBT with biodrying. The following paragraph will describe typical MBT plants with biodrying technology. For the first example, in Phitsanulok Province, Thailand, an MBT facility with biodrying, depicted in Figure 2.6, was implemented in this province to manage mixed MSW. This MBT system collaborated with a national cement company, producing RDF that is primarily transported to the cement kiln. Although the MBT facility is now inactive, it significantly diminished landfill waste volume in the region, concurrently reducing the municipality's waste management budget [1]. The capacity of this facility was 100 ton_{MSW}/day on average, and mixed MSW contained an initial moisture of 52.9%, with 40.3% being organic waste [1].

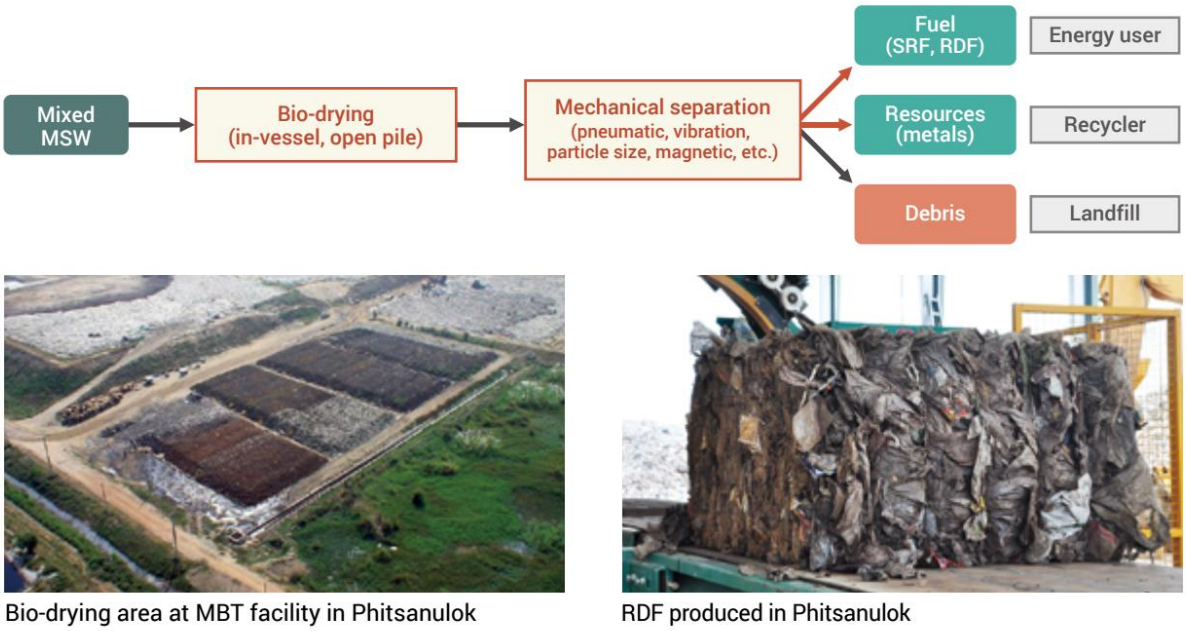

Figure 2.6 MBT with Biodrying in Phitsanulok, Thailand

Source: [1]

Noted: The cement company has internal quality standards for RDF, mandating a minimum lower heating value of 18.8 MJ/kg (4,493.2 kcal/kg), and chlorine content below 0.8%.

Another example of MBT with biodrying is in Mitoyo City, Japan. According to [1], the city manages MSW as residual combustible waste, averaging 31.5 tonnes per day. MSW is mixed with timber and wood twigs. Their treatment process is an in-vessel biodrying with air circulation, and the average drying time of 17 days. The final product, averaging 13.3 tonnes per day, is sold as feedstock to a solid fuel production company. Subsequently, the SRF is utilized in paper mills, a predominant industry in this region. The constant consumption of SRF is a crucial factor for the success of this MBT approach. Figure 2.7 presents the MBT process in Mitoyo, Japan.

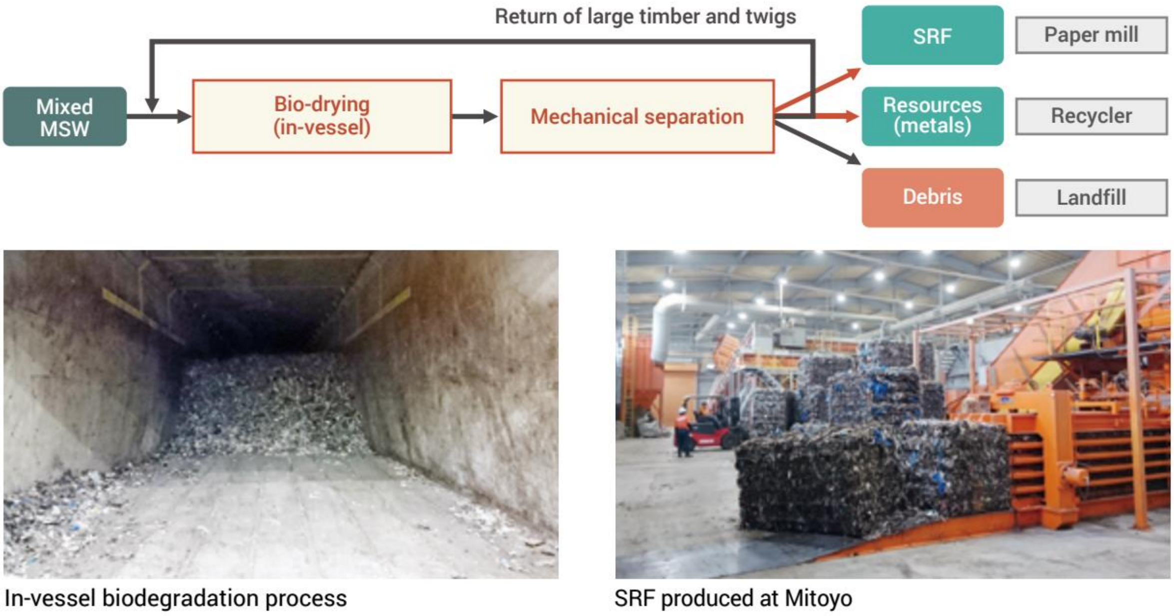

Figure 2.7 MBT with Biodrying in Mitoyo, Japan
Source: [1]

An example of MBT with biodrying in Europe, this case is in Końskie City, located in the central part of Poland. This MBT process includes two stages. The initial stage involves mechanical operations, specifically sieving with an 80 mm mesh, followed by the second biological stage, incorporating a biodrying reactor. This cuboid-shaped, 150 m^3 steel reactor integrates active aeration pattern that connects to a bio-filter for eliminating odors. According to Latosińska et al. [12], the biodegradable proportion of MSW (kitchen waste and paper) was estimated at approximately 27.7%. Throughout the biodrying process within 14 days, the recorded changes in moisture content of MSW decreased from an initial 56.5% to a range of 30 to 35%. Figure 2.8 exhibits the application of biodrying in Końskie, Poland.

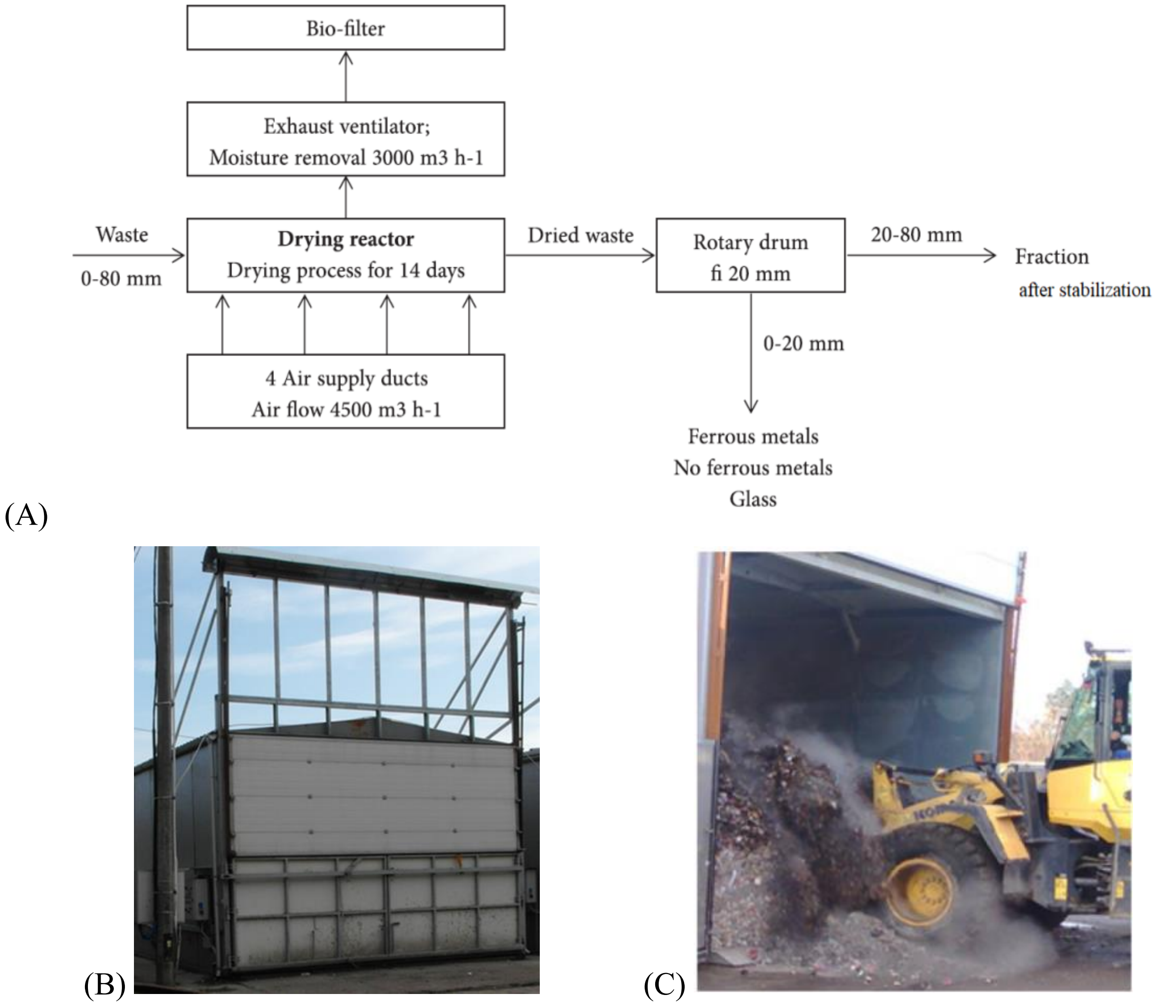

Figure 2.8 Application of Biodrying in Końskie, Poland
(A) Process flow diagram, (B) Biodrying reactor,
(C) The unloading of waste after a 14-days biodrying period.
Source: [12]

Noted: This diagram flow shows only the biological stage as the 2nd stage of this MBT process.

To sum up, biodrying MBT systems are employed globally, notably in Asia and Europe. It improves MSW quality by reducing moisture, enhancing mechanical separation efficiency, and producing solid fules. MBT with biodrying can be grouped into thin-layer, windrow, and bunker/in-vessel types. Examples include a facility in Phitsanulok, Thailand, reducing landfill waste and collaborating with a cement company; Mitoyo City, Japan, utilizing in-vessel biodrying for solid fuel production for paper industry; and Końskie City, Poland, employing a two-stage process with a biodrying reactor to reduce MSW moisture. These cases present diverse applications of MBT with biodrying across continents.

2.5 Review of Solid Waste Biodrying Research

In this section, data related to MSW biodrying were collected from published research papers and academic articles. This review summarizes and highlights various MSW biodrying systems, key biodrying parameters and indicators for performance evaluation, and alternative techniques used in MSW biodrying. The objective is to identify existing research gaps and challenges in developing biodrying technology for moisture reduction in MSW. The compiled information from the literature review (Table 2.3) also provides a foundation of biodrying research and supporting information for the rationale of this study as presented in each chapter.

Table 2.3 Compilation of Biodrying Research from Systematic Literature Review

Abbreviations in Table 2.3

Feedstock types: MSW = Municipal solid waste, MRS = Mechanically sorted residue

Evaluation index: AE: air efficiency (g water/m^3 supply air), BA: biodry air ratio (air input per stoichiometric air demand (%)), BI: biodrying index (water loss per organic loss(mass-based index)), HVC: Heating value change (%), MCR: moisture content reduction (%), SE: sorting efficiency (%), TI: temperature integration (◦C), ΣFP: airflow rate and vapor pressure difference (m^{3}kPa)

No.	Year	Country	Feedstock types	Density (kg/m3)	Evaluation Index	Scale	Retention Time (days)	Initial MC (%w/w)	Final MC (%w/w)	% Moisture reduction	% Initial Organic Content	% Final Organic Content	Water Loss to Organic Loss Ratio	Initial LHV (kcal/kg)	Final LHV (kcal/kg)	Selected Condition(s)	Ref.
1	2022	Thailand	MSW	300	BA, BI, TI, MCR, HVC	Lab	7	48.5 ± 10.6	22.2 ± 12.6	54.23	49.6 ± 3.4	64.2 ± 10.1	20.51 gH2O/g VS	2,844	4,938	T1 airflow rate: 0.5 m^3/kg/day constant rate and negative aeration	[13]

No.	Year	Country	Feedstock types	Density (kg/m3)	Evaluation Index	Scale	Retention Time (days)	Initial MC (%w/w)	Final MC (%w/w)	% Moisture reduction	% Initial Organic Content	% Final Organic Content	Water Loss to Organic Loss Ratio	Initial LHV (kcal/kg)	Final LHV (kcal/kg)	Selected Condition(s)	Ref.
2	2022	China	Food Waste	n/a	AE, BI, MCR	Lab	5	57.86 61.87	37.45 34.47	35.27 44.29	~93% ~90%	~94% ~83%	4.9 gH_2O/gVS 2.39 gH_2O/gVS	n/a	n/a	**<u>Tial A-1</u>** airflow rate: 1 L/kg/min (1.44 $m^3/kg/day$), aeration temperature = 65 °C kitchen waste: corn crop: 1:1.5 **<u>Tial B-1</u>** airflow rate: 0.8 L/kg/min (1.15 $m^3/kg/day$), aeration temperature = 55 °C kitchen waste: corn crop: 1:1	[14]
3	2022	Thailand	MRS	232	BI, TI, MCR, HVC	Lab	5	44.91	36.62	18.46 (7.286 kg)	n/a	n/a	0.171 kg water/kg degradable material	3,207	4,908	0.6AR airflow rate: 0.6 $m^3/kg/day$ negative aeration	[15]
4	2019	India	MSW	220 199	TI, MCR, HVC	Pilot	11	62.45 60.06	47.1±7.8 36.74±5.0	24.58 38.83	n/a	n/a	n/a	2,141.44 2,404.34	4,361.75 6,771.65	**<u>Experiment NO.1</u>** airflow rate: 0.35 $m^3/kg/day$ **<u>Experiment NO.2</u>** airflow rate: 0.66 $m^3/kg/day$	[16]
5	2021	Mexico	Food Waste	331 339	MCR, HVC	Lab	46	75.00 88.00	14.40 11.90	80.80 86.48	93.69 95.41	73.69 69.59	0.89 g water/g organic matter 1.02 g water/g organic matter	n/a	3,650.01 3,783.85	**<u>P1</u>** initial volume: 1.49 m^3 %composition: orange peel (79.8): mulch (10.2): carrot bagasse (10) **<u>P2</u>** initial volume: 1.13 m^3 %composition: orange peel (79.8): mulch (3.5): sugar bagasse (16.7)	[17]
6	2021	Thailand	MSW	253.97	BI, TI, MCR, HVC	Pilot	10	57.76 ±10.41	21.26 ±12.60	63.19	n/a	n/a	4.48 kg water/kg organic carbon	1,688.55± 98.07	5,078.57 ±1,396.87	0.78AR airflow rate: 0.78 $m^3/kg/day$ continuous aeration positive aeration	[18]

No.	Year	Country	Feedstock types	Density (kg/m3)	Evaluation Index	Scale	Retention Time (days)	Initial MC (%w/w)	Final MC (%w/w)	% Moisture reduction	% Initial Organic Content	% Final Organic Content	Water Loss to Organic Loss Ratio	Initial LHV (kcal/kg)	Final LHV (kcal/kg)	Selected Condition(s)	Ref.
7	2012	Spain	Organic Waste	n/a	MCR, HVC	Lab	12 12	68.30 62.80	16.30 21.00	76.13 66.65	n/a	n/a	n/a	818.76 1,133.26	3,259.96 3,176.72	**1st experiment** **GH2** passive aeration waste material: herbaceous waste (50 %) + wood waste and leaves (50 %) **2nd experiment** **GH1** passive aeration waste material: herbaceous waste (25 %) + wood waste and leaves (75 %)	[19]
8	2017	Turkey	Food Waste	~62.5	MCR, HVC	Lab	7 7	88.00 81.00	45.00 57.00	48.86 29.63	43.03 39.49	32.08 24.54	4.81 3.87 (kg water/kg organic carbon) **Calculated based on available data**	901.03 1,042.04	1,639.54 1,355.13	**T3** positive aeration airflow rate: 7.2 m^3/kg/day shredded vegetable waste (15-20 mm):prune = 4:1 **T4** positive aeration airflow rate: 7.2 m^3/kg/day shredded vegetable waste (80-90 mm):prune = 4:1	[20]
9	2018	China	MSW	513.13± 14.62	BI, TI, MCR, HVC, SE, ΣFP	Lab	18	60.39± 2.40	33.35	44.78	80.91± 0.09	66.57	4.12 kg water/ kg VS	578.86±8.60	2,256.16	**C4** positive aeration airflow rate: 0.3 m^3/kg/day MSW:cornstalks = 9:1 turning rate: every 3 days	[21]

No.	Year	Country	Feedstock types	Density (kg/m3)	Evaluation Index	Scale	Retention Time (days)	Initial MC (%w/w)	Final MC (%w/w)	% Moisture reduction	% Initial Organic Content	% Final Organic Content	Water Loss to Organic Loss Ratio	Initial LHV (kcal/kg)	Final LHV (kcal/kg)	Selected Condition(s)	Ref.
10	2022	China	Food Waste	n/a	MCR, HVC	Pilot	1* This is continuous feeding system	76.63 ± 5.45	31.26–35.21	56.63	80.99 ± 3.99	~73	3.13 kg water/kg VS	383.2	1,602.50–1,688.42	There was only one case with 3 cycles of biodrying continuous feeding (every day) 350 kg of crushed food waste without any bulking agent airflow rate: 2.4 m^3/kg waste/day ventilation frequency of 30 min/h, and ventilation rate of 60 m^3/h	[22]
11	2017	Indonesia	Organic Waste	~121.43	MRC	Lab	21	61	21.15	65.33	87.55	83.99	n/a	n/a	3,595.29	Reactor 2 (R2) positive aeration airflow rate: 14.4 m^3/kg/day	[23]
12	2016	Malaysia	MSW	~240	MRC	Lab	14	65.57 ± 2.67	11.91 ± 1.48	81.84	n/a	n/a	n/a	n/a	n/a	Reactor B intermittent positive aeration: 10 min On/3 h Off airflow rate: 0.005 m^3/kg dry waste/hour (~0.0021 m^3/kg waste/day) turning rate: every 2 days	[24]
13	2022	Korea	MRS	545	MCR, HVC, BI, AE	Pilot	14	40±0.3	15.5± 0.8	61.25	61.6	57.8	5.5 kg water/kg organic solid	1,644.25±25	2,334±153	**U45_50** outlet air auto-controlled aeration (at 45-50 °C) average airflow rate: 0.55 m^3/kg waste/day continuous upward airflow with inverted aeration once (at day 9)	[25]

No.	Year	Country	Feedstock types	Density (kg/m3)	Evaluation Index	Scale	Retention Time (days)	Initial MC (%w/w)	Final MC (%w/w)	% Moisture reduction	% Initial Organic Content	% Final Organic Content	Water Loss to Organic Loss Ratio	Initial LHV (kcal/kg)	Final LHV (kcal/kg)	Selected Condition(s)	Ref.
14	2021	Brazil	MSW	n/a	MCR, HVC	Lab	6	51.67	12.90	75.03	92.33	92.00	n/a	2,344.33	4,690.33	The reported value in this case is average values among 3 rotary drums with the same operational condition 200-Litre rotary drum airflow rate: 1.44 m^3/kg/day rotation frequency: every 3 hours rotation speed: 9 rpm	[26]
15	2010	China	MSW	~212.20	MCR, HVC	Lab	16	73	48.3	34.11	82.50	68.80	n/a	958.41	2,461.76	This study reported only one operational setting airflow rate: 1.344 m^3/kg/day intermittent aeration 7 min on/23 min off turning frequency: every 2 days	[27]
16	2012	China	MSW	280	BI, MCR, TI	Lab	16	74	57.24	22.65	71.00	57.12	5.93	n/a	n/a	CN airflow rate: 0.336 m^3/kg/day continuous aeration turning frequency: 1 time at day 8th	[28]
17	2008	China	MSW	212	MCR	Lab	16	72	50.5	29.86	n/a	n/a	4.19	n/a	n/a	Trial B airflow rate: 0.45 $m^3/kg \cdot m^2 \cdot h$ (1.36 m^3/kg waste/day) Ventilation: 7 min on/23 min off Turning frequency: 1 time per 2 days	[29]

References

[1] National Institute for Environmental Studies (NIES) (2020) Mechanical Biological Treatment (MBT) guideline. Tsukuba

[2] Archer E, Baddeley A, Klein A, et al (2005) Mechanical-Biological Treatment: A guide for decision makers, processes, policies, and markets

[3] Fei F, Wen Z, Huang S, De Clercq D (2018) Mechanical biological treatment of municipal solid waste: Energy efficiency, environmental impact and economic feasibility analysis. J Clean Prod 178:731–739. https://doi.org/10.1016/j.jclepro.2018.01.060

[4] Jewell WJ, Dondero NC, van Soest PJ, et al (1984) High Temperature Stabilization and Moisture Removal from Animal Wastes for By-Product RecoveryFinal Report for the Cooperative State Research Service, SEA/CR 616-15-168. Washington, DC

[5] Yang B, Hao Z, Jahng D (2017) Advances in biodrying technologies for converting organic wastes into solid fuel. Drying Technology 35:1950–1969. https://doi.org/10.1080/07373937.2017.1322100

[6] Jalil NA, Ahmad IK, Basri H, et al (2022) Biodrying of Municipal Solid Waste: A Case Study in Malaysia. Springer, pp 375–434

[7] Tun MM, Juchelková D (2018) Drying methods for municipal solid waste quality improvement in the developed and developing countries: A review. Environmental Engineering Research 24:529–542. https://doi.org/10.4491/eer.2018.327

[8] Velis CA, Longhurst PJ, Drew GH, et al (2009) Biodrying for mechanical–biological treatment of wastes: A review of process science and engineering. Bioresour Technol 100:2747–2761. https://doi.org/10.1016/j.biortech.2008.12.026

[9] Chiemchaisri C (2021) Waste Stabilization in different MBT systems: Case studies in Thailand. In: Webinar on Mechanical-Biological Treatment (MBT), The CCET guideline series on intermediate municipal solid waste treatment technologies. The IGES Centre Collaborating with UNEP on Environmental Technologies (CCET)

[10] Raksanau C, Maneechot P (2017) The Potential of Bio-Drying Processin Improvingquality of The Processed Waste from The Mechanical Biological Treatmentfor Industrial Heating Systems. International Journal of Renewable Energy 12:53–63

[11] De Gisi S, Todaro F, Fedele G, et al (2018) Alternating pure oxygen and air cycles for the biostabilization of unsorted fraction of municipal solid waste. Waste Management 79:404–414. https://doi.org/10.1016/j.wasman.2018.08.011

[12] Latosińska J, Żygadło M, Dębicka M (2022) The Biological Drying of Municipal Waste in an Industrial Reactor—A Case Study. Energies (Basel) 15:1039. https://doi.org/10.3390/en15031039

[13] Payomthip P, Towprayoon S, Chiemchaisri C, et al (2022) Optimization of Aeration for Accelerating Municipal Solid Waste Biodrying. International Journal of Renewable Energy Development 11:878–888. https://doi.org/10.14710/ijred.2022.45143

[14] Li J, Ju T, Lin L, et al (2022) Biodrying with the hot-air aeration system for kitchen food waste. J Environ Manage 319:115656. https://doi.org/10.1016/j.jenvman.2022.115656
[15] Bhatsada A, Wangyao K, Patumsawad S (2022) Effect of Aeration rate on Wet- refuse-derived fuel Biodrying process for increasing Heating value and Water content reduction. In: 2022 International Conference and Utility Exhibition on Energy, Environment and Climate Change (ICUE). IEEE, pp 1–8
[16] Tom AP, Pawels R, Haridas A (2019) Exploration of Biodrying Process for Mixed Municipal Solid Waste Management. The Journal of Solid Waste Technology and Management 45:294–304. https://doi.org/10.5276/JSWTM/2019.294
[17] Contreras-Cisneros RM, Orozco-Álvarez C, Piña-Guzmán AB, et al (2021) The Relationship of Moisture and Temperature to the Concentration of O2 and CO2 during Biodrying in Semi-Static Piles. Processes 9:520. https://doi.org/10.3390/pr9030520
[18] Ngamket K, Wangyao K, Patumsawad S, et al (2021) Quality improvement of mixed MSW drying using a pilot-scale solar greenhouse biodrying system. J Mater Cycles Waste Manag 23:436–448. https://doi.org/10.1007/s10163-020-01152-w
[19] Colomer-Mendoza FJ, Robles-Martinez F, Herrera-Prats L, et al (2012) Biodrying as a biological process to diminish moisture in gardening and harvest wastes. Environ Dev Sustain 14:1013–1026. https://doi.org/10.1007/s10668-012-9369-1
[20] Mohammed M, Ozbay I, Durmusoglu E (2017) Bio-drying of green waste with high moisture content. Process Safety and Environmental Protection 111:420–427. https://doi.org/10.1016/j.psep.2017.08.002
[21] Yuan J, Zhang D, Li Y, et al (2018) Effects of the aeration pattern, aeration rate, and turning frequency on municipal solid waste biodrying performance. J Environ Manage 218:416–424. https://doi.org/10.1016/j.jenvman.2018.04.089
[22] Xin L, Yan X, Xu X, et al (2022) Carbohydrate degradation contributes to the main bioheat generation during kitchen waste biodrying process: A pilot study. Waste Management 137:20–30. https://doi.org/10.1016/j.wasman.2021.10.021
[23] Kristanto GA, Hanany I (2017) Effect of air-flow on biodrying method of municipal solid waste in Indonesia. p 040007
[24] Ab Jalil NA, Basri H, Basri NEA, Abushammala MFM (2016) Biodrying of municipal solid waste under different ventilation periods. Environmental Engineering Research 21:145–151. https://doi.org/10.4491/eer.2015.122
[25] Park J-R, Lee D-H (2022) Effect of aeration strategy on moisture removal in bio-drying process with auto-controlled aeration system. Drying Technology 40:2006–2020. https://doi.org/10.1080/07373937.2021.1912080
[26] FELTRIM F, IZZO RLS, ROSE JL, et al (2021) Evaluation of the bio-drying process of municipal solid waste using rotating drums Bio-drying rotary drum. An Acad Bras Cienc 93:. https://doi.org/10.1590/0001-3765202120200085

[27] Shao L-M, Ma Z-H, Zhang H, et al (2010) Bio-drying and size sorting of municipal solid waste with high water content for improving energy recovery. Waste Management 30:1165–1170. https://doi.org/10.1016/j.wasman.2010.01.011
[28] Shao L-M, He X, Yang N, et al (2012) Biodrying of municipal solid waste under different ventilation modes: drying efficiency and aqueous pollution. Waste Management & Research: The Journal for a Sustainable Circular Economy 30:1272–1280. https://doi.org/10.1177/0734242X12462278
[29] ZHANG D, HE P, SHAO L, et al (2008) Biodrying of municipal solid waste with high water content by combined hydrolytic-aerobic technology. Journal of Environmental Sciences 20:1534–1540. https://doi.org/10.1016/S1001-0742(08)62562-0

Chapter 3

Identification of the Advantages of the Solar Greenhouse Biodrying System and Model Development for Mass and Heat Balance Analysis

Graphical Abstract for Chapter 3

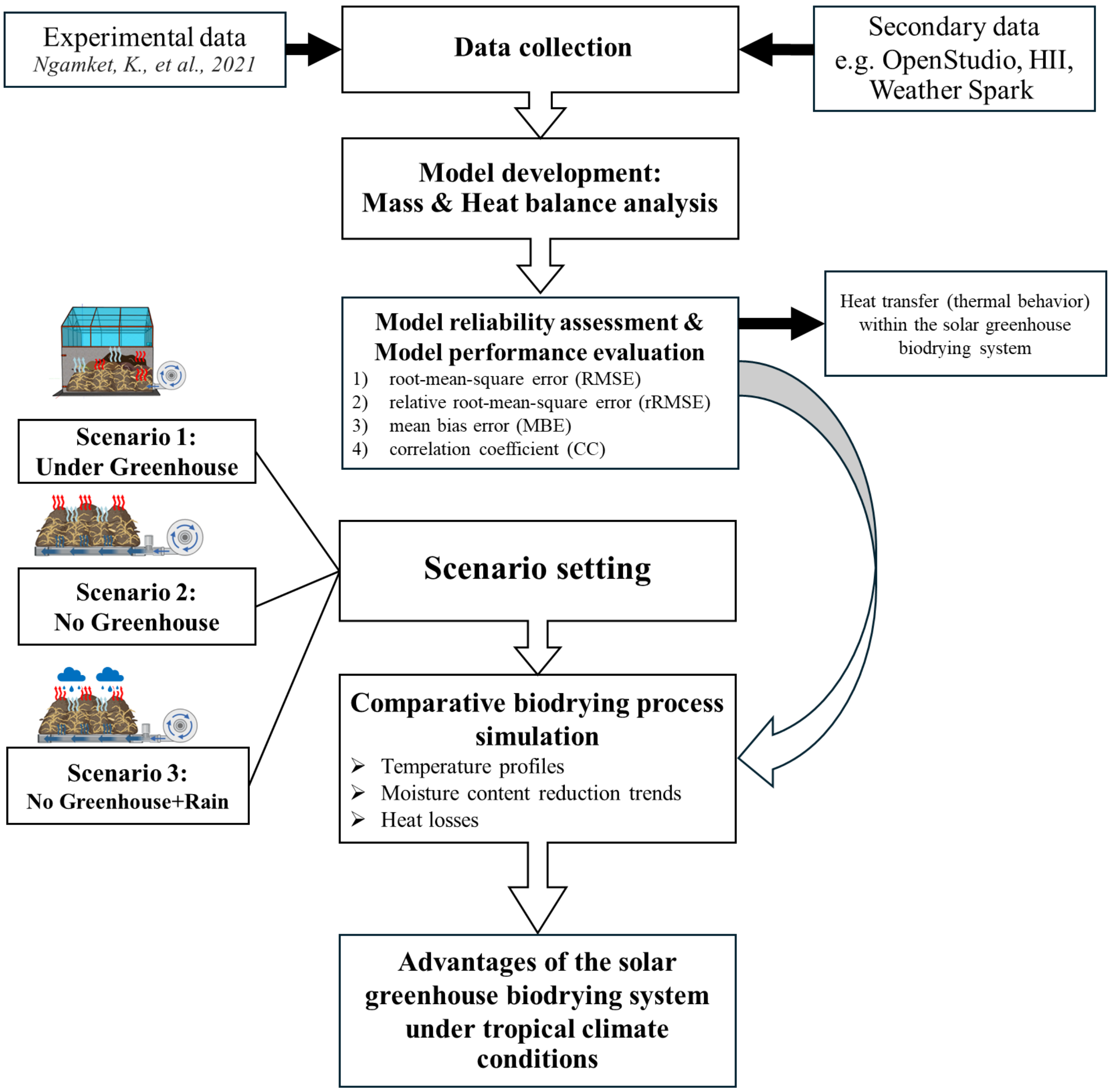

Nomenclature: Parameters and Constant Values

Symbol	Details	Unit	Value
$AH_{MSW \rightarrow GH}$	Absolute humidity of the air passing through the MSW pile to greenhouse headspace	g/m^3	
$AH_{MSW \rightarrow am}$	Absolute humidity of the air from the MSW pile to ambient	g/m^3	

Symbol	Details	Unit	Value
AH_{GH}	Absolute humidity of the air retained within the greenhouse	g/m^3	
AH_{in}	Absolute humidity of inlet air	g/m^3	
$A_{MSW,cvf}$	Area of the MSW surface directly exposed to wind	m^2	
$A_{MSW,nat}$	Area of the MSW surface not directly exposed to wind	m^2	
A_{MSW}	Surface area of top MSW pile	m^2	14
A_{ac}	Surface area of greenhouse receiving sunlight	m^2	22.3545 (for southwest (SW) and southeast (SE) orientation)
$A_{ac,total}$	Total area of acrylic roof	m^2	44.709
A_{c2}	Considered concrete part contacted with the air inside the greenhouse	m^2	15.6
$A_{entire,MSW}$	Total surface area of the MSW pile (for Scenarios 2 and 3)	m^2	32
A_{ref}	Reference surface area for calculating solar radiation flux under open biodrying conditions in scenarios 2 and 3.	m^2	22.3545 (for SW and SE orientation)
A_{side}	Total area of the side concrete wall in contact with the waste pile	m^2	13.8
CC^t	CO_2 concentration at given time	% vol./h	
CV_{OM}	Calorific value of organic matter	kJ/kg	21,558.78
C_{ac}	Heat conductivity of acrylic	kJ/m·°C	0.5472
C_c	Heat conductivity of concrete wall	kJ/m·°C	6.2266
$C_{p,dry\ MSW}$	Specific heat of dry solid	kJ/kg·°C	3
$C_{p,dryair}$	Specific heat of dry air	kJ/kg·°C	1.004
$C_{p,vapor}$	Specific heat of vapor	kJ/kg·°C	1.841
$C_{p,water}$	Specific heat of water	kJ/kg·°C	4.184
E_A	Activation energy in Arrhenius' equation	J/mol	29,000
$F_{MSW\rightarrow GH}$	View factor between MSW and greenhouse headspace	-	0.64
$F_{MSW\rightarrow ac}$	View factor between MSW and acrylic roof	-	0.64
$F_{MSW\rightarrow c2}$	View factor between MSW and concrete part contacted the greenhouse headspace	-	0.36
$F_{MSW\rightarrow sky}$	View factor between MSW and sky	-	1
Fe_{MSW}	Emissivity of the MSW	-	0.85
Fe_{ac}	Emissivity of acrylic roof	-	0.86
Fe_c	Emissivity of concrete	-	0.9
Fe_{sky}	Emissivity of sky	-	0.8
H_o	Metabolic energy per oxygen consumption	kJ/kgO_2	16,000
$J_{d\alpha\theta}$	Inclined direct solar radiation	kJ/h	

Symbol	Details	Unit	Value
$J_{sky\theta}$	Inclined diffuse solar radiation	kJ/h	
$J_{t\alpha\theta}$	Total inclined solar radiation	kJ/h	
K_O	Monod's constant	%	6
K_a	Constant value to convert a_w and MC	-	0.04
K_c	Contois' constant	-	24
$K_{cov,GH\rightarrow ac\rightarrow am}$	Overall thermal transfer coefficient of acrylic roof	kJ/m^2·°C	
$K_{cov,GH\rightarrow c2\rightarrow am}$	Overall thermal transfer coefficient of the concrete wall contacted with the air inside the greenhouse	kJ/m^2·°C	
$K_{tran,c1}$	Overall thermal transfer coefficient of the concrete wall surface connected with the waste pile	kJ/m^2·°C	
L_{ac}	Acrylic thickness	m	0.003
L_c	Concrete thickness	m	0.2
L_w	Latent heat of evaporation	kJ/kg	
LHV	Lower heating value	kcal/kg	
M_{dryair}	Mass of dry air	kg/h	
M_{fo}^t	Mass of degraded food wastes at given hour	kg/h	
M_{rain}	Rainwater quantity	kg/h	
M_s^t	Solid mass at given time	kg/h	
$M_{w,GH}$	Water mass in the greenhouse headspace	kg/h	
$M_{w,GH\rightarrow am}$	Water mass in the exhaust air	kg/h	
$M_{w,MSW\rightarrow GH}$	Water mass in the air releasing from the MSW pile to greenhouse headspace	kg/h	
$M_{w,bio,simu}$	Metabolic water from aerobic biodegradation simulation	kg/h	
$M_{w,bio}$	Metabolic water	kg/h	
$M_{w,in}$	Water mass of inlet air	kg/h	
M_w^t	Water mass in the MSW pile at given hour	kg/h	
MC	Moisture content	%ww.	
O_2	Oxygen concentration	%vol.	
P_{fo}	Food waste	%ww.	
P_{pa}	Paper and cardboard	%ww.	
P_{pl}	Plastics	%ww.	
PP	Precipitation	mm/h	
$Q_{SR,MSW}$	Solar radiation through the entire surface of MSW	kJ/h	
$Q_{SR,ac}$	Transmitted solar radiation heat through acrylic roof	kJ/h	
$Q_{SR,ac\rightarrow MSW}$	Transmitted solar radiation heat through acrylic roof to MSW surface	kJ/h	
Q_a	Sensible heat of the air	kJ/h	
$Q_{absorb,GH}$	Solar radiation absorption by the air	kJ/h	

Symbol	Details	Unit	Value
	inside the greenhouse		
$Q_{air,MSW \rightarrow am}$	Enthalpy of the air from the MSW pile to ambient	kJ/h	
$Q_{air,in}$	Enthalpy of inlet air	kJ/h	
$Q_{air,out}$	Enthalpy of exhaust air	kJ/h	
$Q_{bio,simu}$	Metabolic heat from aerobic biodegradation simulation	kJ/h	
Q_{bio}	Metabolic heat	kJ/h	
$Q_{cov,GH \rightarrow ac \rightarrow am}$	Heat transfer (convection) from greenhouse headspace to outside through the acrylic	kJ/h	
$Q_{cov,GH \rightarrow c2 \rightarrow am}$	Heat transfer (convection) from greenhouse headspace to outside through the concrete material	kJ/h	
$Q_{cov,MSW}$	Heat convection through the entire MSW surface by natural wind	kJ/h	
Q_{eva}	Latent heat of evaporation	kJ/h	
$Q_{rad,MSW \rightarrow GH}$	Heat radiation from the MSW surface to the greenhouse headspace	kJ/h	
$Q_{rad,MSW \rightarrow ac}$	Heat radiation from the MSW surface to acrylic roof	kJ/h	
$Q_{rad,MSW \rightarrow c2}$	Heat radiation from the MSW surface to concrete contacted with the air inside the greenhouse	kJ/h	
$Q_{rad,MSW \rightarrow sky}$	Heat radiation from the MSW surface to sky	kJ/h	
$Q_{tran,MSW \rightarrow c1 \rightarrow am}$	Heat transfer (conduction and convection) between MSW pile and ambient through the concrete wall	kJ/h	
$Q''_{SR,ac \rightarrow MSW}$	Transmitted solar radiation heat through acrylic roof to the MSW surface	MJ	
Q''_{a}	Sensible heat of the air	MJ	
$Q''_{absorb,GH}$	Solar radiation absorption by the air inside the greenhouse	MJ	
$Q''_{air,in}$	Enthalpy of inlet air	MJ	
$Q''_{air,out}$	Enthalpy of exhaust air	MJ	
Q''_{bio}	Metabolic heat	MJ	
$Q''_{cov,GH \rightarrow ac \rightarrow am}$	Heat transfer (convection) from greenhouse headspace to outside through the acrylic	MJ	
$Q''_{cov,GH \rightarrow c2 \rightarrow am}$	Heat transfer (convection) from greenhouse headspace to outside through the concrete material	MJ	
$Q''_{cov,MSW}$	Heat convection through the entire MSW surface by natural wind	MJ	
Q''_{eva}	Latent heat of evaporation	MJ	
Q''_{rad}	Total heat radiation	MJ	
$Q''_{rad,MSW \rightarrow GH}$	Heat radiation from the MSW surface	MJ	

Symbol	Details	Unit	Value
	to the greenhouse headspace		
$Q"_{rad,MSW\rightarrow ac}$	Heat radiation from the MSW surface to acrylic roof	MJ	
$Q"_{rad,MSW\rightarrow c2}$	Heat radiation from the MSW surface to concrete contacted with the air inside the greenhouse	MJ	
$Q"_{rad,MSW\rightarrow sky}$	Heat radiation from the MSW surface to sky	MJ	
$Q"_{tranfer}$	Total heat transfer in Scenario 1	MJ	
$Q"_{tran,MSW\rightarrow c1\rightarrow am}$	Heat transfer (conduction and convection) between MSW pile and ambient through the concrete wall	MJ	
R	Gas constant	J/mol·K	8.314
$R_{O/S}$	Oxygen consumption per substrate consumption	kgO/kgS	1.1
RH_{GH}	Relative humidity of the air retained within the greenhouse	%	
$RH_{MSW\rightarrow GH}$	Relative humidity of the air passing through the MSW pile to greenhouse headspace	%	
$RH_{MSW\rightarrow am}$	Relative humidity of the air from the MSW pile to ambient	%	83.94
RH_{in}	Relative humidity of inlet air	%	
S	Substrate mass	kg	
$T_{GH,cal}$	Headspace temperature from the model	°C	
$T_{GH,mix}$	Headspace temperature, representing the stage where air moves through the waste pile and mixes with the greenhouse headspace	°C	
T_H	Maximum temperature for microbial growth	°C	70
T_M	Optimum temperature for microbial growth	°C	50
$T_{MSW,cal}$	Waste temperature from the model	°C	
T_S	The ideal temperature, contributing to the maximum biomass growth rate with no oxygen and water limitations	°C	50
$T_{ac,in}$	Internal surface temperature of the acrylic roof	°C	
T_{am}	Ambient temperature from the experiment	°C	
$T_{c2,in}$	Internal surface temperature of the concrete connected to the greenhouse headspace	°C	
T_{sky}	Sky temperature	°C	
V_{GH}	The volume of greenhouse headspace	m³	42.12
$V_{MSW\rightarrow GH}$	The volume of the air passing through the MSW pile to greenhouse	m³	

Symbol	Details	Unit	Value
	headspace		
V_{in}	The volume of inlet air	m³	130
V_{out}	The volume of the air flowing out from the greenhouse system	m³	
X	Microbial mass	kg	
$Y_{X/S}$	Microbial yield	kgX/kgS	0.2
a_{MSW}	Heat transfer coefficient between MSW and concrete walls	kJ/m^2·°C	33.6
$a_{ac,in}$	Interior convective heat transfer coefficient on acrylic material	kJ/m^2·°C	20.27
$a_{c2,in}$	Interior convective heat transfer coefficient on concrete contacted with the air inside the greenhouse	kJ/m^2·°C	22.32
a_{cvnat}	Natural convective heat transfer coefficient	kJ/m^2·°C	
a_o	Heat convection coefficient on the exterior surface	kJ/m^2·°C	
a_w	Water activity	-	
a_{w0}	Minimum water activity for microbial growth	-	0.91
$q_{MSW \rightarrow GH}$	The volume of the air passing through the MSW pile to greenhouse headspace	m³/h	
$q_{MSW \rightarrow am}$	The volume of the air passing through the MSW pile to ambient	m³/h	
q_{in}	The volume of inlet air	m³/h	130
q_{out}	The volume of the air flowing out from the greenhouse system	m³/h	
v_{in}	Air velocity inside the greenhouse	m/s	0.00258
v_{wind}	Wind speed	m/s	
w_H	Maximum moisture content for microbial growth	%ww.	80
w_L	Minimum moisture content for microbial growth	%ww.	30
w_M	Optimum moisture content for microbial growth	%ww.	60
α_{MSW}	The solar radiation absorptivity of the MSW surface	-	0.2570
$\eta_{SR,air}$	Absorption coefficient of solar radiation by the air inside the greenhouse	-	0.05-0.55
μ_s	Maximum specific growth rate at 50 °C	1/h	0.18
ρ_{GH}	Density of the air retained in the greenhouse	kg/m^3	
$\rho_{MSW \rightarrow GH}$	Density of the air from the MSW pile to greenhouse headspace	kg/m^3	
$\rho_{MSW \rightarrow am}$	Density of the air from the MSW pile to ambient	kg/m^3	

Symbol	Details	Unit	Value
$\rho_{air,in}$	Density of inlet air	kg/m^3	
$\rho_{air,out}$	Density of exhaust air	kg/m^3	
σ	Stefan-Boltzmann constant	W /m^2·K^4	5.667x10^{-8}
τ_{ac}	Acrylic transmittance	-	0.9125
ΔM_{CO2}	The amount of generated CO_2	mol/h	
ΔM_{OM}	The amount of degraded organic matter	kg/h	
ΔO_x	Oxygen consumption	kg/h	
$\Delta O_x/\Delta t$	Oxygen consumption rate	kg/h	
Δq_{co2}	The volume of CO_2 generated for an hour	m³/h	
$\Delta T_{GH,cal}/\Delta t$	Change in greenhouse headspace temperature	°C/h	
$\Delta T_{MSW,cal}/\Delta t$	Change in waste temperature	°C/h	
$\Delta S/\Delta t$	The substrate consumption rate	kg/h	
ΔW	Water mass change in the waste pile	kg/h	
$\Delta X/\Delta t$	Microbial growth rate	kg/h	

3.1 Introduction

Across the globe, there is a notable seeking for renewable energy resources as a sustainable alternative instead of the rapidly declining fossil fuel resources. Waste to energy (WtE) is one of the circular economy solutions, contributing to economic, social, and environmental co-benefits by efficient natural resource utilization, that leads to greenhouse gas emission reduction, job creation, and fostering innovation [1]. The waste-to-energy market in the Asia-Pacific region was forecasted to grow by more than 15% annually, with an anticipated value of 13.66 billion USD by 2023 [2]. The study by Sutthasil et al. [3] indicated that conversion of municipal solid waste (MSW) to refuse-derived fuel (RDF) via the Mechanical Biological Treatment (MBT) process for electricity production resulted in declining greenhouse gas (GHG) emissions by 117%, 87%, and 50% compared to anaerobic landfill as the conventional waste disposal method, when the distance between the RDF facility and the power plant was 100 km, 200 km, and 300 km, respectively.

MBT could potentially be the suitable processes as a waste management tool to reduce the environmental impact associated with the final disposal of biodegradable waste [4]. The operational units in MBT facilities can be flexible, depending on the goals of the waste management strategy. Additionally, the advantages of MBT are not only in terms of suitable mixed MSW management but also in terms of resource recovery, such as RDF production or metal recovery via the sorting process [5]. High moisture content of MSW contributes to low efficiency of mechanical separation and thermal conversion process. The drying step is possible to reduce moisture content together with a decrease in the volume of MSW. Advantages of drying are the decline of transportation costs, microbiological inactivation in organic waste materials, safe waste storage, and the reduction of hazard levels [6].

A biodrying process is an alternative drying method which evaporate water in solid waste by heat convection from microbial activity [7]. In contrast to thermal drying, biodrying is a sustainable option for treating MSW, as it operates without the need of external heat [8]. Additionally, the biodrying technology is a cost-effective and environmentally beneficial technology because the heat required for drying is generated by the decomposition of organic waste in MSW, with the aid of aeration, which consume minimal electricity [9]. According to Kaza et al. [10] in those middle-income and low-income countries, over half of the total waste (> 50%) consists of organic waste (food and green wastes). Therefore, biodrying presents the potential drying method that can be implemented in many countries.

The biodrying under greenhouse condition is appropriate for developing countries where high solar radiation is available, and it is inexpensive and can be operated by local accessible technologies [11]. Biodrying under greenhouse condition could potentially be the solution for moisture reduction in MSW, but there are a few studies conducting experiments on this method. The study by Robles-Martínez et al. [12], indicated that biodrying process within a greenhouse cover had the combined effects of the heat capture and the energy produced by microbial activity in market food waste. The combination of biodrying and greenhouse technologies enhanced the efficiency of water removal in the waste compared to open solar drying. Contreras-Cisneros et al. [13] conducted the greenhouse biodrying experiment in semi-static piles with passive aeration over 46 days. Although oxygen consumption dropped to near zero by day 34, moisture content continued to decrease due to convective drying driven by temperature differences in the greenhouse. Even during inactive biodrying, a notable 14–15% moisture reduction from the initial level was observed, highlighting the ability of the greenhouse system to enhance and sustain drying even without microbial activity. Moreover, the greenhouse cover can shield against excess rainfall water entering the MSW pile without obstructing sunlight. Overall, the solar greenhouse biodrying system offers multiple advantages, including enhanced heat capture, improved water removal efficiency, sustained drying even without active microbial activity, and protection from rainfall, making it suitable for tropical regions.

The potential of greenhouse technology application for the biodrying process to reduce moisture content has been identified, but a comprehensive understanding of the energy source contribution in the biodrying with the greenhouse system remains elusive. To address this gap, it is important to conduct a detailed heat balance analysis to quantify the contributions of various energy sources involved in the water removal process and the thermodynamic behavior within the solar greenhouse biodrying system. Prior studies on the biodrying heat balance analysis employed different approaches for calculating the heat elements involved in biodrying systems. For instance, the model proposed by Zawadzka et al. [14] considered three primary sources of heat input, including the heat from the incoming air, the heat contained within the raw biomass, and the biological heat generated during the process. In contrast, several studies only considered biological heat produced by the biodegradation of organic waste as the source of heat input in their biodrying system [8, 15, 16]. Advanced mathematical models, such as the finite difference method, can be applied in heat balance analysis and this method is powerful tools for numerically solving complex problems, including thermo-diffusion in materials and 3D temperature profiling within waste piles [17, 18]. For example, Orozco-Álvarez et al. [18] employed this method to model temperature profiles during pilot-scale biodrying in a greenhouse-type structure at multiple recording points within an organic solid waste pile. The limitations of this method include high computational cost and time due to memory requirements and solving time as well as calculation complexity. A recent study by Lai et al. [19] on heat balance analysis and temperature profiling in aerobic digestion of food waste successfully adapted and modified Monod-type kinetic models to predict temperature variations during composting. The Monod kinetics model showed superior performance over the first-order model, achieving a relative root mean square error (rRMSE) of 10% in an intermittently aerated in-vessel composting system.

Based on the literature survey, few studies have conducted heat balance analysis of MSW biodrying under a greenhouse system. It is crucial to develop mathematical models that can predict temperature profiles within both the waste pile and the air inside greenhouse. Given the complexity of MSW biodrying in a greenhouse, the process involves multiple heat sources and losses, including metabolic heat, inlet air heat content, solar radiation, heat conduction and convection as well as thermal radiation to the air and material structure. Radiation is a heat transfer process that transmits heat through electromagnetic waves and generates heat in the airflow containing liquid particles [20]. In this study, we propose a novel calculation methodology for heat balance in biodrying under a greenhouse condition. This proposed model differs from existing models by accounting for comprehensive heat inputs and outputs within the pilot-scale solar greenhouse biodrying system, as well as explicitly incorporating the heat balance in the greenhouse headspace. Experimental data was used from previously published work [21] to compare the temperature profiles between actual observations and the simulated data generated by the developed mass and heat balance models. The key difference between the previous work and the current study is that while the previous work reported observed results from a pilot-scale experiment, the present study aims to develop a mathematical model to realistically represent the biodrying process within a greenhouse system. Also, this research aims to investigate the influence of heat sources on temperature changes and water evaporation during the biodrying process. Furthermore, we have elucidated the merits of solar greenhouse biodrying through comparative data simulations by comparison between the biodrying under greenhouse and non-greenhouse conditions. The simulations have been conducted under consideration of precipitation to demonstrate the benefits of applying a greenhouse in the biodrying process within tropical regions.

This study addresses three main research questions related to the biodrying process within the greenhouse system: (1) What are the contributions of heat sources and heat utilization to both the waste pile and the air (headspace) inside the greenhouse. (2) How does the thermal behavior of the biodrying process vary during daytime and nighttime. (3) What are the advantages of applying greenhouse technology in the biodrying process. The outcomes derived from this study have the potential to enhance our comprehension of biodrying under a greenhouse condition and constitute a novel contribution in this research field.

3.2 Material and Methods

3.2.1 MSW Feedstock and Characterization

The MSW used in this study was sourced from the On-nut Waste Transfer Station in Bangkok, Thailand. A representative sample of mixed MSW was collected for analysis of waste composition and characteristics. Subsequently, the sampled MSW was divided among three greenhouse reactors for the experiment.

Moisture content (MC) of the MSW was determined using the oven-drying method at 105 °C, following the ASTM D-3173 1997 standard before and after 10-day experimental period. Also, initial and final MSW weight values were measured by truck scale, and a greenhouse reactor received approximately 4,000 kg of MSW, with an initial operational setting that included a feedstock height of 1.2 m, a length of 4 m, and a width of 3.5 m. The initial MC was 57.76±10.41% by mass. The waste composition primarily consisted of organic waste, constituting 48.73% of the mass, which included food waste (15.64% by mass), yard waste (10.23% by mass), and organic scraps (22.86% by mass). Plastic and paper fractions accounted for 20.22% and 6.60% of the total mass, respectively. The initial composition of MSW is provided in Appendix A.

3.2.2 Experimental Procedure

The experimental results from the previous study [21] were used as the primary data, supplemented by secondary data such as weather information from satellites and estimated the heat generation factor from food waste degradation by literature. These data were essential for calculating mass and heat balance models, as well as conducting simulations to compare biodrying processes with and without greenhouse covers. Thus, it is necessary to descript the experimental procedure of the pilot-scale solar greenhouse biodrying (SGB) reactors in the previous study.

Three greenhouse reactors are located in the On-nut sewage treatment plant, near the On-nut Waste Transfer Station in Bangkok, Thailand (13°42'46.6"N 100°40'54.0"E). As shown in Figure 3.1, each reactor in the SGB system comprises concrete bunkers measuring 3.50 m in width, 4.35 m in length, and 2.20 m in height. These bunkers were topped with roofs made of a metal structure covered by acrylic material with 3 mm of thickness. The ground was levelled up to 0.25 m, allowing for the creation of internal gutters within the greenhouse reactors. Each greenhouse reactor has two gutters, each serving two purposes: facilitating the air pathway and draining leachate. Air supply systems were positioned at the backside of the greenhouses. These systems comprised centrifuge blowers, enclosures, and aeration pipelines measuring 6 inches in diameter (0.1524 m). Ventilation fans were used to extract exhaust air for reducing humidity levels inside the greenhouse.

We conducted three treatments under different conditions. Two conditions operated under force aeration at varying airflow rates: 0.78 and 1.96 m^3/kg waste/day. The other condition was passive aeration (no forced aeration). All treatments were monitored for a duration of 10 days. In this study, the condition of the aeration rate at 0.78 m^3/kg waste/day was used for performing mass and heat balance analysis in order to simulate the temperature profile in the SGB system. The comparison between actual and simulated temperature data was conducted due to the abundance and reliability of the temperature measurements obtained in this pilot-scale experiment. Temperature measurements were conducted using type-K thermocouples, and four thermocouples were installed in the core layer (below 60 cm from the top of the waste pile), with other four in the surface layer (5–10 cm from the top). One thermocouple was placed near the exhaust gas sampling channel, while ambient temperature was also monitored outside the greenhouse. Temperature data were hourly collected and recorded using Graphtec data loggers (GL240, Japan) placed behind the reactors in the controller boxes. Solar radiation intensity was measured using a pyranometer (RK200-03, China) positioned on the top of the greenhouse. Daily accumulation of solar radiation intensity (MJ/m^2/day) during the biodrying process was recorded by a data logger (RK600, China). Carbon dioxide (CO_2) and methane (CH_4) produced during the process were analyzed using a portable analyzer (Biogas5000, UK), which measures CO_2 and CH_4 concentrations by volume. A channel at the top-backside of the acrylic cladding, near the ventilation fan, was used for sampling exhaust gas.

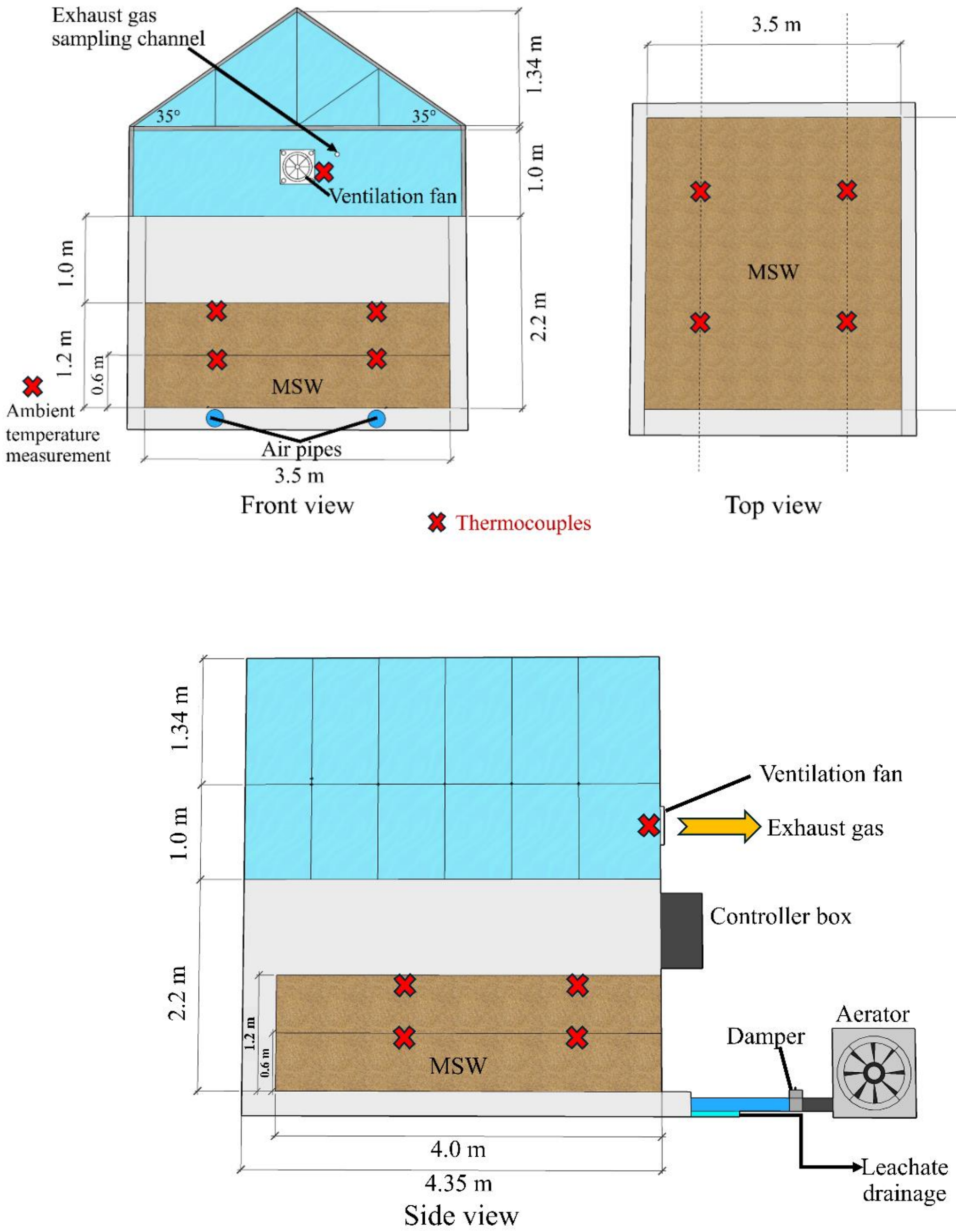

Figure 3.1 The Configuration and Components of the SGB System

3.2.3 Calculation of Mass Balance in MSW pile

3.2.3.1 Calculation of Solid Mass

In the greenhouse, the MSW mass was decreased by aerobic degradation of organic matter and water evaporation, and CO_2 was generated. The solid mass degraded by microorganisms was estimated from the CO_2 concentration at the outlet air from the greenhouse, assuming that the CO_2 was generated by only aerobic degradation.

First, the amount of air flowing out from the greenhouse system (q_{out}, m^3/h) was determined using the ambient temperature and the greenhouse headspace temperature by Eq.1. Air was assumed to behave as an ideal gas, following Charles's Law, which states that at constant pressure, the volume of a gas is directly proportional to its temperature in Kelvin [22].

$$q_{out} = q_{in} \times \frac{T_{GH,cal}+273.15}{T_{am}+273.15} \qquad \text{Eq. 3- 1}$$

Where the volume of inlet air (q_{in}) is 130 m^3/h, $T_{GH,cal}$ is headspace temperature (°C) from the model, and T_{am} is ambient temperature (°C).

Next, the volume of CO_2 generated for an hour (Δq_{co2}, m^3/h) and the amount generated CO_2 (ΔM_{CO2}, mol/h) were calculated by the CO_2 concentration in the air by Eqs. 3-1&2, respectively.

$$\Delta q_{co2} = \left[V_{GH} \cdot \frac{(CC^t - CC^{t-1})}{100} \right] + \left[V_{out} \cdot \frac{CC^t}{100} \right] - \left[V_{in} \cdot \frac{0.03}{100} \right] \qquad \text{Eq. 3- 2}$$

$$\Delta M_{CO2} = \frac{\Delta q_{co2}}{0.0224} \qquad \text{Eq. 3- 3}$$

Where V_{GH} is the volume of greenhouse headspace (42.12 m^3), V_{out} is the volume of the air flowing out from the greenhouse system (m^3), and V_{in} is the inlet air volume (130 m^3). Alos, it was assumed that one mole of an ideal gas at standard temperature and pressure (STP) is equal to 22.4 L/mol (0.0224 m^3/mol).

After that, the amount of degraded organic matter was estimated stoichiometrically (Eq. 3-4), assuming that the chemical composition of organic matter used in the study was $C_{18}H_{26}O_{10}N$ (molecular weight = 416), suggested by Haug [23].

$$4C_{18}H_{26}O_{10}N + 75O_2 = 72CO_2 + 46H_2O + 4NH_3 \qquad \text{Eq. 3- 4}$$

Therefore, the amount of degraded organic matter (ΔM_{OM}, kg/h) in the MSW was calculated by Eq. 3-5.

$$\Delta M_{OM} = -\Delta M_{CO2} \times \frac{4}{72} \times \frac{416}{1000} \qquad \text{Eq. 3- 5}$$

Lastly, it was possible to estimate the solid mass in MSW at the given hour (M_s^t, kg/h) using Eq. 3-6.

$$M_s^t = M_s^{t-1} + \Delta M_{OM}^t - (\Delta M_{OM}^t \times Y_{X/S}) \qquad \text{Eq. 3- 6}$$

Where, t-1 in the superscription refers to the previous hour of the process. $Y_{X/S}$ is microbial yield ($Y_{X/S}$= 0.2 kg microbial mass/kg degraded solid), suggested by Kaneko et al. [24].

3.2.3.2 Calculation of Water Mass

In the MSW pile, the MC change was considered as the water loss from evaporation together with moisture addition from metabolic water and humidity of inlet air. Thus, the water mass change (ΔW, kg/h) and the water mass in MSW pile at the given hour (M_w^t, kg/h) were calculated by Eqs. 3-7 and 3-8.

$$\Delta W = M_{w,bio} + M_{w,in} - M_{w,MSW \rightarrow GH} \qquad \text{Eq. 3- 7}$$
$$M_w^t = M_w^{t-1} + \Delta W^t \qquad \text{Eq. 3- 8}$$

To calculate ΔW, there are three associated variables.

The metabolic water ($M_{w,bio}$, kg/h) was also estimated stoichiometrically using Eq. 9. The amount of water produced and consumed by microorganisms was obtained from the calculation of the ΔM_{CO2} value in Eq. 3-3.

$$M_{w,bio} = \Delta M_{CO2} \times \frac{46}{72} \times \frac{18}{1000} \qquad \text{Eq. 3- 9}$$

The water mass from inlet air ($M_{w,in}$, kg/h) was estimated from the inlet air volume (q_{in}, m^3/h) and the absolute humidity (AH_{in}, g/m^3) at ambient temperature, as shown in Eq.10 [25]. Here are the steps for calculating $M_{w,in}$:

$$AH_{in} = 217 \times \left(\frac{6.1078 \times 10^{\frac{7.5 \times T_{am}}{T_{am}+237.3}}}{T_{am}+273.15} \right) \times \left(\frac{RH_{in}}{100} \right) \qquad \text{Eq. 3- 10}$$

$$M_{w,in} = \frac{AH_{in} \times q_{in}}{1000} \qquad \text{Eq. 3- 11}$$

Where RH_{in}(%) refers to the relative humidity of the inlet air in hour scale, obtained from the weather station (by Hydro-Informatics Institute, Thailand [26]) near the location of the pilot-scale biodrying system.

The water mass in the air releasing from the MSW pile to the greenhouse headspace ($M_{w,MSW \rightarrow GH}$, kg/h): The air volume passing through the MSW pile ($q_{MSW \rightarrow GH}$, m^3/h) was estimated by Eq.12, and then this amount of water mass was calculated as same as the previous step (Eqs. 10-11). Here are the steps for calculating $M_{w,MSW \rightarrow GH}$:

$$q_{MSW\rightarrow GH} = q_{in} \times \frac{T_{MSW,cal}+273.15}{T_{am}+273.15}$$ Eq. 3- 12

$$AH_{MSW\rightarrow GH} = 217 \times \left(\frac{6.1078\times10^{\frac{7.5\times T_{MSW,cal}}{T_{MSW,cal}+237.3}}}{T_{MSW,cal}+273.15} \right) \times \left(\frac{RH_{MSW\rightarrow GH}}{100}\right)$$ Eq. 3- 13

$$M_{w,MSW\rightarrow GH} = \frac{AH_{MSW\rightarrow GH}\times q_{MSW\rightarrow GH}}{1000}$$ Eq. 3- 14

Where $T_{MSW,cal}$ is calculated waste temperature (°C), and $RH_{MSW\rightarrow GH}$ is the relative humidity of the air passing through the MSW pile to greenhouse headspace (%).

In the greenhouse headspace, the water mass of the exhaust air ($M_{w,GH\rightarrow am}$, kg/h) was determined by two components: the water mass in the air released from the MSW pile into the greenhouse headspace ($M_{w,MSW\rightarrow GH}$, kg/h) and the water mass retained within the greenhouse ($M_{w,GH}$, kg/h). The calculation of $M_{w,GH\rightarrow am}$ is based on the following equations:

$$M_{w,GH\rightarrow am} = M_{w,MSW\rightarrow GH} - M_{w,GH}$$ Eq. 3- 15

Meanwhile, $M_{w,GH}$ was estimated by Eqs.3-16 and 3-17.

$$AH_{GH} = 217 \times \left(\frac{6.1078\times10^{\frac{7.5\times T_{GH,cal}}{T_{GH,cal}+237.3}}}{T_{GH,cal}+273.15} \right) \times \left(\frac{RH_{GH}}{100}\right)$$ Eq. 3- 16

$$M_{w,GH} = \frac{AH_{GH}\times V_{GH}}{1000}$$ Eq. 3- 17

Where $T_{GH,cal}$ is within the greenhouse (%) calculated headspace temperature (°C), and RH_{GH} is the relative humidity of the air retained in greenhouse headspace.

3.2.4 Calculation of Heat Balance

The heat balance of the SGB system was calculated and analyzed from experimental data. In this study, there were six key temperature points that interacted and contributed to the dynamic temperature changes inside the system. These temperatures included: 1) waste temperature, 2) headspace temperature (the air inside the greenhouse), 3) concrete temperature in contact with the waste pile (denoted as c1), 4) concrete temperature in contact with the air inside the greenhouse (denoted as c2), 5) acrylic temperature, and 6) ambient temperature. Although these considered temperatures were heterogeneous in actual situation due to moisture and temperature gradients in waste pile, greenhouse headspace, and structural materials, we assumed that they were homogeneous objects for the purpose of model calculations. Moreover, calculations were performed in hour scale for 10 days. The temperatures of the waste pile and headspace were determined through individual heat balance equations. In contrast, the acrylic and concrete temperatures were derived using the heat transfer equation. The ambient temperature was obtained from experimental data reported in the previous study. The temperature change for one hour was calculated in each heat element entering and departing each system. The following sections describe the detailed calculations in each heat element. It was assumed that the heat inputs were almost entirely converted into heat outputs, thereby representing heat utilization (heat losses) within the biodrying process. Lateral heat transfer from the center to both sides of the waste pile may occur, representing a potential form of unaccounted heat loss in the system. However, this type of heat loss was observed to contribute less than 0.1% of the total heat loss in the pilot-scale system [16]. Given its minimal contribution, the effect of this heat transfer is considered practically insignificant. Therefore, excluding it from the heat balance model is a reasonable simplification that does not affect the model's reliability. The reliability assessment of the heat balance model was confirmed by comparing the minimum and maximum of observed MSW temperature profile as well as the greenhouse headspace temperature with the calculated value of temperatures obtained from the heat balance calculation.

3.2.4.1 Heat Balance within the MSW Pile

The heat balance within the MSW pile in the SGB system is presented in Eq. 3-18 with nine heat elements. The heat inputs included metabolic heat generated within the waste (Q_{bio}), solar radiation transmitted through the acrylic roof of the greenhouse to MSW surface ($Q_{SR,ac \rightarrow MSW}$), and enthalpy of inlet air ($Q_{air,in}$). The remaining elements contributed to heat utilization within the system. These included the latent heat of evaporation (Q_{eva}), sensible heat of the air passing through the MSW pile (convection) (Q_a), radiative heat losses from the MSW surface to the surrounding materials ($Q_{rad,MSW \rightarrow c2}$ and $Q_{rad,MSW \rightarrow ac}$) and air within the greenhouse ($Q_{rad,MSW \rightarrow GH}$), and heat transfer through the concrete walls (conduction and convection) ($Q_{tran,MSW \rightarrow c1 \rightarrow am}$). Each of these heat elements interacts dynamically, contributing to the temperature changes within the waste pending the biodrying process. Figure 3.2 presents the boundary of heat balance analysis within the waste pile, and the overall heat input and output formula for the MSW component is as follows:

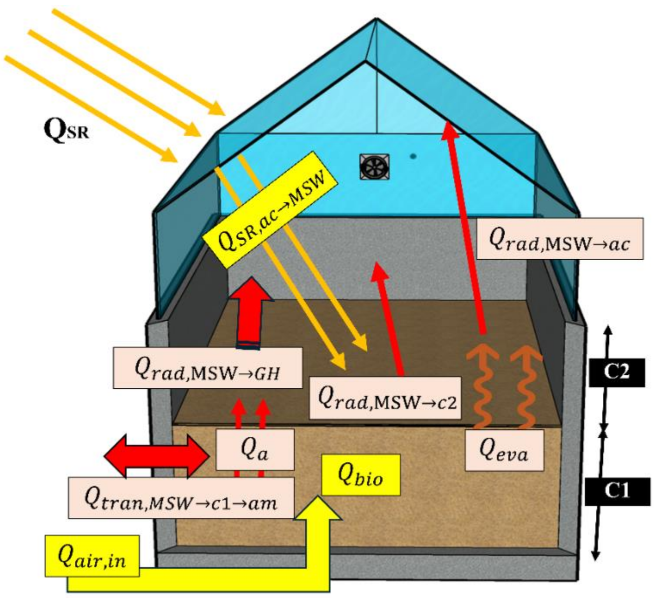

Figure 3.2 The Boundary of the Heat Balance Analysis within the Waste Pile

$$\left(C_{p,dry\ MSW} \cdot M_s + C_{p,water} \cdot M_w\right) \times \frac{\Delta T_{MSW,cal}}{\Delta t} = Q_{air,in} + Q_{bio} + Q_{SR,ac\rightarrow MSW} - Q_a - Q_{eva} - Q_{rad,MSW\rightarrow GH} - Q_{rad,MSW\rightarrow c2} - Q_{rad,MSW\rightarrow ac} - Q_{tran,MSW\rightarrow c1\rightarrow am} \quad \text{Eq. 3- 18}$$

From Eq. 3-18, Each heat element was calculated as shown in Table 3.1.

Table 3.1 Details and description of each heat element for heat balance within the MSW pile

Heat elements	Formulas	Parameters and constants
Enthalpy of inlet air ($Q_{air,in}$)	$Q_{air,in} = (1.0065 \times T_{am} \times \rho_{air,in} \times q_{in}) + ((1.805 \cdot T_{am} + 2501) \times AH_{in} \times 10^{-3} \times q_{in})$ (Eq. 3- 19)	$\rho_{air,in} = 1.293 \times \frac{273.15}{273.15+T_{am}}$ AH_{in} can be estimated by Eq. 3-10.
Metabolic heat (Q_{bio})	$Q_{bio} = -\Delta M_{OM} \times CV_{OM}$ (Eq. 3- 20)	CV_{OM}= 21,558.78 kJ/kg (Estimated from the chemical composition ($C_{18}H_{26}O_{10}N$) suggested by Haug [23].
Transmitted solar radiation through the acrylic roof to MSW surface ($Q_{SR,ac\rightarrow MSW}$)	$Q_{SR,ac\rightarrow MSW} = Q_{SR,ac} \times \alpha_{MSW}$ (Eq. 3- 21)	$Q_{SR,ac} = J_{t\alpha\theta} \times \tau_{ac} \times A_{ac}$ $J_{t\alpha\theta} = J_{d\alpha\theta} + J_{sky\theta}$ (See also Appendix A) τ_{ac} = 0.9125 [27] A_{ac} = 22.3545 m^2 (for both south-east and south-west directions) α_{MSW} = 0.2570
Sensible heat of the air (Q_a)	$Q_a = [C_{p,dryair} \cdot M_{dryair} \cdot (T_{MSW,cal} - T_{am})] + [C_{p,vapor} \cdot (M_{w,MSW\rightarrow GH} \cdot T_{MSW,cal} - M_{w,in} \cdot T_{am})]$ (Eq. 3- 22)	$C_{p,dryair}$ = 1.004 kJ/kg·°C $M_{dryair} = q_{in} \times \rho_{in}$ $C_{p,vapor}$ = 1.841 kJ/kg·°C
Latent heat of water evaporation (Q_{eva})	$Q_{eva} = L_w \times \Delta W$ (Eq. 3- 23)	$L_w = 2{,}500.8 - 2.3668 \times T_{MSW,cal}$
Heat radiation from the MSW surface to the greenhouse headspace ($Q_{rad,MSW\rightarrow GH}$)	$Q_{rad,MSW\rightarrow GH} = Fe_{MSW} \cdot F_{MSW\rightarrow GH} \cdot \sigma \cdot A_{MSW} \times [(T_{MSW,cal} + 273.15)^4 - (T_{GH,mix} + 273.15)^4]$ (Eq. 3- 24)	Fe_{MSW} = 0.85 [8] $F_{MSW\rightarrow GH}$ = 0.64 σ = 5.667×10^{-8} W/m^2·K^4 A_{MSW} = 14 m^2 $T^t_{GH,mix} = T^{t-1}_{MSW,cal} - [(T^{t-1}_{MSW,cal} - T^{t-1}_{GH,cal}) \times \frac{V_{GH}}{(V_{in} + V_{GH})}]$

Heat elements	Formulas	Parameters and constants
Heat radiation from the MSW surface to the concrete part connected to the greenhouse headspace (**$Q_{rad,MSW\rightarrow c2}$**)	$Q_{rad,MSW\rightarrow c2} = Fe_{MSW} \cdot Fe_c \cdot F_{MSW\rightarrow c2} \cdot \sigma \cdot A_{MSW} \times [(T_{MSW,cal} + 273.15)^4 - (T_{c2,in} + 273.15)^4]$ (Eq. 3- 25)	Fe_c = 0.9 $F_{MSW\rightarrow c2}$ = 0.36 $T_{c2,in}$: the internal surface temperature of the concrete connected to the greenhouse headspace (See also Appendix A)
Heat radiation from the MSW surface to acrylic material (**$Q_{rad,MSW\rightarrow ac}$**)	$Q_{rad,MSW\rightarrow ac} = Fe_{MSW} \cdot Fe_{ac} \cdot F_{MSW\rightarrow ac} \cdot \sigma \cdot A_{MSW} \times [(T_{MSW,cal} + 273.15)^4 - (T_{ac,in} + 273.15)^4]$ (Eq. 3- 26)	Fe_{ac} = 0.86 [28] $F_{MSW\rightarrow ac}$ = 0.64 $T_{ac,in}$: the internal surface temperature of acrylic material (See also Appendix A)
Heat transfer through the concrete walls (**$Q_{tran,MSW\rightarrow c1\rightarrow am}$**)	$Q_{tran,MSW\rightarrow c1\rightarrow am} = K_{tran,c1} \times A_{side} \times (T_{MSW,cal} - T_{am})$ (Eq. 3- 27)	$K_{tran,c1} = \frac{1}{\frac{1}{a_{MSW}} + \frac{L_c}{C_c} + \frac{1}{a_o}}$ a_{MSW} = 33.6 kJ/m^2·°C [29] L_c = 0.2 m C_c = 6.2266 kJ/m·°C $a_o = \begin{cases} (2 + 1.2V_{wind}) \times 3.6, if\ v_{wind} < 4 \\ 2V_{wind}^{0.8} \times 3.6, if\ v_{wind} \geq 4 \end{cases}$ A_{side} = 13.8 m^2

Noted:

1) For Eq. 3-21, given the heterogeneous composition of MSW, the solar radiation absorptivity of the MSW surface was estimated to be α_{MSW} = 0.2570 in this study.
2) Eqs. 3-24 and 3-26, which relate to the calculation of thermal radiative heat, and the estimated view factors (including $F_{MSW\rightarrow GH}$, $F_{MSW\rightarrow c2}$, and $F_{MSW\rightarrow ac}$) used in this study, were adopted from Baehr et al. [30]. All equations were in units of W, so the values were converted to kJ/h using a factor of 3.6
3) Fe_{MSW}= 0.85 represents the emissivity factor used to account for non-black-body radiation [8, 30]
4) For Eq. 3-25, thermal emissivity value of concrete (Fe_c = 0.9) was obtained from the OpenStudio® Sorfware developed by The National Renewable Energy Laboratory (U.S.) (NERL) operated by the Alliance for Sustainable - Energy, LLC. In this study, it was assumed that the thermal absorptivity of the concrete material was equal to its thermal emissivity.
5) For Eq. 3-27, the heat convection coefficient on the exterior surface (a_o) was calculated by applying the method outlined by Zhang et al. [31]. The environmental wind speed data (v_{wind}) required for this calculation were obtained from Weather Spark [32]. Additionally, the heat conductivity of concrete, initially reported as C_c= 1.7296 W/m·K in the OpenStudio software by NERL, was converted to kJ/m·°C using a conversion factor of 3.6.

3.2.4.2 Heat Balance in the Greenhouse Headspace

The heat balance of the air in the greenhouse headspace was calculated by considering seven heat elements including four heat elements for the heat input side and three heat elements for the heat output side. For the heat input side, there were 1) Sensible heat of the air (Q_a), 2) Latent heat of evaporation (Q_{eva}), and 3) Heat radiation from the MSW surface to the greenhouse headspace ($Q_{rad,MSW\rightarrow GH}$), and 4) Solar radiation absorption by the air inside the greenhouse ($Q_{absorb,GH}$). For heat output side (heat dissipation), heat transfer (convection) from greenhouse headspace to outside through the acrylic material ($Q_{cov,GH\rightarrow ac\rightarrow am}$) and concrete (c2) ($Q_{cov,GH\rightarrow c2\rightarrow am}$) were taken into account in this heat balance equation as well as enthalpy of exhaust air ($Q_{air,out}$). Figure 3.3 expresses the boundary of heat balance analysis in the greenhouse headspace. The overall heat balance for the greenhouse headspace expresses in Eq. 3-28.

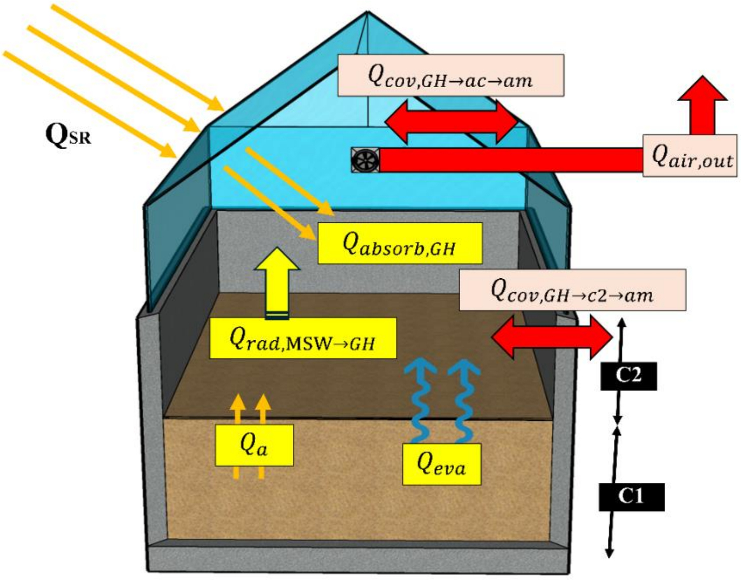

Figure 3.3 The Boundary of Heat Balance Analysis in the Greenhouse Headspace

$$\left[\left(C_{p,vapor} \cdot \left(M_{w,MSW \to GH} + M_{w,GH}\right)\right) + \left(C_{p,dryair} \cdot \left(\rho_{MSW \to GH} \cdot V_{MSW \to GH} + \rho_{GH} \cdot V_{GH}\right)\right)\right] \frac{\Delta T_{GH,cal}}{\Delta t} = Q_a + Q_{eva} + Q_{rad,MSW \to GH} + Q_{absorb,GH} - Q_{cov,GH \to ac \to am} - Q_{cov,GH \to c2 \to am} - Q_{air,out} \quad \text{(Eq. 3- 28)}$$

Where $M_{w,MSW \to GH}$ was determined by Eq.3-14. Moreover, the density of the air retained within the greenhouse (ρ_{GH}, kg/m^3) was calculated by Eq. 3-29, and the water mass in the greenhouse headspace ($M_{w,GH}$, kg/h) was calculated by Eq. 3-17, respectively. Those parameters were used in Eq. 3-28.

$$\rho_{GH} = 1.293 \times \frac{273.15}{273.15 + T_{GH,cal}} \quad \text{Eq. 3- 29}$$

Each heat element used in calculating the heat balance within the greenhouse headspace is shown in Table 3.2.

Table 3.2 Details And Description of Each Heat Element for Heat Balance in the Greenhouse Headspace

Heat elements	**Formulas**	**Parameters and constants**
Sensible heat of the air ($\boldsymbol{Q_a}$)	Refer to Eq. 3-22	
Latent heat of water evaporation ($\boldsymbol{Q_{eva}}$)	Refer to Eq. 3-23	

Heat elements	Formulas	Parameters and constants
Heat radiation from the MSW surface to the greenhouse headspace ($\boldsymbol{Q_{rad,MSW\to GH}}$)	Refer to Eq. 3-24	
Solar radiation absorption by the air inside the greenhouse ($\boldsymbol{Q_{absorb,GH}}$)	$Q_{absorb,GH}= Q_{SR,ac} \times \eta_{SR,air}$ (Eq. 3- 30)	$\eta_{SR,air}$= 0.05-0.55 (This variable was optimized based on time, see also Appendix A for further details.)
Heat transfer (convection) from greenhouse headspace to outside through the acrylic ($\boldsymbol{Q_{cov,GH\to ac\to am}}$)	$Q_{cov,GH\to ac\to am} = K_{cov,GH\to ac\to am} \times A_{ac,total} \cdot (T_{GH,mix} - T_{am})$ (Eq. 3- 31)	$K_{cov,GH\to ac\to am} = \frac{1}{\frac{1}{a_{ac,in}} + \frac{L_{ac}}{C_{ac}} + \frac{1}{a_o}}$ $a_{ac,in} = 5.678 \times \left[m + n\left(\frac{v_{in}}{0.3048}\right)^p\right] \times 3.6$ (m=0.99, n=0.21, p=1.00, v_{in}=0.00258 m/s) L_{ac} = 0.003 m C_{ac} = 0.5472 kJ/m·°C [33] $A_{ac,total}$ = 44.709 m^2
Heat transfer (convection) from greenhouse headspace to outside through the concrete material (c2) ($\boldsymbol{Q_{cov,MSW\to c2\to am}}$)	$Q_{cov,GH\to c2\to am} = K_{cov,GH\to c2\to am} \times A_{c2} \cdot (T_{GH,mix} - T_{am})$ (Eq. 3- 32)	$K_{cov,GH\to c2\to am} = \frac{1}{\frac{1}{a_{c2,in}} + \frac{L_c}{C_c} + \frac{1}{a_o}}$ $a_{c2,in} = 5.678 \times \left[m + n\left(\frac{v_{in}}{0.3048}\right)^p\right] \times 3.6$ (m=1.09, n=0.23, p=1.00) A_{c2} = 15.6 m^2
Enthalpy of exhaust air ($\boldsymbol{Q_{air,out}}$)	$Q_{air,out} = (1.0065 \times T_{GH,cal} \times \rho_{air,out} \times q_{out}) + ((1.805 \cdot T_{GH,cal} + 2501) \times M_{w,GH\to am})$ (Eq. 3- 33)	$\rho_{air,out}$ = $1.293 \times \frac{273.15}{273.15+T_{GH,cal}}$ $M_{w,GH\to am}$ can be calculated by Eq. 3-15.

Noted:

1) The interior convective heat transfer coefficient ($a_{ac,in}$ and $a_{c2,in}$) were determined using McAdams's model. As reported by Mirsadeghi et al. [34], this model was based on wind tunnel experiments involving a vertical square copper plate (0.5 x 0.5 m²) subjected to a uniform airflow parallel to the plate. The parameters m, n, and p are roughness factors that account for both smooth and rough surface conditions. Using this method, it is appropriate for estimating heat convection within the SGB system.
2) The heat convection coefficient on the exterior surface (a_o) in Eqs. 3-31&32 was determined using the same method proposed by Zhang et al. [31].

3.2.4.3 Heat Balance of Surface Materials (Concrete and Acrylic)

The surface temperatures of materials such as concrete and acrylic were considered due to their interaction with MSW and the greenhouse headspace temperatures. The concrete (c1 and c2) and the acrylic roof temperatures were determined using the heat transfer equations. Detailed descriptions of each calculation method for concrete and acrylic temperatures are provided in Appendix A.

3.2.5 Model Performance Evaluation

In this study, the temperatures of the waste and greenhouse headspace at the current time (t) were calculated as the summation of heat elements from the previous time step (t-1). This calculation approach follows an explicit method, where the state of the system at the current time is determined based on the state of the system at the previous time step. In order to assess the reliability of the outcomes from the model, the results from the model were compared with the experimental temperature data. This was because temperature data for both the waste and the greenhouse headspace were abundant, unlike MC, which exhibited a high bias error due to the heterogeneous nature of MSW. Therefore, we compared the waste and headspace temperatures obtained from the model with those from the experimental data. To evaluate the model's accuracy, four statistical indicators including 1) root-mean-square error (RMSE), 2) relative root-mean-square error (rRMSE), 3) mean bias error (MBE), and 4) correlation coefficient (CC), were used. These indicators are expressed in Eqs. 3-34 and 3-37.

$$RMSE = \left[\frac{1}{n}\sum_{i=1}^{n}(T_{cal,i} - T_{exp,i})^2\right]^{0.5} \quad \text{Eq. 3- 34}$$

$$rRMSE = 100 \cdot \frac{1}{T_{exp,avr}} \cdot RMSE \quad \text{Eq. 3- 35}$$

$$MBE = \frac{1}{n}\sum_{i=1}^{n}(T_{cal,i} - T_{exp,i}) \quad \text{Eq. 3- 36}$$

$$CC = \frac{\sum_{i=1}^{n}(T_{exp,i} - T_{exp,avr}) \cdot (T_{cal,i} - T_{cal,avr})}{n \cdot sd_{exp} \cdot sd_{cal}} \quad \text{Eq. 3- 37}$$

Where $T_{cal,i}$ is the modeled temperature at given time, while $T_{cal,avr}$ is the average modeled temperature. $T_{exp,i}$ is the experimental temperature at given time, while $T_{exp,avr}$ is the average experimental temperature. sd_{exp} and sd_{cal} are the standard deviation of the experimental and modeled temperatures, respectively. n represents the number of hours, which was 240 in this study. The model with the lower RMSE value is considered to have better performance compared to a model with a higher RMSE. RMSE is always positive, and an ideal model would have an RMSE of zero, indicating perfect predictions. In addition, there is good agreement between the modeled and experimental temperature when the rRMSE ranges between 10% and 20%, while values below 10% indicate excellent agreement [19]. Meanwhile, MBE provides information on the long-term performance of a model [35]. MBE can be positive, meaning the model tends to overestimate, or negative, meaning the model tends to underestimate. Nevertheless, one limitation of MBE is that overestimation in one individual observation can be offset by underestimation in another observation. Lastly, considering the CC value, the model is regarded as a good predictor if the CC is close to or greater than 0.8 [36], and the CC value also reflects the level of consistency between the experimental and the modeled temperature. Hence, all indicators were used together to evaluate model performance in this study.

Moreover, this present study aims to optimize the accuracy of temperature prediction in the heat balance model of the pilot-scale SGB system. The target parameters for optimization were MBE and RMSE of both waste and headspace temperatures. Sensitivity analysis was conducted to identify the variables that significantly influence these errors. The results revealed that the relative humidity of the air passing through the MSW pile ($\%RH_{MSW \rightarrow GH}$) was the most critical factor, as a 20% increase in this variable led to substantial reductions in MBE and RMSE for both waste (by 39.87% for MBE and by for 17.87% RMSE) and headspace temperatures (by 35.94% for MBE and by 5.98% for RMSE). The solar radiation absorptivity of the MSW surface (α_{MSW}) was identified as the second most influential parameter, while the absorption coefficient of solar radiation by air inside the greenhouse ($\eta_{SR,air}$) showed a comparatively minor effect. The details of the sensitivity analysis of the selected variables for minimizing MBE and RMSE in the heat balance model are presented in Appendix A.

Following the reliability of the calculation method to a satisfactory level, we proceeded to set up the different scenarios of biodrying processes for the next section. Subsequently, the biodegradation process simulation was conducted, and the heat balance was compared under three different conditions.

3.2.6 Process Simulation

In this section, three different scenarios of biodrying process were performed. Since the objective of this study was to introduce the advantages of greenhouse application in biodrying process, the three different scenarios are as follows:

Scenario 1: Forced aeration with greenhouse cover.
Scenario 2: Forced aeration without greenhouse cover.
Scenario 3: Forced aeration without greenhouse cover, considering available precipitation.

Among three different scenarios, the airflow rate was set at 0.78 m^3/kg waste/day. The calculation methodology of heat balance was similar to the previous section for scenario 1. Nevertheless, total heat balance and determined heat elements were different in the open biodrying condition, since Scenarios 2 and 3 were performed with in the outdoor environment. Table 3.3 indicates all considered heat elements for Scenarios 2 and 3. The key differences for heat balance analysis were 1) Solar radiation was considered as an open solar drying, directly exposing the entire surface of the MSW pile. 2) In Scenarios 2 and 3, heat radiation was considered as being directly emitted from the MSW surface to the open sky, contrasting with Scenario 1, where heat radiation was emitted from the MSW surface to the greenhouse headspace. 3) Both Scenarios 2 and 3 accounted for direct heat convection through the entire MSW surface by natural wind. Eq. 3-38 expressed the overall equation for heat balance analysis in scenarios 2 and 3.

$$\left(C_{p,dry\,MSW} \cdot M_s + C_{p,water} \cdot M_w\right) \times \frac{\Delta T_{MSW,cal}}{\Delta t} = Q_{air,in} + Q_{bio,simu} + Q_{SR,MSW} - Q_a - Q_{eva} - Q_{rad,MSW\rightarrow sky} - Q_{cov,MSW} - Q_{air,MSW\rightarrow am} \quad \text{Eq. 3- 38}$$

Table 3.3 Details and Description of Each Heat Element for Heat Balance in Scenario 2 and 3

Heat elements	Formulas	Parameters and constants
enthalpy of inlet air (**$Q_{air,in}$**)	Refer to Eq.3-19	
Metabolic heat derived from biodegradation simulation (**$Q_{bio,simu}$**)	$Q_{bio,simu} = H_o \times \Delta O_x$ (Eq. 3- 39)	H_o = 16,000 kJ/kgO_2 [24] ΔO_x: oxygen consumption (see also section 2.6.1)
Solar radiation through the entire surface of MSW (**$Q_{SR,MSW}$**)	$Q_{SR,MSW} = J_{t\alpha\theta} \times A_{ref} \times \alpha_{MSW}$ (Eq. 3- 40)	$J_{t\alpha\theta} = J_{d\alpha\theta} + J_{sky\theta}$ (See also Appendix A) A_{ref} = 22.3545 m^2 (for both south-east and south-west directions)
Sensible heat of the air (**Q_a**)	Refer to Eq.3-22	
Latent heat of water evaporation (**Q_{eva}**)	Refer to Eq.3-23	
Heat radiation from the MSW surface to sky (**$Q_{rad,MSW\rightarrow sky}$**)	$Q_{rad,MSW\rightarrow sky} = Fe_{MSW} \cdot Fe_{sky} \cdot F_{MSW\rightarrow sky} \cdot \sigma \cdot A_{entireMSW} \times [(T_{MSW,cal} + 273.15)^4 - (T_{sky} + 273.15)^4]$ (Eq. 3- 41)	Fe_{sky} = 0.8 [31] $F_{MSW\rightarrow sky}$ = 1 $A_{entireMSW}$ = 32 m^2 $T_{sky} = 0.0559 \times T_{am}^{1.5}$ [31]
Heat convection through the entire MSW surface by natural wind (**$Q_{cov,MSW}$**)	$Q_{cov,MSW} = [a_o \cdot A_{MSW,cvf} \cdot (T_{MSW,cal} - T_{am})] + [a_{cvnat} \cdot A_{MSW,nat} \cdot (T_{MSW,cal} - T_{am})]$ (Eq. 3- 42)	$A_{MSW,cvf}$ (see also at note under this table) $a_{cvnat} = 1.98 \times (T_{MSW,cal} - T_{am})^{0.25} \times 3.6$ [37] $A_{MSW,nat} = A_{entireMSW} - A_{MSW,cvf}$
Enthalpy of the air from the MSW pile to ambient (**$Q_{air,MSW\rightarrow am}$**)	$Q_{air,MSW\rightarrow am} = (1.0065 \times T_{MSW,cal} \times \rho_{MSW\rightarrow am} \times q_{MSW\rightarrow am}) + ((1.805 \cdot T_{MSW,cal} + 2501) \times AH_{MSW\rightarrow am} \times 10^{-3} \times q_{MSW\rightarrow am})$ (Eq. 3- 43)	$\rho_{MSW\rightarrow am} = 1.293 \times \frac{273.15}{273.15+T_{MSW,cal}}$ $q_{MSW\rightarrow am} = q_{in} \times \frac{T_{MSW,cal} + 273.15}{T_{am} + 273.15}$ $AH_{MSW\rightarrow am} = 217 \times \left(\frac{6.1078 \times 10^{\frac{7.5\times T_{MSW,cal}}{T_{MSW,cal}+237.3}}}{T_{MSW,cal} + 273.15}\right) \times \left(\frac{RH_{MSW\rightarrow am}}{100}\right)$ $RH_{MSW\rightarrow am}$ = 83.94%

Noted:

1) In Eq. 3-41, the value was expressed in units of W and it was crucial to use a conversion factor of 3.6 for converting the value to kJ/h.
2) The surface areas of the MSW exposed to wind ($A_{MSW,cvf}$) in Eq. 3-42 were determined based on wind direction. It was assumed that natural convection occurred simultaneously on the sides not exposed to forced convection by wind. When the wind originated from the north or south, $A_{MSW,cvf}$ was determined as 18.20 m². For wind from the east or west, $A_{MSW,cvf}$ was 18.80 m². Winds coming from the southwest, southeast, northwest, or northeast resulted in the largest exposed surface area, determining as 23.00 m². In cases the wind was absent, there was no surface area exposed to forced convection ($A_{MSW,cvf}$= 0 m^2, if v_{wind}= 0 m/s).
3) The natural convective heat transfer coefficient (a_{cvnat}) was estimated following the methodology outlined in Tanaka et al. [37], with a conversion factor of 3.6 applied to convert the values to kJ/m$^2\cdot$°C.
4) The relative humidity of the air passing through from the MSW pile to the ambient environment ($RH_{MSW\rightarrow am}$) in scenarios 2 and 3 was assumed to be 83.94%, derived from the average %RH of the air passing through the MSW in scenario 1.

3.2.6.1 Aerobic Biodegradation Simulation

In this simulation, microbial activity must be change because factors including temperature, MC, organic mass, and oxygen concentration vary in scenarios 2 and 3. In the model developed in Section 2.3.1, microbial activity was evaluated based only on observed CO_2 generation. But in this section, microbial activity related to metabolic energy should be able to be compared across all scenarios. The simulation equation developed by Kaneko et al. [24], was adopted in this study. Although the study focused on the composting process, it is important to note that biodrying is quite similar, as both rely on aerobic biodegradation. However, since the objective of biodrying is moisture reduction, unlike composting which aims for organic waste stabilization, certain parameters related to the biodegradation process, such as the temperature range for microbial growth and the minimum water activity for microbial growth, were adjusted to reflect the conditions of the biodrying simulation (see also Table 4). The flow of calculation was to calculate the growth rate of microorganisms, then calculated the consumption rate of organic substrates and oxygen. After that metabolic heat was obtained by oxygen consumption. Furthermore, metabolic water was estimated by the consumption rate of organic substrates.

To determine the microbial growth rate ($\Delta X/\Delta t$) affected by temperature ($f(T)$), moisture content ($f(MC)$), oxygen concentration ($f(O_x)$), the amount of organic substrate and microbial mass ($f(S,X)$), it is described by the following equation.

$$\frac{\Delta X}{\Delta t} = \mu_s \cdot f(T) \cdot f(MC) \cdot f(O_2) \cdot f(S,X) \qquad \text{Eq. 3- 44}$$

It is noted that μ_s stands for maximum biomass growth rate with no oxygen and water limitations at the temperature 50 °C (T_S). This constant value is 0.18 h^{-1} [24]. Each factor affecting microbial growth is described in Table 4.

Table 3.4 Details and Description of Factors Affecting Microbial Growth

Factors	Formula and parameters
Temperature ($f(T)$)	$f(T)\begin{cases} \exp\left[\left(\frac{-E_A}{R}\right)\cdot\left(\frac{1}{T_{MSW,cal}+273.15}-\frac{1}{T_S+273.15}\right)\right], if\ T_{MSW,cal} \le T_M \\ \exp\left[\left(\frac{-E_A}{R}\right)\cdot\left(\frac{1}{T_{MSW,cal}+273.15}-\frac{1}{T_S+273.15}\right)\right]\cdot\frac{T_H-T_{MSW,cal}}{T_H-T_M}, if\ T_M < T_{MSW,cal} \le T_H \\ 0, if\ T_{MSW,cal} > T_H \end{cases}$ (Eq. 3- 45) The optimum temperature for microbial growth (T_M) was set to 50 °C, and the maximum temperature for microbial growth (T_H) was set to 70 °C in this calculation. Activation energy in Arrhenius' equation (E_A) = 29,000 J/mol Gas constant (R) = 8.314 J/mol·K

Factors	Formula and parameters
Moisture content ($f(MC)$)	$f(MC)\begin{cases}\frac{(a_w-a_{w0})}{(1-a_{w0})}, if\ w_L < MC \le w_M \\ \frac{(a_w-a_{w0})}{(1-a_{w0})}\cdot\frac{(w_H-MC)}{(w_H-w_M)}, if\ w_M < MC \le w_H \\ 0, if\ MC \le w_L\ or\ MC > w_H\end{cases}$ (Eq. 3- 46) The optimal MC (w_M) for microbial growth was set at 60%, the upper limit (w_H) at 80%, and the lower limit (w_L) was set at 30% in this study. Minimum water activity for microbial growth (a_{w0}) was 0.91 at 30% MC. Water activity (a_w) is closely linked to MC value of MSW and it can be estimated through the following: $a_w = \frac{MC}{((1-K_a)\times MC)+K_a}$ (Eq. 3- 47) Where constant value to convert a_w and MC (K_a) = 0.04
Oxygen concentration ($f(O_x)$),	$f(O_2) = \frac{O_2}{K_O+O_2}$ (Eq. 3- 48) O_2 is oxygen concentration (%) Monod's constant (K_O) = 6%
Organic substrate and microbial mass ($f(S,X)$)	$f(S,X) = \frac{X\times S}{(K_c\cdot X)+S}$ (Eq. 3- 49) Easily biodegradable substrate (S) and microbial biomass (X) are measured in kg. Contois' constant (K_c) = 24

Noted:

1) The minimum water activity (a_{w0}) required for the growth of spoilage bacteria in highly perishable fresh foods is 0.91 [38], which corresponds to a moisture content (MC) of approximately 30%. Additionally, Contreras-Cisneros et al. [13] observed that when the moisture content dropped below 30–35% (corresponding to a_w = 0.90), microbial activity ceased entirely in the biodrying process under greenhouse cover. In contrast, the composting process requires a minimum water activity of 0.94 (40% MC) to sustain microbial activity [24].
2) The S value, used in Eq. 3-49, was considered as the percentage of food waste in the waste composition analysis at the beginning of the experiment together with the initial mass of MSW by truck scale. The initial mass of the substances (kg) was input as the initial value of S at t=0.

After $\Delta X/\Delta t$ had been obtained from Eq. 44, the substrate consumption rate ($\Delta S/\Delta t$) was calculated afterwards by Eq. 50.

$$-\frac{\Delta S}{\Delta t} = \frac{1}{Y_{X/S}} \times \frac{\Delta X}{\Delta t} \quad \text{Eq. 3- 50}$$

To this stage, both metabolic water ($M_{w,bio,simu}$, kg/h) and oxygen consumption rate ($\Delta O_x/\Delta t$) were possible to determine based on the $\Delta S/\Delta t$ value from Eq. 3-50.

$$M_{w,bio,simu} = \frac{\Delta S}{\Delta t} \times \frac{1}{416} \times \frac{46}{4} \times 18 \quad \text{Eq. 3- 51}$$

$$\frac{\Delta O_x}{\Delta t} = R_{O/S} \times \frac{\Delta S}{\Delta t} \times (1 - Y_{X/S}) \quad \text{Eq. 3- 52}$$

The oxygen consumption per substrate consumption catabolically ($R_{O/S}$, kgO/kgS) was estimated to be 1.1. [24]

3.2.6.4 Calculation of Rainwater Entering MSW Pile

In Scenario 3, it was assumed that rainwater entering the MSW pile. The precipitation data was from Bangkok, Thailand during the actual experiment period (7─14 September 2019). Hour-scale rainwater data in Bangkok during this period was based on Global Satellite Mapping of Precipitation (GSMaP) data provided by JAXA [39]. The GSMaP data were from the point closest to the experimental site at 13.75°N latitude and 100.65°E longitude. The hourly rainfall data (PP, mm/h) was used for estimating the among of rainwater entering the MSW pile (M_{rain}, kg/h) by Eq. 3-53. the top surface of MSW (A_{MSW}) was 14 m^2.

$$M_{rain} = PP \times A_{MSW} \qquad \text{Eq. 3- 53}$$

3.2.7 Heating Value Estimation

The biodried waste could potentially be taken into RDF production, so that the potential of heating value after biodrying process should be assessed. In this study, heating value was reported in terms of lower heating value (LHV). Consideration of LHV is needed because it provides a more accurate representation of the energy content available in a fuel. The calculation methods by Chang et al. [40] adopted in this study, as this calculation method provided a consistent initial and final LHV value based on the experiments from the previous study [21]. In addition, the coefficient of multiple determination for this calculation method was 0.975, demonstrating better accuracy compared to conventional models for LHV estimation. The equation for estimating LHV of MSW is shown as follows:

$$LHV = [39.04P_{pa} + 101.47P_{pl} + 38.47P_{fo})] \times \left(\frac{100-MC}{100}\right) - 6MC \qquad \text{Eq. 3- 54}$$

From the above equation, the physical composition of MSW is a crucial parameter for estimating the LHV. In this context, P_{pa} represents the percentage of paper, P_{pl} denotes the percentage of plastic, and P_{fo} is the percentage of food waste. These values were derived from waste composition analysis. The LHV values changed during the biodrying process due to the degradation of food waste, which represents easily biodegradable materials. To determine the mass of degraded food waste (M_{fo}, kg) and its proportion (P_{fo}, %ww.) over time, the equation below can be used.

$$M_{fo}^{t} = M_{fo}^{t-1} - (\Delta S/\Delta t)^{t-1} + (\Delta X/\Delta t)^{t-1} \qquad \text{Eq. 3- 55}$$

$$P_{fo}^{t} = \frac{M_{fo}^{t}}{M_{s}^{t}+M_{w}^{t}} \qquad \text{Eq. 3- 56}$$

3.3 Results and Discussion

3.3.1 Model Reliability

The calculated temperatures of both waste and headspace from the heat balance model were compared with the measured MSW temperature from pilot-scale experiment, and minimum and maximum MSW temperatures were also taken into consideration for model reliability assessment. The heterogeneity of MSW was assumed as a homogeneous object with a certain temperature for simplifying the calculation of the heat balance model. Figure 3.4 Comparisons of Calculated and Measured Temperatures:illustrates comparisons of calculated and measured temperatures.

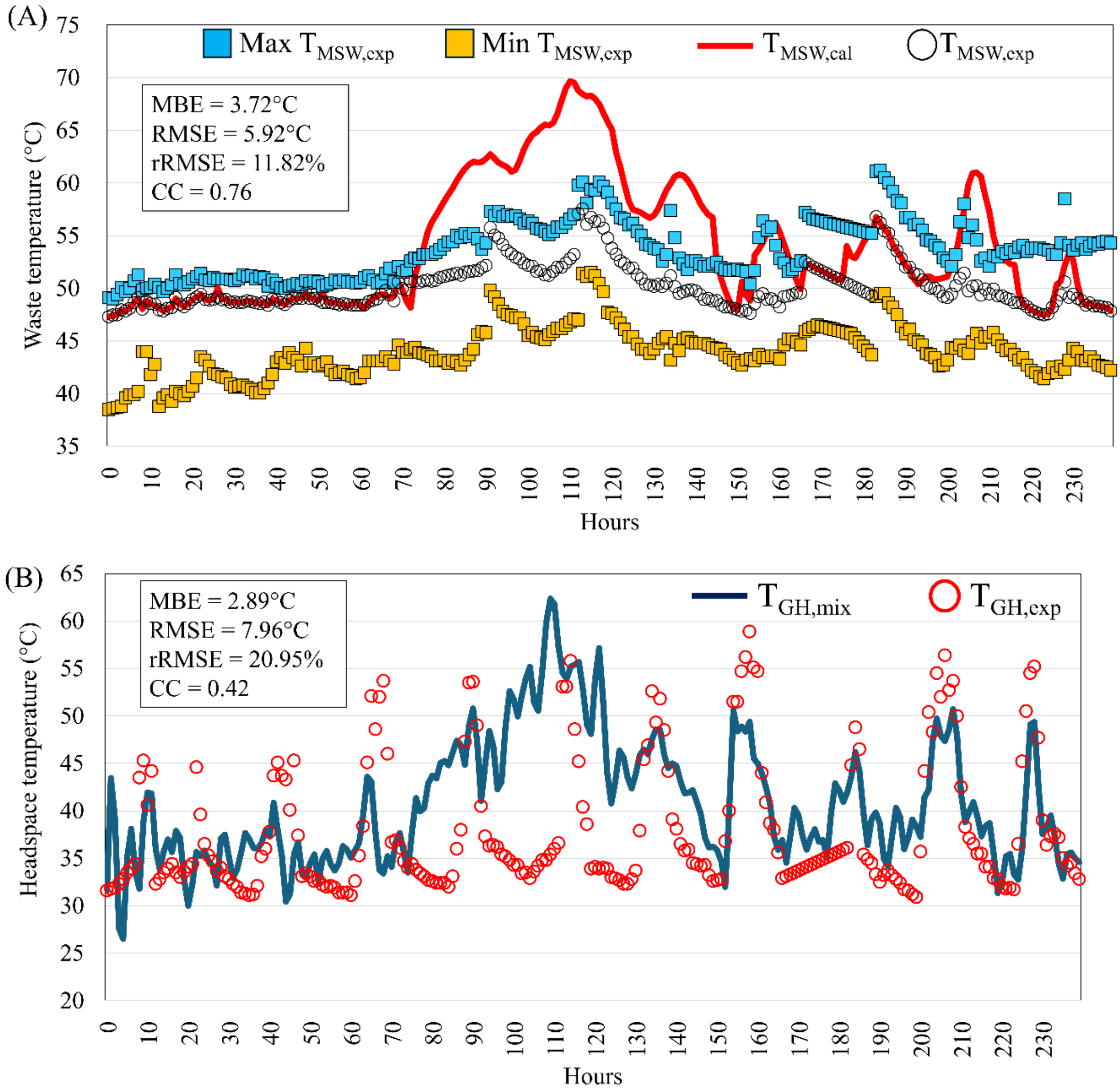

Figure 3.4 Comparisons of Calculated and Measured Temperatures:
(A) Waste temperature from model ($T_{MSW,cal}$) and experiment ($T_{MSW,exp}$)
(B) Headspace temperature from model ($T_{GH,mix}$) and experiment ($T_{GH,exp}$)

Noted: Max $T_{MSW,exp}$ and Min $T_{MSW,exp}$ are maximum and minimum waste temperatures from experimental data.

For the waste temperature, the model's predictions matched the measured temperature values. Based on temperature data points (n=240), $T_{MSW,cal}$ was aligned within the maximum-minimum MSW temperature range of 155 points (accounting for approximately 65% within the range). Moreover, $T_{MSW,cal}$ expressed a similar pattern along with the fluctuation of experimental MSW temperature profile till the end of biodrying process. MBE showed 3.72 °C, indicating that the model performed accurate prediction in waste temperature on average, and RMSE of 5.92 °C fell slightly above the observed standard deviation range of 1.79 °C to 5.48 °C across the eight temperature sensor points, suggesting that the model's error remained within a reasonable margin relative to the actual spatial variability within the waste matrix. The model achieved the CC value of 0.76, indicating a strong positive correlation, and it implied that the model was able to perform a high degree of consistency. The rRMSE was 11.81%, which falls within the generally accepted threshold of 10–20% [19, 41], and this low rRMSE indicated that the model's prediction was able to perform a good agreement between model and experimental temperature data. A recent study on temperature profiling during the aerobic treatment of food waste reported higher rRMSE values under continuous aeration, ranging from 10.82 to 33.85, compared to intermittent aeration, which ranged from 2.61 to 8.63 [19]. This indicates that aeration pattern can significantly influence waste temperature profiling.

A notable temperature difference in the waste was observed between hours 71 to 144. During this period, the CO_2 concentration by volume increased from 0.5% to 1.8%, with values consistently exceeding 1.4%. This elevated CO_2 concentration might have contributed to the enlarged discrepancy between the model and experimental data. Furthermore, the discrepancy between the actual and model's predicted temperatures were due to the heterogeneous properties of MSW, which might hinder the occurrence of peak temperatures during the thermophilic phase of the biodrying process, and the thermosensors could not detect these high temperatures within the heterogeneous texture of MSW. It was suggested that adding more sensors and incorporating more than two layers for waste temperature monitoring could improve the accuracy in obtaining representative waste temperature measurements.

Considering the headspace temperature, the temperature from the model showed fluctuations, but the overall pattern of temperature change was consistent with the actual headspace from the experiment. MBE was 2.89 °C, meaning that the temperature predictions were overestimated but remain close to the experimental headspace temperature values on average. However, the RMSE was 7.96 °C, indicating a relatively large deviation, as evidenced by the notable fluctuations in headspace temperature. It had a CC of 0.42, indicating a moderate consistency between the modeled and experimental headspace temperatures [42], and the high rRMSE of 20.95% further emphasized the limited predictive accuracy of the model in capturing headspace temperature dynamics. It is difficult to establish a high accuracy model for predicting indoor air temperature like the greenhouse headspace temperature, and many studies about indoor air modeling have shown that indoor temperature changes often lag because of external factors, such as weather conditions, as well as system adjustments, including temperature and volume of the supplied air [43].

The final mass from the experiment was 2,990 kg, while the model predicted a final mass of 1,473 kg. The discrepancy was 1,517 kg, which was a relatively large difference considering the nearly three tons of final MSW mass that had processed in the pilot-scale biodrying system. This discrepancy occurred because the model assumed a uniform MSW pile, whereas heterogeneous MSW in actual situation consisted of various materials with different moisture retention abilities. Additionally, actual MSW underwent compaction during the biodrying process, but the model did not account for this factor to simplify calculations. Lastly, non-uniform airflow in the pilot-scale experiment may have led to uneven drying, while the model assumed perfectly distributed aeration. Subsequently, the model assumed perfect water evaporation without accounting for water condensation. Among the factors evaluated in the proposed heat balance model, the relative humidity of the air passing through the MSW pile ($RH_{MSW \rightarrow GH}$) was the most influential factor in the heat balance model. A 20% increase reduced RMSE by 17.87% for waste temperature (See also Appendix A). This could have resulted in an overestimation of water evaporation within the system, while simultaneously reducing the modeling error for waste temperature profiling. Therefore, these limitations of the heat balance model in the pilot-scale experiment indicate the need to address these issues in future improvement of the model for a biodrying process within a greenhouse system.

The model demonstrated reasonable accuracy, with small MBE in waste temperature and MBE in headspace temperature. Also, the CC and rRMSE values for waste temperature indicated good performance in terms of the model's predictive ability. Although the higher RMSE in headspace temperature was due to both internal and external factors, the overall pattern was moderately consistent with the experimental headspace temperature. Therefore, it was reasonable to apply this model setting to describe the biodrying process under the greenhouse system and also to use it for comparison with non-greenhouse biodrying process simulation in order to introduce the merits of the greenhouse application in the next section.

3.3.2 Heat Balance Analysis

This section expresses the overall results from the heat balance models, describing the heat sources in the system, and the heat used for water evaporation as well as the heat losses during the biodrying process of the pilot-scale SGB system. This heat balance model provides an analysis of heat flow within the system, considering all relevant heat transfer components. According to heat balance analysis, each heat element was divided into heat input and heat output. The heat input in this context refers to the heat generation by microbial activity ($Q"_{bio}$) and the heat acquisition from solar energy ($Q"_{SR,ac \rightarrow MSW}$) as well as the heat content of inlet air ($Q"_{air,in}$). It was assumed the heat input would be mostly transformed into heat output, which represented the heat utilization in the biodrying process. Table 3.5 and Table 3.6 indicate a detailed breakdown of the heat balance in the waste pile and greenhouse headspace including overall process, daytime and nighttime periods. In the MSW pile, the majority of the heat input was attributed to metabolic heat at 66% (6,036 MJ), followed by 27% (2,486 MJ) from enthalpy of inlet air. Meanwhile, the heat derived from transmitted solar radiation to the MSW surface accounted for 7% of the total heat input, amounting to 687 MJ. On the heat output side, the largest portion of heat was accounted for by evaporation at 59% (5,444 MJ). In terms of thermal radiation from the top surface of the MSW pile ($Q"_{rad,MSW\rightarrow GH}$ + $Q"_{rad,MSW\rightarrow c2}$ + $Q"_{rad,MSW\rightarrow ac}$), it accounted for 20% (1,800 MJ). Of the total thermal radiation, the MSW surface emitted more radiation towards the acrylic material (8%, 745 MJ) than to the concrete wall (c2) (5%, 419 MJ). It was obvious that the latent heat of evaporation accounted for the majority of heat consumption in the biodrying process, which is a common characteristic of the heat balance in biodrying process. In the study by Yuan et al. [44], they conducted lab-scale MSW biodrying with positive aeration for an 18-day drying process. The latent heat of evaporation accounted for a range of 50.6% to 68%. The proportion of evaporation latent heat in our study was within the range reported in the previously mentioned study. The higher heat loss in the pilot-scale biodrying was probable because the heat losses from the side walls, as well as the heat radiation to structural materials in the calculation of this study, was higher than the heat loss typically observed in small-scale biodrying reactors. In the greenhouse headspace, this heat balance model revealed the role of solar radiation absorption by the air inside the greenhouse ($Q"_{absorb,GH}$). Solar radiation absorbed by the air contributed to maintaining the higher temperature conditions within the greenhouse compared to ambient temperature, and this heat element accounted for 276 MJ, or 4% of the total heat input. The heat output within this system came from heat transfer, with 317 MJ (4%) lost through the concrete material ($Q"_{cov,GH\rightarrow c2\rightarrow am}$) and 1,093 MJ (15%) through the acrylic ($Q"_{cov,GH\rightarrow ac\rightarrow am}$). The largest portion of heat loss, 6,125 MJ (81%), was due to the enthalpy of the exhaust air ($Q"_{air,out}$), which carried away heat from the greenhouse. It was remarkable that the higher enthalpy of the exhaust air compared to the inlet air. The exhaust air is often warmer and more humid due to the heat and moisture extracted from the waste during the biodrying process.

A detailed breakdown of the heat balance during daytime and nighttime was also conducted, and this analysis was different from other studies on the biodrying heat balance analysis. A key factor that contributed to the difference in heat balance between day and night was the availability of transmitted solar energy during the daytime. From the result of the heat balance in the waste pile, it was found that the total heat input was significantly higher at 4,999 MJ during the daytime, primarily due to the addition of transmitted solar radiation (687 MJ), which constituted 14% of the total heat input during daytime. The transmitted solar radiation as the heat source was absent at night, resulting in a total heat input of only 4,210 MJ. Considering the latent heat of evaporation, it was higher during the daytime (2,996 MJ), accounting for 18% more than during nighttime (2,449 MJ). In contrast, the heat consumption related to thermal radiation was slightly higher at night, exceeding daytime by 70 MJ (8%). Overall, during the daytime, the net heat gain exhibited a positive value (+191 MJ), whereas a negative value (-83

MJ) was observed at night. This indicated the advantage of using the greenhouse system in biodrying for heat refilling, as well as enhancing water evaporation during daytime with the availability of solar energy. From the result of the heat balance in the greenhouse headspace, during the daytime, the total heat input was significantly higher, amounting to 4,162 MJ. In contrast, at night, the total heat input decreased to 3,368 MJ. The absence of solar radiation during the night meant that heat input was primarily driven by latent and sensible heat, and it was lower compared to daytime due to the lack of sunlight and reduced evaporation heat. The total heat output remained relatively consistent both day and night. During the daytime, 4,169 MJ of heat was lost, while at night, the heat loss was slightly reduced to 3,365 MJ. The higher heat loss during the daytime can be attributed to increased temperatures and moisture content within the greenhouse headspace, which resulted in greater heat content in the exhaust air.

It was remarkable that there was a minor 1.18% error from the comparison between heat input and output within the waste pile. Concerning the other study that conducted the heat balance analysis of biodrying using a similar calculation method, the error was reported 5% [16]. Hence, this established heat balance model was suitable for comparing different biodrying operation scenarios and indicating the heat utilization within the biodrying under the greenhouse system. Furthermore, when considering the heat balance within the greenhouse headspace, the discrepancy between heat input and output was minimal, with an error margin of only 0.07%.

Table 3.5 Detailed Breakdown of the Heat Balance in the Waste Pile

Heat balance	Heat elements	Overall		Daytime		Nighttime	
		MJ	%	MJ	%	MJ	%
Heat inputs (MJ)	Enthalpy of inlet air ($Q"_{air,in}$)	2,486	27%	1,243	25%	1,244	30%
	Metabolic heat ($Q"_{bio}$)	6,036	66%	3,070	61%	2,967	70%
	Transmitted solar radiation through the acrylic roof to MSW surface ($Q"_{SR,ac\rightarrow MSW}$)	687	7%	687	14%	-	0%
	Total heat input	9,210	100%	4,999	100%	4,210	100%
Heat outputs (MJ)	Sensible heat of the air ($Q"_{a}$)	1,173	13%	595	12%	578	14%
	Latent heat of water evaporation ($Q"_{eva}$)	5,444	59%	2,996	60%	2,449	58%
	Heat radiation from the MSW surface to the greenhouse headspace ($Q"_{rad,MSW\rightarrow GH}$)	636	7%	294	6%	341	8%
	Heat radiation from the MSW surface to the concrete part connected to the greenhouse headspace ($Q"_{rad,MSW\rightarrow c2}$)	419	5%	203	4%	215	5%
	Heat radiation from the MSW surface to acrylic material ($Q"_{rad,MSW\rightarrow ac}$)	745	8%	367	7%	378	9%

Heat balance	Heat elements	Overall		Daytime		Nighttime	
		MJ	%	MJ	%	MJ	%
	Heat transfer through the concrete walls ($Q"_{tran,MSW \rightarrow c1 \rightarrow am}$)	684	7%	352	7%	332	8%
	Total heat output	9,101	98.82%	4,808	96%	4,293	102%
	Heat input-Heat output	108	1.18%	191	4%	-83	-2%

Table 3.6 Detailed Breakdown of the Heat Balance in the Greenhouse Headspace

Heat balance	Heat elements	Overall		Daytime		Nighttime	
		MJ	%	MJ	%	MJ	%
Heat inputs (MJ)	Sensible heat of the air ($Q"_{a}$)	1,173	16%	595	14%	578	17%
	Latent heat of water evaporation ($Q"_{eva}$)	5,444	72%	2996	72%	2,449	73%
	Heat radiation from the MSW surface to the greenhouse headspace ($Q"_{rad,MSW \rightarrow GH}$)	636	8%	294	7%	341	10%
	Solar radiation absorption by the air inside the greenhouse ($Q"_{absorb,GH}$)	276	4%	276	7%	-	0%
	Total heat input	7,529	100%	4,162	100%	3,368	100%
Heat outputs (MJ)	Heat transfer (convection) from greenhouse headspace to outside through the concrete material ($Q"_{cov,GH \rightarrow c2 \rightarrow am}$)	317	4%	178	4%	139	4%
	Heat transfer (convection) from greenhouse headspace to outside through the acrylic ($Q"_{cov,GH \rightarrow ac \rightarrow am}$)	1,093	15%	618	15%	475	14%
	Enthalpy of exhaust air ($Q"_{air,out}$)	6,125	81%	3,373	81%	2,752	82%
	Total heat output	7,535	100%	4,169	100%	3,365	100%
	Heat input-Heat output	-5	-0.07%	-8	-0.19%	2	0.07%

Noted: For Table 3.5 and Table 3.6, the percentages (%) represent the proportion of each heat element relative to the total heat input in the biodrying process.

Table 3.7 presents a comparison of heat balance models, highlighting the performance and advantages of the model developed in this study, compared with a general heat balance model commonly applied in batch biodrying systems. In terms of predictive accuracy for waste temperature, the proposed model exhibited improvements across all statistical indicators. A key strength of the proposed model is its ability to predict headspace temperature, which the general model does not address. Although the correlation for headspace temperature was modest, the inclusion of this parameter is valuable because it influences heat and moisture dynamics within the greenhouse biodrying system. Furthermore, the proposed model incorporated a more comprehensive set of heat sources and radiative heat transfer mechanisms. In contrast to the general model, which considers only metabolic heat, the new model includes the enthalpy of inlet air and transmitted solar radiation through the acrylic roof. These factors are especially important in greenhouse-type systems, where solar radiation and airflow play critical roles in determining thermal behavior. Moreover, the model accounted for the complex thermal interactions within the greenhouse, including radiation from MSW surface to the greenhouse headspace, the concrete structures connected to the headspace, and the acrylic roof. This enhanced the model's realism in the biodrying under the greenhouse system.

Table 3.7 Comparison of Heat Balance Models

Model	Waste temperature				Headspace temperature				Heat inputs in the waste pile	Relative thermal radiation
	RMSE	rRMSE	MBE	CC	RMSE	rRMSE	MBE	CC		
General heat balance model in batch biodrying [8, 15, 16]	7.23	14.41	3.96	0.74	n/a	n/a	n/a	n/a	Metabolic heat	Heat radiation from the waste surface to the environment
Heat balance model in this study	5.92	11.81	3.72	0.76	7.96	20.95	2.89	0.42	1) Enthalpy of inlet air, 2) Metabolic heat, 3) Transmitted solar radiation through the acrylic roof	Heat radiation from the MSW surface to 1) the greenhouse headspace, 2) concrete parts connected to headspace, 3) acrylic roof

Noted:

1) n/a = not available
2) These results were derived by calculating each heat element, followed by using an explicit method to simulate the temperature profile and compared the model results with the experimental data.
3) An rRMSE between 10% and 20% indicates a good fit between the model and experimental data, while values under 10% reflect a highly accurate or excellent match [19].
4) The model is considered a good predictor if the correlation coefficient (CC) is close to or greater than 0.8 [36].

3.3.3 Comparison of Temperature Profile and MC reduction from Process Simulation Data among Three Different Scenarios

The process simulation involved three scenarios, including Scenario 1 utilized forced aeration with a greenhouse cover, Scenario 2 involved forced aeration without a greenhouse cover, and Scenario 3 incorporated forced aeration while considering available precipitation. These scenarios were assumed to operate under the same airflow rate at 0.78 m^3/kg waste/day. The heat balance models in sections 2.4 and 2.6 were applied to simulate the temperature profile and MC reduction trend among three different scenarios. Figure 3.5 presents temperature profiles of the three different scenarios, and Figure 3.6 shows MC reduction trend with the amount of precipitation. The results from biodrying process simulation found that there was significant difference in the MSW temperature change patterns between greenhouse cover and non-greenhouse cover conditions in the first 2 days of the biodrying process. The scenario 1 was able to maintain a higher waste temperature rather than the other scenarios. However, during the latter half of the biodrying process (after the 6th day), the temperature in the MSW began to decline, with varying decrease rates depending on the specific scenario. In Scenario 1, the temperature of the MSW pile in this process simulation remained at approximately 47 °C or higher until the end of the process. Meanwhile, the waste temperature was dropped in the latter half of the biodrying process in Scenario 2. For Scenario 3, The waste temperature rose again due to additional water from rainfall, which increased water activity and reactivated microbial growth in the waste pile. Overall, the temperature of the MSW remained higher during the first two days and after the 6th day in Scenario 1, with moderate fluctuations throughout the biodrying process. In contrast, Scenarios 2 and 3 experienced unstable waste temperatures, showing strong fluctuations influenced by external environmental factors including wind and precipitation.

Considering MC change among three different scenarios, Fig. 6 includes the MC criteria (<30%) line required by user's criteria as cement plant [45]. At the end of the biodrying process, the final MC values were less than 30% for Scenario 1, 56% for Scenario 2, and 64% for Scenario 3, respectively. The decrease in MC in Scenario 1 had potential to reach MC value below 30% within 7 days, compared to Scenario 2, which had potential to reduce MC value below 30% more than 8 days. Meanwhile, Scenario 3, MC change trend increased owing to additional water in the MSW pile from precipitation, and it was unable to reach MC below 30%. Biodrying under the greenhouse system appeared to have a slightly faster reduction in MC in comparison to outdoor conditions. This simulation results were consistent with the experimental study by Robles-Martínez et al. [12], that conducted under both outdoor and greenhouse conditions. Additional evidence that supported these simulation results was found in the study by Sutthasil et al. [46], which examined a full-scale windrow pile MBT system with MSW piles (2–4 m height) and containing 73.93% biodegradable components. After one year, the MC of MSW ranged from 38.93% to 57.41%, compared to an initial MC of approximately 48.94% to 60.17%. In addition, another study by Wangyao et al. [47] investigated a shallow windrow pile MBT system with piles heights of 0.5–1 m. The MC of MSW after 16 months was 42.3%, compared to 77.3% for initial waste (fresh MSW). These findings suggested that achieving a significant reduction in MC required a long processing time in those case studies. Intense precipitation in tropical regions not only delays the drying process but also CH_4 emissions from the waste pile. High CH_4 emissions were observed during periods of heavy rainfall in the initial phase of outdoor biodrying, when the degradable organic carbon content in the waste was still high under a full-scale windrow pile with a passive aeration [46].

Up to this point, it was evident that Scenario 1, within the greenhouse system, demonstrated significant differences in the pattern of MSW temperature changes and MC reduction when compared to non-greenhouse scenarios. However, advantages of the biodrying process under the greenhouse system raises questions about its efficacy in water evaporation and heat transfer within the MSW pile, and the subsequent section about comparative heat balance between greenhouse and non-greenhouse covers will be discussed in order to provide a comprehensive understanding of the biodrying under the greenhouse system.

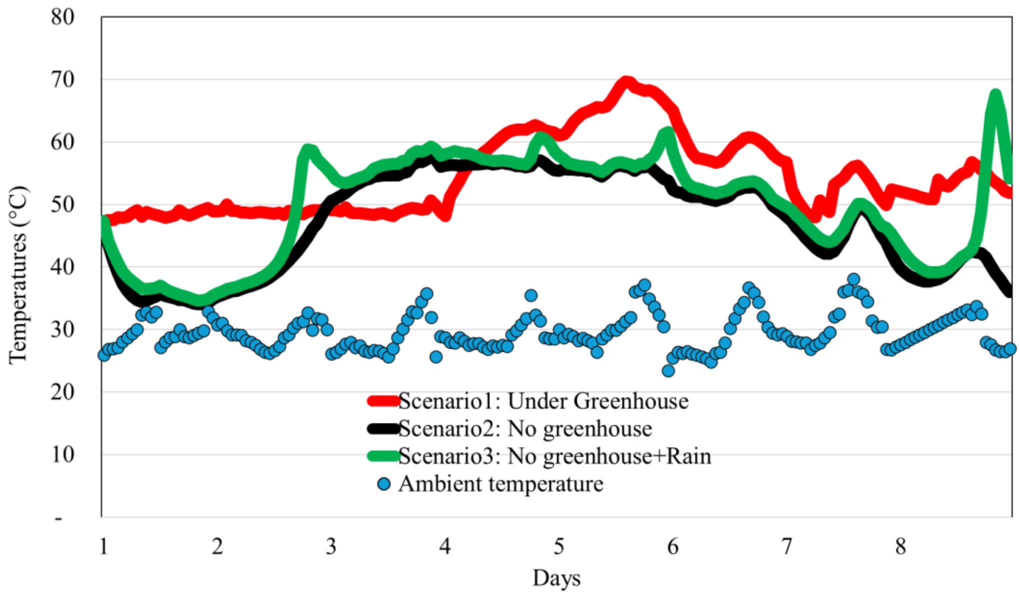

Figure 3.5 Temperature Profiles of the Three Different Scenarios

Noted: The waste temperature profiles of Scenarios 1-3 were represented as the calculated temperatures from the model, while the ambient air temperature was reported from the experiment.

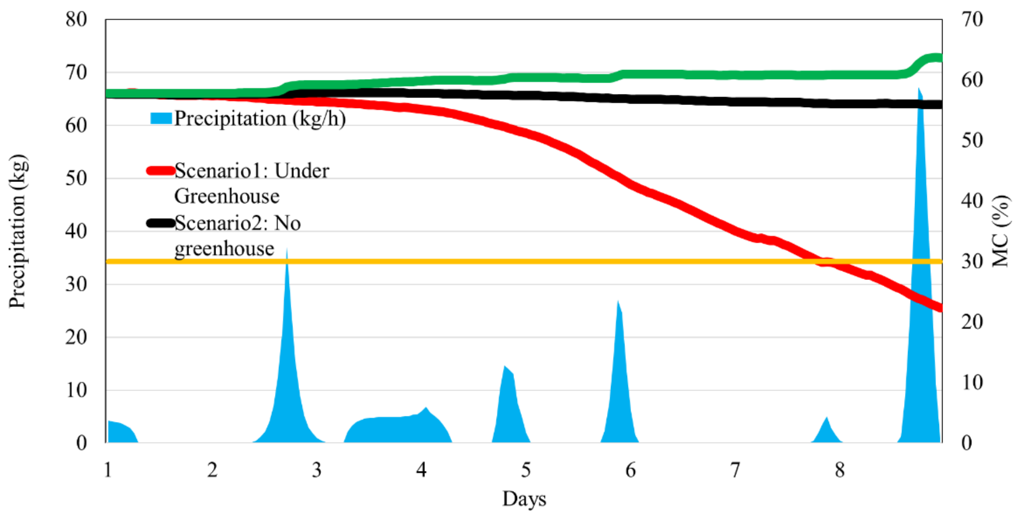

Figure 3.6 MC Reduction Trend with the Amount of Precipitation

3.3.4 Heat Balance Analysis from Process Simulation Data among Three Different Scenarios

According to heat balance analysis from process simulation data, Figure 3.7 shows a comparison of heat consumption among three different scenarios. Over 8-day periods, the sensible heat of the air ($Q"_a$) ranged from 650 to 962 MJ, depending on the specific scenario. Remarkably, Scenario 1 performed the highest latent heat for evaporation ($Q"_{eva}$) with 4,439 MJ. Meanwhile, the proportion of evaporation heat was lowest in Scenario 3 (791 MJ, 6% of total heat consumption), due to the outdoor condition and the influence of precipitation. The exposure to external factors, including rainfall and fluctuating wind speed, contributed to increased moisture retention, thereby reducing the efficiency of heat-driven water evaporation. Additionally, an obvious difference could be found in heat radiation from MSW pile. In Scenario 1, the heat radiation exhibited 1,471 MJ, accounting for 20% of total heat loss, following by 2,609 MJ (21%) in Scenario 2, and 2,899 (23%) in Scenario 3, respectively. Although Scenario 1 involved more heat elements related to thermal radiations ($Q"_{rad,MSW \rightarrow GH}$ $+Q"_{rad,MSW \rightarrow c2}$$+Q"_{rad,MSW \rightarrow ac}$), it did not exceed the heat radiated from the entire surface of the MSW to the environment (as sky temperature) ($Q"_{rad,MSW \rightarrow sky}$) in Scenarios 2 and 3. This was possible because operating biodrying without a greenhouse cover created a greater temperature difference between the waste pile and the surrounding air. These results highlighted the contributions of heat radiation and latent heat for evaporation across the comparative scenarios between greenhouse and non-greenhouse conditions. Within the greenhouse system, there was a higher amount of latent heat for evaporation, accompanied by lower radiative heat loss from the top surface of the MSW to the surrounding air and greenhouse structure material. Thus, this aspect indicated one of the key advantages of conducting the biodrying process within the greenhouse system.

The distinction between greenhouse and outdoor conditions was evident in the presence of heat convection by wind ($Q"_{cov,MSW}$). In Scenarios 2 and 3, there was a notable heat loss due to convection by wind, resulting in 1,925–2,218 MJ of heat loss (16–18% of total heat loss). This highlighted one of the advantages of operating biodrying under a greenhouse system, as it minimized heat loss caused by exposure to wind. The convective heat from the wind was one of the factors contributing to the higher total heat loss or heat consumption in the waste pile in Scenarios 2 and 3 compared to Scenario 1. Moreover, the higher convective heat by wind as well as the higher radiative heat from the MSW surface resulted in a decrease in MSW temperature, leading to a reduction in water evaporation and lower latent heat for evaporation in non-greenhouse conditions. Thus, another benefit of using a greenhouse cover was that it maintained the MSW temperature by protecting it from direct wind and outside environmental conditions.

Regarding the MC change profile (Figure 3.6) in the previous section together with the heat balance analysis, it was evident that, during the rainy season, the MC of MSW under

Scenario 3 significantly increased, reaching a final MC over 60%. This phenomenon has potentially obstructed the drying process. Although Scenario 3 generated greater metabolic heat due to the remaining abundance of moisture in the waste pile by rainfall, there was also a higher amount of heat loss. Therefore, the biodrying under the greenhouse system not only prevented heat loss from convection by wind and minimized heat radiation but also shielded the waste from remoisturization caused by heavy rainfall, while enhancing water evaporation within the waste pile.

While the solar greenhouse biodrying offers several advantages, its practical implementation involves economic and environmental trade-offs should be considered. Based on the bill of quantities (BOQ) and local prices of materials and equipment, the initial investment cost for the greenhouse roof accounted for approximately 26–31% of the total capital cost, while the cost of the aeration system ranged from 4–7%, depending on the scale of the waste treatment facility. Electricity consumption for forced aeration was estimated to represent about 27% of the annual operational cost. However, these expenses may be offset by several benefits, including shorter drying durations, the elimination of leachate treatment costs at the biodrying pretreatment stage, and improved RDF quality. In the previous study, the RDF market value reached approximately 569.43 Baht per ton of MSW, or about 17.11 USD/t MSW (at an exchange rate of 1 USD = 33.27 Baht) [21]. Additionally, implementing biodrying may reduce reliance on imported fossil fuels for use in industrial sectors, such as the cement industry [45]. Therefore, further comprehensive economic assessments of the full-scale biodrying within the greenhouse system as a pretreatment step prior to thermal conversion are recommended to consider for decision-making from multiple perspectives.

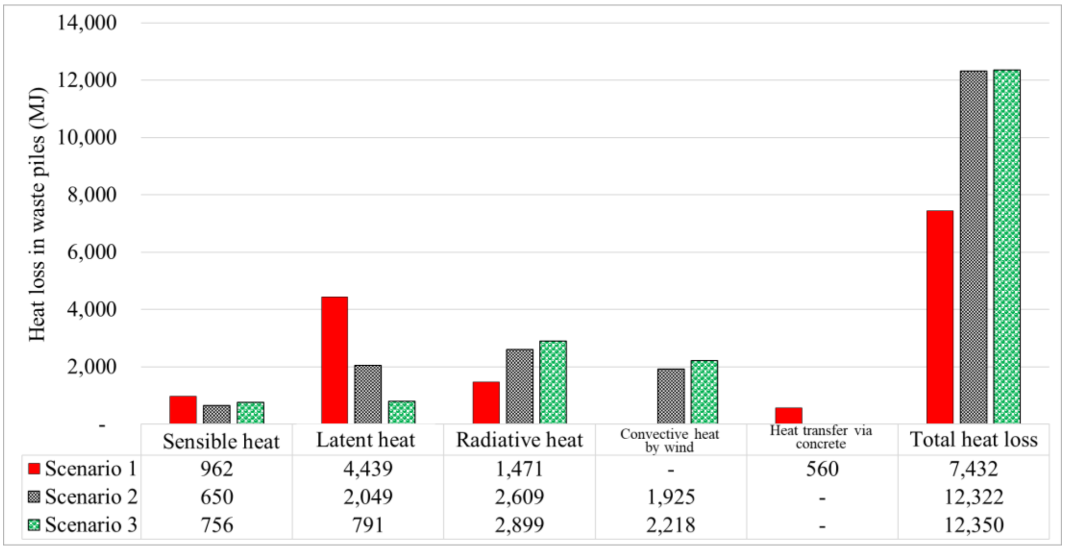

Figure 3.7 Comparison of Heat Consumption among Three Different Scenarios

Noted:

1) In Scenario 1, $Q"_{tranfer}$ refers to heat transfer through the concrete walls ($Q_{tran,MSW\rightarrow c1\rightarrow am}$) in Eq. 3-27

2) $Q"_{rad}$ stands for thermal radiation from MSW surface to greenhouse headspace, concrete, and acrylic cover

($Q_{rad,MSW\to GH}$ +$Q_{rad,MSW\to c2}$+$Q_{rad,MSW\to ac}$) in Eqs. 3-24 to 3-26 for Scenario 1. Meanwhile, $Q"_{rad}$ for Scenarios 2 and 3 refer to heat radiation from the MSW surface to sky ($Q_{rad,MSW\to sky}$) in Eq. 3-41.

3) In this context, total heat consumption refers to heat losses within the waste pile.

3.3.5 Estimation of the LHV in Biodried Waste from Different Scenarios

This section presents and discusses the potential of the biodrying process among different scenarios for upgrading biodried waste quality in terms of the heating content. Figure 3.8 expresses changes in solid mass and LHV across different biodrying process scenarios. In Scenario 1, the solid mass decreased to 1,503 kg, yielding a final LHV at 4,186 kcal/kg. For Scenario 2, the solid mass decreased to 1,140 kg, resulting in a final LHV at 1,286 kcal/kg. Scenarios 2 and 3 showed a similar trend in solid mass decline but yielded significantly different LHV values at the final stage because of remoisturization from rainfall in Scenario 3. Scenario 3 potentially produced biodried waste with the lowest heating value (1,131 kcal/kg), as moisture content was inversely proportional to LHV. As depicted in Figure 3.8, Scenario 1, with a greenhouse cover, retained the highest amount of solid mass, implying lower organic degradation compared to the non-greenhouse condition. According to the primary objective of biodrying, which aims to reduce MC while retaining carbon content, the biodrying process under the greenhouse system in this study demonstrated a key advantage by preserving more of the MSW's energy content within the system. This was achieved by limiting organic degradation, allowing for greater retention of the material's calorific value while also facilitating effective water removal within the system. Nevertheless, further investigation through experiments is important to confirm these findings, as well as to explore the biological effects such as microbial ecosystem within the biodrying under the greenhouse system. Addressing these aspects also contributes to closing the existing research gap in this field.

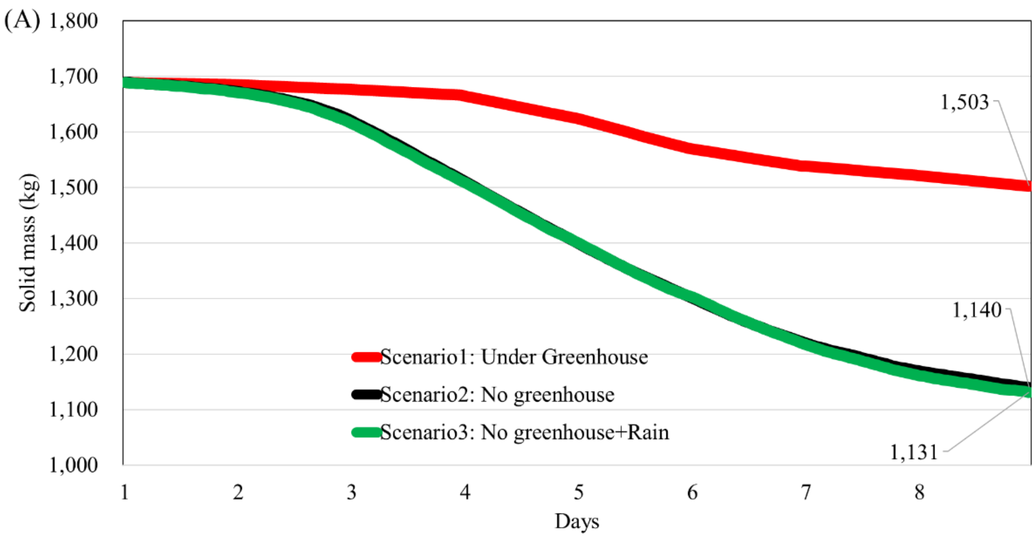

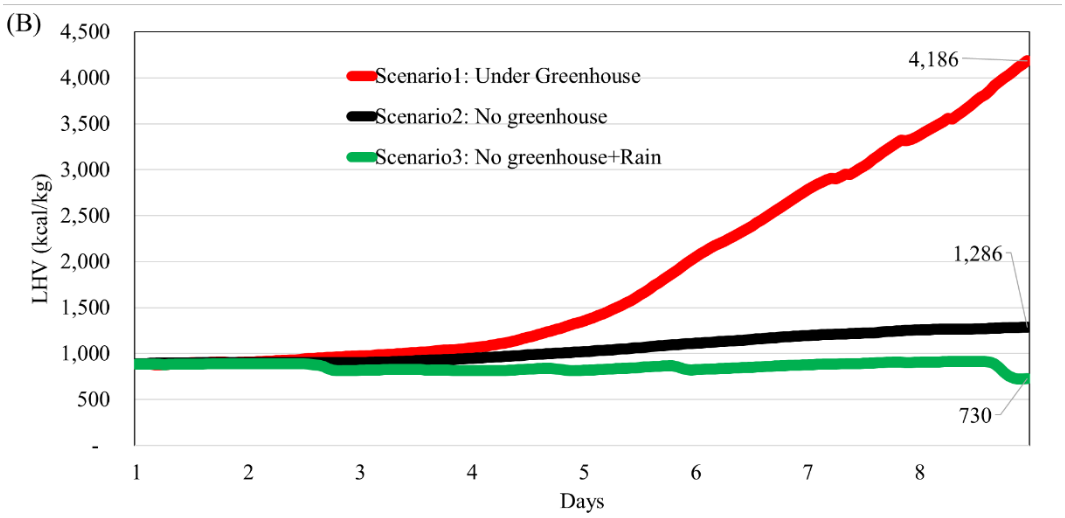

Figure 3.8 Changes in (A) Solid Mass and (B) LHV across Different Biodrying Process Scenarios

3.4. Conclusion

This chapter conducted heat balance analysis in the biodrying within the greenhouse system, aiming to provide a comprehensive understanding of the heat contribution and thermal behavior for this system. A heat balance model was developed to assess the benefits of biodrying within the greenhouse condition. Comparative simulations were performed to contrast biodrying within greenhouse and without greenhouse covers, as well as to mimic environmental conditions in tropical climates with frequent rainfall. The heat balance model developed in this study showed clear advantages over conventional batch biodrying models. It provided higher accuracy in predicting waste temperature, extending the modeling scope to include headspace temperature. These results contribute to the model more suitable for biodrying within the greenhouse system, particularly under tropical climate conditions where solar radiation and temperature of inlet air are critical factors.

This study has achieved its aim by responding comprehensively to the research questions. Key findings are summarized as follows:

The findings revealed that the heat inputs to the waste in the biodrying process within the greenhouse system consisted of metabolic heat (66%), enthalpy of inlet air (27%), and solar radiation (7%). Meanwhile, a significant portion of heat consumption was attributed to latent heat for evaporation (59%). For the greenhouse headspace, heat transfer mainly occurred in the forms of sensible and latent heat to the air inside the greenhouse, accounting for 88% of the total heat input to the headspace. Heat losses occurred through the greenhouse structure (19%) and via the heat content of exhaust air (81%). In this case, solar radiation absorbed by the air inside the greenhouse contributed 4% to the dynamic warming of the greenhouse headspace. The thermal behavior of the solar greenhouse biodrying process exhibited differences between daytime and nighttime. During the daytime, total heat input was significantly higher, primarily due to transmitted solar radiation, which contributed 14% of the total input, equivalent to an additional 687 MJ. The latent heat of evaporation was also higher during the daytime at 2,996 MJ, which was over 18% greater than the nighttime at 2,449 MJ. However, thermal radiation heat loss was slightly higher at night, by 70 MJ (8%).

The application of a greenhouse offers several advantages in the biodrying process. First, it enhanced heat input through transmitted solar radiation, thereby improving water evaporation during the daytime. Second, simulation results showed that the greenhouse system achieved the target moisture content (<30%) within 7 days, demonstrating higher evaporation efficiency due to greater latent heat utilization compared to outdoor biodrying. Third, the greenhouse roof reduced heat loss caused by wind-driven convention and thermal radiation to ambient, effectively acting as an insulating layer over the waste pile. Lastly, it can prevent rainwater intrusion, ensuring satisfactory biodried waste quality and potentially reducing methane emissions, as rainfall decreases void space and promotes anaerobic conditions

The results also offer valuable insights for policymakers, industry stakeholders, and both engineering and operational perspectives. From a policy perspective, while windrow biodrying presents a lower-cost option compared to greenhouse-type biodrying facilities, the latter offers additional benefits such as improved drying efficiency. Therefore, waste management policymakers should consider integrating solar greenhouse biodrying into an appropriate proportion by balancing the use of indoor biodrying systems with outdoor methods to optimize environmental and economic outcomes. For the industrial sector, the improved quality and shorter drying time of RDF produced through the solar greenhouse biodrying system supports the reduction of fossil fuel consumption in energy-intensive industries, such as cement and paper manufacturing, particularly in co-combustion processes. This may contribute to enhanced energy security by decreasing reliance on fossil fuels and reducing production costs. From engineering and operational perspective, understanding the heat transfer mechanisms involved enables the optimization of bioreactor design, site selection, and operational strategies. For example, selecting locations and bunker shapes that maximize solar energy capture, avoiding sites with high wind speeds to minimize convective heat loss, employing cover insulation on a greenhouse roof to reduce thermal radiation losses at night, and balancing aeration rates to maintain heat within the system while ensuring efficient moisture removal can improve overall system performance.

Future research could follow two directions. First, further refinement of the heat balance model is necessary to better account for the heterogeneity of MSW, compaction effects, and non-uniform airflow in the biodrying within the greenhouse system. These aspects will validate the simulation results, enhancing the model's ability to predict the potential biodried products and drying times with greater accuracy. Moreover, simulating biodrying process variations across seasons, while considering factors such as solar irradiance, air humidity, and rainfall frequency in different seasons, holds the potential to establish adaptable operational guidelines for the solar greenhouse biodrying technique. Second, feasibility studies and economic evaluations are needed to support policy decisions and practical adoption of the solar greenhouse biodrying in waste management systems.

References

[1] Asian Development Bank (2020) Waste to energy in the circular economy handbook

[2] Lim W Bin, Yuen E, Bhaskar AR (2019) Waste-to-Energy: Green solutions for emerging markets. In: KPMG International Limited. https://kpmg.com/xx/en/home/insights/2019/10/waste-to-energy-green-solutions-for-emerging-markets.html. Accessed 26 Aug 2024

[3] Sutthasil N, Chiemchaisri C, Chiemchaisri W, et al (2023) Life cycle greenhouse gas emissions of emerging municipal solid waste management options: a case study in Thailand. J Mater Cycles Waste Manag 25:662–673. https://doi.org/10.1007/s10163-022-01584-6

[4] Archer E, Baddeley A, Klein A, et al (2005) Mechanical-Biological Treatment: A guide for decision makers, processes, policies, and markets

[5] National Institute for Environmental Studies (NIES) (2020) Mechanical Biological Treatment (MBT) guideline. Tsukuba

[6] Perazzini H, Freire FB, Freire FB, Freire JT (2016) Thermal treatment of solid wastes using drying technologies: A review. Drying Technology 34:39–52. https://doi.org/10.1080/07373937.2014.995803

[7] Tom AP, Haridas A, Pawels R (2016) Biodrying process efficiency: -Significance of reactor matrix height. Procedia Technology 25:130–137. https://doi.org/10.1016/j.protcy.2016.08.240

[8] He P, Zhao L, Zheng W, et al (2013) Energy balance of a biodrying process for organic wastes of high moisture content: A review. Drying Technology 31:132–145. https://doi.org/10.1080/07373937.2012.693143

[9] Jalil NA, Ahmad IK, Basri H, et al (2022) Biodrying of Municipal Solid Waste: A Case Study in Malaysia. Springer, pp 375–434

[10] Kaza S, Yao LC, Bhada-Tata P, Van Woerden F (2018) What a waste 2.0: A global snapshot of solid waste management to 2050. Washington, DC

[11] Tun MM, Juchelková D (2018) Drying methods for municipal solid waste quality improvement in the developed and developing countries: A review. Environmental Engineering Research 24:529–542. https://doi.org/10.4491/eer.2018.327

[12] Robles-Martínez F, Silva-Rodríguez EM, Espinosa-Solares T, et al (2012) Biodrying under Greenhouse Conditions as Pretreatment for Horticultural Waste. J Environ Prot (Irvine, Calif) 03:298–303. https://doi.org/10.4236/jep.2012.34038

[13] Contreras-Cisneros RM, Orozco-Álvarez C, Piña-Guzmán AB, et al (2021) The Relationship of Moisture and Temperature to the Concentration of O2 and CO2 during

Biodrying in Semi-Static Piles. Processes 9:520. https://doi.org/10.3390/pr9030520
[14] Zawadzka A, Krzystek L, Stolarek P, Ledakowicz S (2010) Biodrying of Organic Fraction of Municipal Solid Wastes. Drying Technology 28:1220–1226. https://doi.org/10.1080/07373937.2010.483034
[15] Yuan J, Zhang D, Li Y, et al (2017) Effects of adding bulking agents on biostabilization and drying of municipal solid waste. Waste Management 62:52–60. https://doi.org/10.1016/j.wasman.2017.02.027
[16] Yu B, Chen T, Zheng G, et al (2022) Water-heat balance characteristics of the sewage sludge bio-drying process in a full-scale bio-drying plant with circulated air. Waste Management 141:220–230. https://doi.org/10.1016/j.wasman.2022.01.041
[17] Hobiny AD, Abbas IA (2021) Finite Element Analysis of Thermal-Diffusions Problem for Unbounded Elastic Medium Containing Spherical Cavity under DPL Model. Mathematics 9:2782. https://doi.org/10.3390/math9212782
[18] Orozco-Álvarez C, Díaz-Megchún J, Osorio-Mirón A, et al (2022) Finite difference modeling of the temperature profile during the biodrying of organic solid waste. Sustainability 14:14705. https://doi.org/10.3390/su142214705
[19] Lai JC, Then YL, Hwang SS, et al (2025) Modelling Temperature Profiles in Food Waste Composting: Monod Kinetics Under Varied Aeration Conditions. Process Integration and Optimization for Sustainability. https://doi.org/10.1007/s41660-024-00480-w
[20] Anantha Kumar K, Sugunamma V, Sandeep N (2020) Effect of thermal radiation on MHD Casson fluid flow over an exponentially stretching curved sheet. J Therm Anal Calorim 140:2377–2385. https://doi.org/10.1007/s10973-019-08977-0
[21] Ngamket K, Wangyao K, Patumsawad S, et al (2021) Quality improvement of mixed MSW drying using a pilot-scale solar greenhouse biodrying system. J Mater Cycles Waste Manag 23:436–448. https://doi.org/10.1007/s10163-020-01152-w
[22] Çengel YA, Boles MA, Kanoğlu M (2019) Thermodynamics: An Engineering Approach, 9th ed. McGraw-Hill Education, New York
[23] Haug RT (1993) The practical handbook of compost engineering. Routledge
[24] Kaneko H, Hirayama K, Fujita K (2001) Simulation of composting reaction. Japan Society of Waste Management Research 12:122–130
[25] Electrical Information (2020) An easy-to-understand explanation of how to calculate the amount of saturated water vapor! In: Electrical Information. https://detail-infomation.com/#google_vignette. Accessed 5 Sep 2024
[26] Hydro-Informatics Institute (HII) (2021) Resource data: Hourly relative humidity data. In: Hydro-Informatics Institute (HII). https://tiservice.hii.or.th/opendata/data_catalog/humidity/2019/201909/. Accessed 27 Aug 2024
[27] Kommareddy AAG (2003) Design and construction of light guides for efficient transfer

of light in to a dense algal culture in a Photo-Bio Reactor (PBR). In: 2003, Las Vegas, NV July 27-30, 2003. American Society of Agricultural and Biological Engineers, St. Joseph, MI
[28] ThermoWorks (2020) Infrared emissivity table. In: ThermoWorks. https://www.thermoworks.com/emissivity-table/. Accessed 26 Aug 2024
[29] Fujita K (1993) Composting technology: Technology for effective use of waste. Gihodo Publishing
[30] Baehr HD, Stephan K (2011) Heat and Mass Transfer, 3rd ed. Springer Berlin Heidelberg, Berlin, Heidelberg
[31] Zhang G, Ding X, Li T, et al (2020) Dynamic energy balance model of a glass greenhouse: An experimental validation and solar energy analysis. Energy 198:. https://doi.org/10.1016/j.energy.2020.117281
[32] Weather Spark (2019) Suvarnabhumi International Airport in Thailand climate history for September 2019. In: Weather Spark. https://ja.weatherspark.com. Accessed 27 Aug 2024
[33] Thermtest Incorporated (2024) Materials thermal properties database. In: Thermtest Inc. https://thermtest.com/thermal-resources/materials-database. Accessed 13 Sep 2024
[34] Mirsadeghi M, Cóstola D, Blocken B, Hensen JLM (2013) Review of external convective heat transfer coefficient models in building energy simulation programs: Implementation and uncertainty. Appl Therm Eng 56:134–151
[35] Khalil SA, Shaffie AM (2013) A comparative study of total, direct and diffuse solar irradiance by using different models on horizontal and inclined surfaces for Cairo, Egypt. Renewable and Sustainable Energy Reviews 27:853–863. https://doi.org/10.1016/j.rser.2013.06.038
[36] Huiliñir C, Pérez J (2017) A new model of batch biodrying of sewage sludge, Part 2: Model calibration and validation. Drying Technology 35:666–679. https://doi.org/10.1080/07373937.2016.1206124
[37] Tanaka S, Takeda J, Iwata T, et al (2015) Latest Architectural Environmental Engineering, 4th ed. Inoue Shoin, Tokyo
[38] Majumdar A, Pradhan N, Sadasivan J, et al (2018) Food Degradation and Foodborne Diseases: A Microbial Approach. In: Microbial Contamination and Food Degradation. Elsevier, pp 109–148
[39] Japan Aerospace Exploration Agency (JAXA) (2024) World rainfall distribution bulletin. In: Japan Aerospace Exploration Agency (JAXA). https://sharaku.eorc.jaxa.jp/GSMaP/index_j.htm. Accessed 27 Aug 2024
[40] Chang YF, Lin CJ, Chyan JM, et al (2007) Multiple regression models for the lower heating value of municipal solid waste in Taiwan. J Environ Manage 85:891–899. https://doi.org/10.1016/j.jenvman.2006.10.025
[41] Despotovic M, Nedic V, Despotovic D, Cvetanovic S (2016) Evaluation of empirical

models for predicting monthly mean horizontal diffuse solar radiation. Renewable and Sustainable Energy Reviews 56:246–260. https://doi.org/10.1016/j.rser.2015.11.058
[42] Schober P, Boer C, Schwarte LA (2018) Correlation Coefficients: Appropriate Use and Interpretation. Anesth Analg 126:1763–1768. https://doi.org/10.1213/ANE.0000000000002864
[43] Li X, Han Z, Zhao T, et al (2021) Modeling for indoor temperature prediction based on time-delay and Elman neural network in air conditioning system. Journal of Building Engineering 33:101854. https://doi.org/10.1016/j.jobe.2020.101854
[44] Yuan J, Zhang D, Li Y, et al (2018) Effects of the aeration pattern, aeration rate, and turning frequency on municipal solid waste biodrying performance. J Environ Manage 218:416–424. https://doi.org/10.1016/j.jenvman.2018.04.089
[45] Itsarathorn T, Towprayoon S, Chiemchaisri C, et al (2022) The situation of RDF utilization in the cement industry in Thailand. In: 2022 International Conference and Utility Exhibition on Energy, Environment and Climate Change (ICUE). IEEE, pp 1–7
[46] Sutthasil N, Chiemchaisri C, Chiemchaisri W, et al (2020) Greenhouse gas emission from windrow pile for mechanical biological treatment of municipal solid wastes in tropical climate. J Mater Cycles Waste Manag 22:383–395. https://doi.org/10.1007/s10163-020-00999-3
[47] Wangyao K, Sutthasil N, Chiemchaisri C (2021) Methane and nitrous oxide emissions from shallow windrow piles for biostabilisation of municipal solid waste. J Air Waste Manage Assoc 71:650–660. https://doi.org/10.1080/10962247.2021.1880498

Chapter 4

Experimental Study of Different Aeration Patterns in the Solar Greenhouse Biodrying under Various External Environmental Conditions

Graphical Abstract for Chapter 4

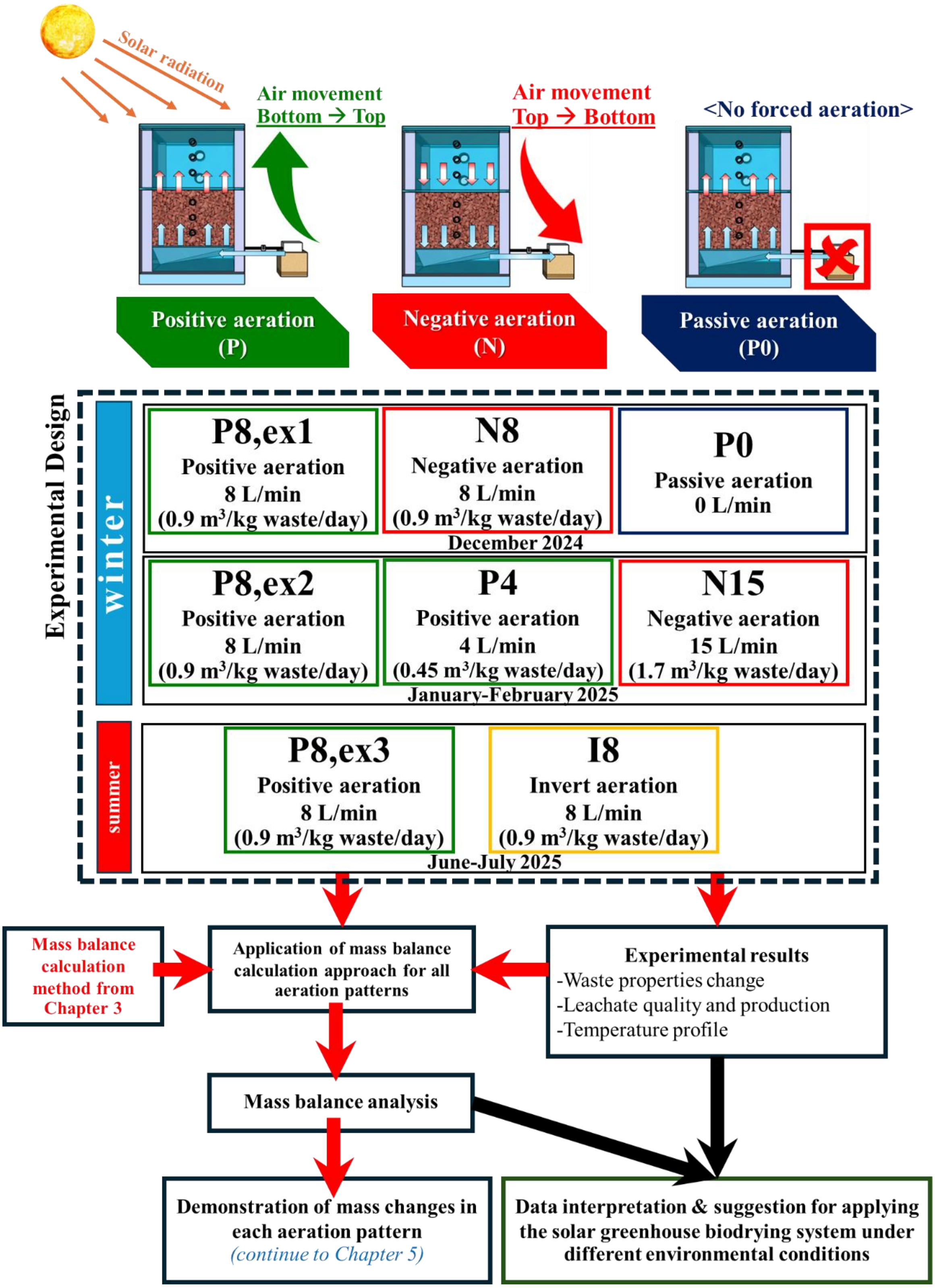

4.1. Introduction

Landfills are the most widely used waste disposal methods worldwide. From the literature, it was shown that majority of the countries have adopted landfilling as waste management systems [1]. In middle-income countries, around 18% to 54% of waste was managed through landfills, while 30% to 60% was disposed of in open dumps [2]. Siddiqua et al. [1] conducted a desk review methodology from 42 articles and found that landfilling causes environmental pollution, including groundwater contamination from leachate, air pollution from suspended particles, odor from municipal solid waste (MSW), and marine pollution from runoff. Additionally, people may confront potential health risks from polluted water and gas emissions, including carcinogenic effects and other illnesses.

Furthermore, organic waste within MSW often contains high levels of moisture content (MC), causing challenges for waste management practices. Siddiqua et al. [1] reported that food waste and organic fines contributed approximately 70–80% of moisture within MSW in summer and autumn, and around 50–60% in winter and spring. High MC in MSW increases the weight of waste, leading to higher transportation costs and reduced efficiency of separation process. Also, it could reduce the recycling rate of recoverable materials, cause operational instability in Waste-to-Energy (WtE) facilities, and increase combustion costs [3]. High moisture levels could reduce the calorific value of MSW, which is critical for energy recovery processes like incineration, and drying waste could increase its calorific value significantly, enhancing its suitability for energy generation [4].

Mechanical Biological Treatment (MBT) offers a potential solution to enhance recycling efficiency, reduce dependence on landfilling, and mitigate its negative impacts. MBT involves a combination of mechanical processes (such as crushing, densification, magnetic separation, and separation by size or density) and biological treatments (via aerobic or anaerobic degradation) (Edo-Alcón et al., 2024; NIES, 2020). MBT also allows for resource recovery, such as Refuse-derived fuel (RDF) production or metal recovery from sorting machines. Biodrying, a form of aerobic decomposition, is optional to be employed in MBT facilities to reduce moisture and partially stabilize MSW [7]. Since the MC in MSW is inversely proportional to its heating value, a lower MC results in a higher heating value of the waste. The basic principle in biodrying is the utilization of metabolic energy from microbial activity to degrade the organic waste and this process is assisted by aeration [8]. Biodrying differs from composting in that it focuses on drying and preserving most of the biomass or solid content within the waste, rather than achieving full waste stabilization [7]. Therefore, biodrying technology offers several benefits, such as reducing waste moisture and volume, lowering transportation costs, improving separation efficiency, and supporting energy and resource recovery.

Biodrying within a greenhouse system can allow solar energy to assist the drying process, thereby reducing the reliance on metabolic heat from biodegradation for moisture reduction.

According to the study Robles-Martínez et al. [9], biodrying in a greenhouse system have two main heat sources for evaporation, including the heat capture from solar thermal energy by the greenhouse cladding and the metabolic heat from biodegradation, resulting in acceleration of MC reduction in the waste. The study by Colomer-Mendoza et al. [10] demonstrated that the covered greenhouse trial provided lower MC in the final product compared to uncovered one. MC decreased by 82% in the biodrying in the greenhouse system, and by 48% in the non-greenhouse biodrying. Moreover, biodrying within a greenhouse system has the potential to reduce MC in organic solid waste with an initially high moisture level. According to the study by Contreras-Cisneros et al. [11], biodrying within a greenhouse system, using passive aeration and turning every seven days, reduced the moisture content of organic waste (including orange peel, mulch, and carrot bagasse from agro-industry) from 75% to 14.4% within 46 days. The solar thermal energy plays an important role in warming up the air inside the greenhouse as call as the headspace temperature. Evidence from Ngamket et al. [12] indicated a positive correlation between solar radiation intensity and the daily average headspace temperature, with r values ranging from 0.56 to 0.79, depending on operational conditions. This suggested that biodrying in a greenhouse system can enhance the air's water-holding capacity.

Given that air movement is still essential for reducing the weight of MSW and its MC, the aeration system is an indispensable component of the biodrying process, whether it operates in conventional biodrying systems or solar greenhouse biodrying systems [8, 12]. Aeration is a critical parameter in the biodrying process. The important roles of aeration in biodrying, as summarized from Xu et al. [13], are as follows: 1) It enhances microbial activity by providing the necessary oxygen for their metabolism, promoting the degradation of organic materials. 2) Aeration improves moisture reduction by enhancing water evaporation and dispersion, facilitating dewatering. 3) Suitable air supply promotes effective heat transfer, ensuring uniform temperature distribution. Although high aeration rates can enhance the moisture removal, it may concurrently elevate heat loss within the biodrying system, potentially limiting the overall effectiveness of biodrying. [14]. Therefore, achieving a balance between aeration for water removal and the waste pile's self-heating ability remains crucial for optimizing the biodrying process.

From literature, positive aeration (forced aeration) and passive aeration (no forced aeration) had been conducted in biodrying in the greenhouse system [9–12, 15]. An alternative air supply method, such as air suction or negative aeration, needs further investigation in the case of the biodrying process under a greenhouse system. In terms of positive aeration, this method refers to air blowing upward through waste materials, while negative aeration involves drawing air down through waste materials. Each method haves both advantages and disadvantages. Previous research indicated that negative aeration resulted in a higher ratio of water loss to volatile solids (VS) loss compared to positive aeration [16]. This could be possible because of a greater VS degradation in the biodrying with positive aeration. Additionally, the study by Tom et al. [17] observed heterogeneous moisture distribution from biodrying with positive aeration method, and this was because the condensation of evaporated water within the reactor occurred. Up to this point, there is interest in integrating negative aeration into biodrying in the greenhouse system to assess its impact on the biodrying performance, temperature distribution within the waste pile, and the quality attributes of the biodried product. Furthermore, a comprehensive comparison of biodrying under the greenhouse system with different aeration patterns should be conducted to fully understand their effects on moisture reduction during the biodrying process in a greenhouse system. It is important to note that the term of aeration pattern in this context refers to both the aeration direction and the airflow rate used in the operational settings of the biodrying process. Therefore, the primary goal of this study is to conduct a comprehensive comparison of biodrying under the greenhouse system with different aeration patterns. Additionally, the impact of external factors, such as ambient temperature and solar radiation intensity, will be observed in this experimental study. This study explores the impact of different aeration patterns on the solar greenhouse biodrying process through three primary research questions. First, how varying aeration patterns lead to distinct temperature profiles and mass changes within the waste materials during biodrying. Second, how seasonal variations in weather conditions (external environmental factors) affect the biodrying process within a greenhouse system. By addressing these questions, this study enhances the understanding of aeration strategies in solar greenhouse biodrying and contributes to the optimization of biodrying systems for improved waste management efficiency. This comparative investigation of biodrying under greenhouse conditions with varying aeration patterns represents a novel contribution to the field of biodrying technology.

4.2 Materials and Methods

4.2.1 Preparation of Waste Materials

The synthetic waste composition used in this study was designed to simulate typical organic-rich waste. The materials were selected based on their availability and representativeness of the organic waste materials. This synthetic waste consisted predominantly of organic materials, with cabbage, bananas and white bread making up the largest portions at approximately 27%, 25–26%, and 5% by wet weight, respectively. These were supplemented with paper (13%) and sawdust (21%) to represent slowly degradable materials, along with a smaller fraction of plastics in the form of polystyrene (PS) resin (8%) as a non-degradable component. All materials were manually mixed to achieve a homogeneous texture prior to characterization and the biodrying experiment. The total waste mass per reactor was maintained at approximately 13.03±0.31 kg, and the initial bulk density was recorded as 271.46 ± 6.41 kg/m³. The initial MC was found to be 62.28 ± 2.55% (wet basis). The volatile solids (VS) content, measured on a dry weight basis, was 91.28 ± 5.75%. Additionally, the details of each waste material are provided in Appendix B.

4.2.2 Reactor Configuration and Related Equipment

The reactor used in this study was designed in a rectangular cuboid shape, with dimensions of 52 × 52 × 77 cm (width × depth × height). The main body was constructed from acrylic material and insulated on all sidewalls using 5 cm-thick foam panels to minimize heat loss. On the right side of the reactor, four circular channels (5 cm inner diameter) were installed. The lower two were designated for waste sampling, while the upper channel served as a ventilation outlet. The left side of the reactor featured six smaller channels (2.5 cm inner diameter) intended for the insertion of thermos-sensors. These channels were sealed with silicone corks to prevent heat loss, except for the upper-right channel, which functioned as the ventilation outlet and remained open during the biodrying operation.

Internally, each reactor was divided into three functional sections. The bottom section was used for leachate collection and air supply or exhaust, depending on the aeration pattern. For positive aeration, air entered through the bottom section via an air pump. Meanwhile, for negative aeration pattern, it functioned as the outlet air passing from the waste. The middle section, used for loading the waste material, was separated from the bottom part by a stainless-steel porous plate with pores of 2 mm in diameter. This plate facilitated airflow through the waste and simultaneously provided structural support for the waste layer. The top section, called the headspace, played a crucial role in absorbing incoming solar radiation and capturing moisture evaporated from the waste matrix. The top of the reactor was made of transparent acrylic to allow solar energy penetration.

Thermo-sensors were installed at three vertical positions within the waste pile (bottom, middle, and top layers) to monitor temperature distribution. Additional sensors were placed on the reactor's sidewall, top surface, within the headspace. Also, temperatures were measured in the headspace within the reactor and surrounding air outside the reactor. All temperature measurements were conducted using Type-K thermocouples, connected to a data logger (Graphtec GL240, Japan) for continuous monitoring.

The experimental setup also included a digital balance (Ohaus D3000 Series, Japan) to monitor weight changes, and an air supply system connected to the back of each reactor using silicone tubing. A flow meter was installed to regulate the aeration rate, and air was supplied using an air pump (YP-40VC module, Japan). In the case of negative aeration, a water trap was placed between the flow meter and the air outlet channel to prevent moisture intrusion to the air pump.

Three identical greenhouse reactors were placed inside the horticulture building at Hokkaido University's farm. To maintain a warmer environment during the winter experimental period (December 2024 to February 2025), the building was equipped with a heater. A detailed schematic of the reactor configuration and associated equipment is presented in Figure 4.1.

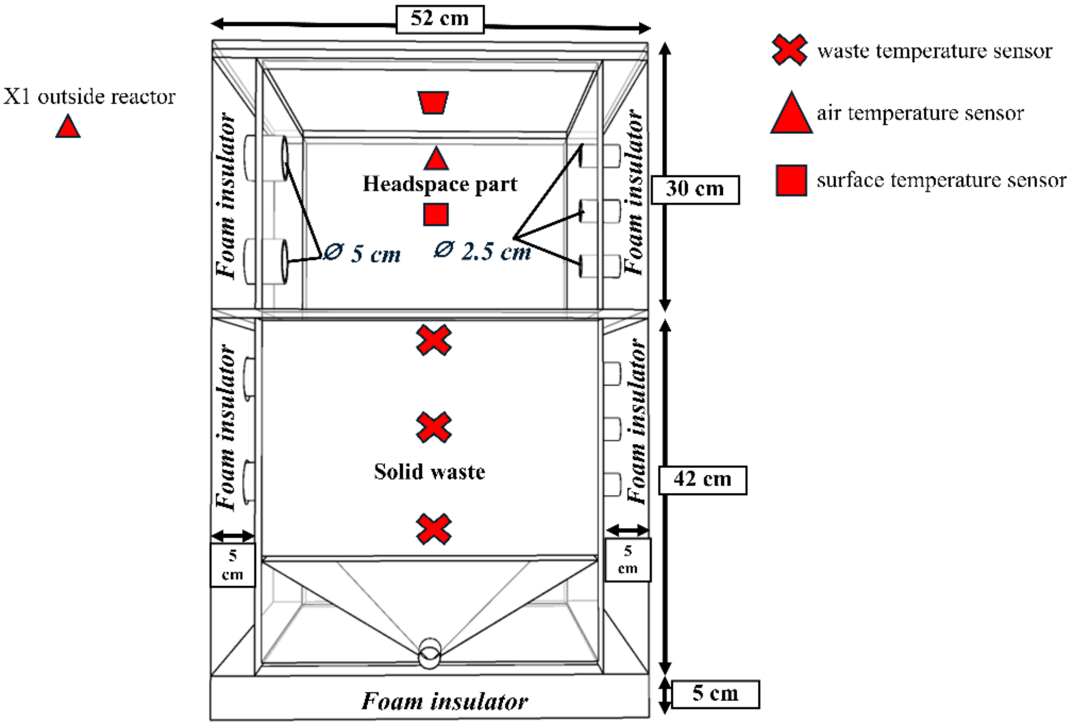
52 cm
waste temperature sensor
air temperature sensor
surface temperature sensor
X1 outside reactor
Foam insulator
Foam insulator
Headspace part
Ø 5 cm
Ø 2.5 cm
30 cm
Foam insulator
Foam insulator
Solid waste
42 cm
5 cm
5 cm
Foam insulator
5 cm

(A)

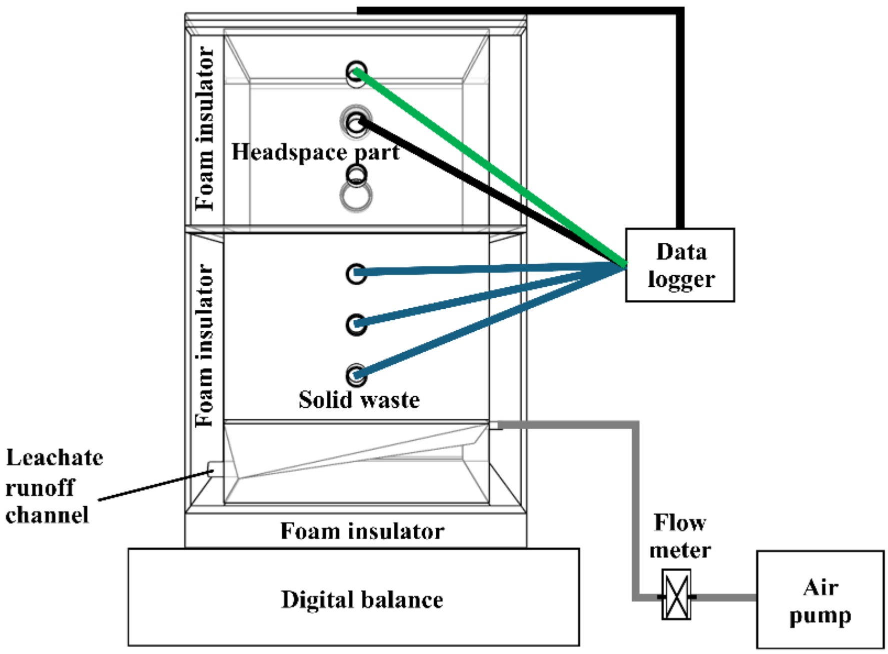
Foam insulator
Headspace part
Foam insulator
Solid waste
Data logger
Leachate runoff channel
Foam insulator
Flow meter
Digital balance
Air pump

(B)

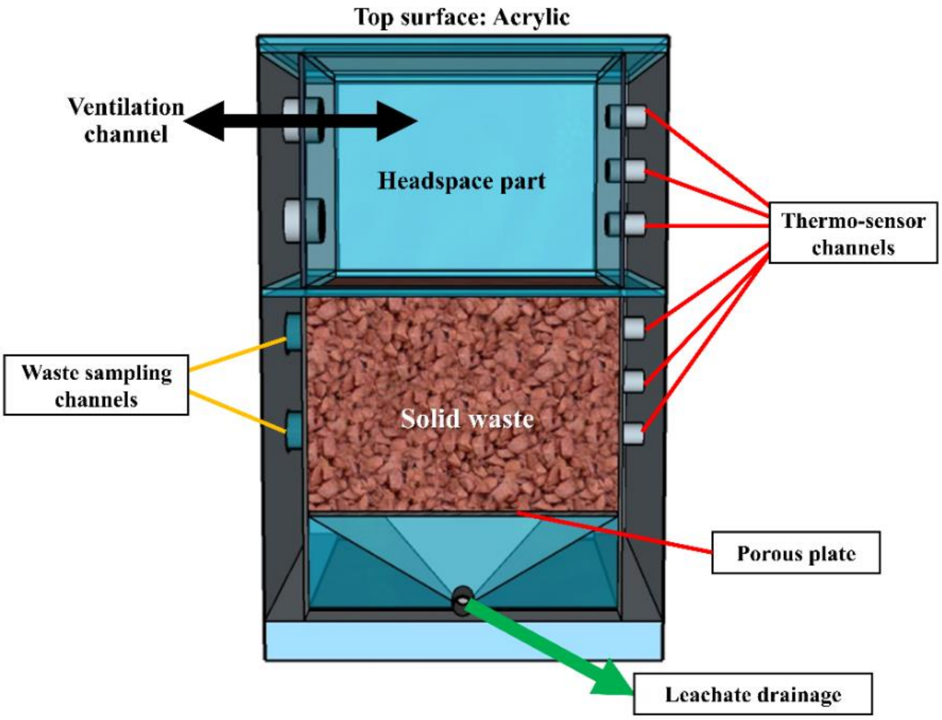

(C)

Figure 4.1 Reactor Configuration

(A) Thermo-sensor insertion points, (B) Reactor and associated equipment setup, (C) Reactor components

4.2.3 Experimental design

This experimental design was performed to investigate the effects of aeration patterns, aeration rates, and experimental period on temperature profiles, mass changes, and biodrying performance. A total of 8 trial conditions were conducted, as summarized in Table 4. 1. The nomenclature for the trial names is as follows: “P” indicates positive aeration, “N” indicates negative aeration, and “P0” refers to passive aeration (i.e., no forced aeration). The number following the letter denotes the airflow rate in liters per minute (L/min). For example, P8 refers to positive aeration at 8 L/min, while N15 indicates negative aeration at 15 L/min. To examine the effect of aeration pattern, three trials (P8,ex1; N8; and P0) were conducted during the same period (11–25 December 2024). The effect of airflow rate was assessed by comparing four trials (P8,ex2; P4; N8; and N15) with varying airflow rates. P8,ex3 and I8 were also conducted in summer to observe the season effect and the potential of inverted aeration application. Additionally, to assess the impact of different experimental periods, ‘P8,ex1’, ‘P8, ex2’, and ‘P8,ex3’ were conducted with the same aeration conditions at 8 L/min. This approach enabled the evaluation of external environmental influences such as solar radiation intensity, relative humidity of surrounding air, and ambient temperature on the biodrying process.

Table 4.1 Summary of Experimental Design and Comparison Objectives

Trial names	P8,ex1	N8	P0	P8,ex2	P4	N15	P8,ex3	I8
Initial moisture content (%MC, wet basis)	57.82±7.6%			64.69±1.16%			64.04±0.45%	
Initial volatile solid (%VS, dry basis)	97.13±0.87%			85.58±0.79%			81.75±0.04%	
Initial mass (kg)	12.52	13.46	13.35	12.97	12.94	12.94	12.92	13.07
Bulk density (kg/m3)	260.83	280.42	278.13	270.21	269.58	269.58	269.23	272.29
Airflow rate (L/min)	8	8	0	8	4	15	8	8
Airflow rate (m3/kg waste/day)	0.9	0.9	0	0.9	0.45	1.7	0.9	0.9
Experimental periods (date)	11-25 Dec 2024			18 Jan-1 Feb 2025			27 Jun-11 July 2025	

4.2.4 Parameter monitoring

During the biodrying experiment, physical, chemical, and environmental parameters were monitored to evaluate the performance and dynamics of the biodrying process within the greenhouse system. Table 4. 2 summarizes the measured parameters, the tools and methods used for each parameter, and their respective sampling or monitoring schedules. Key waste characteristics such as MC and VS were periodically analyzed to track the drying efficiency and organic matter reduction. Environmental conditions including temperatures, relative humidity, and solar radiation were continuously monitored to assess their influence on the biodrying process.

Table 4.2 Summary of Parameters, Measurement Methods, and Sampling Schedule During the Biodrying Experiment

Parameters	Measurement tools and methods	Day of Sampling or monitoring
Moisture content (MC)	The samples were dried in an oven at 105 °C.	Day 0, 5, 10, 15
Volatile solid (VS)	The dried samples were combusted in a muffle furnace at 600 ± 50 °C for a duration of 6 hours	Day 0, 5, 10, 15
Oxygen (O_2)	Gas samples were collected from the headspace every 8 to 12 hours, and analyzed by Gas chromatography (Shimadzu GC-8A, Japan)	Daily
Weight (Mass loss)	Digital Weighing Balance (Ohaus D3000 Series, Japan)	Daily
Temperatures (waste, headspace, materials, air outside the reactor)	Real-time temperature data were recorded by a data logger (Graphtec GL240, Japan) at hourly intervals.	Daily
Relative humidity (RH) of both inlet and outlet air	This parameter was measured using a temperature and humidity data logger (Ondotori TR-72nw, Japan). For the inlet air, measurements were recorded every hour, while the %RH in the headspace was measured every 8 to 12 hours throughout the experiment.	Daily
Radiation intensity	Method 1: To obtain the daily solar radiation intensity	Daily

Parameters	Measurement tools and methods	Day of Sampling or monitoring
	profile, actual measurements taken at the experimental site using a lux meter (LX1330B, China) were compared with simulated data from the EnergyPlus program. A daily correction factor was then applied accordingly. The conversion factor used was 0.00862 $W \cdot m^{-2}/lx$ (modified from 1 W/m^2 = 116 lx), as suggested by Michael et al. [18]. Method 2: Measured by a pyranometer (ML-01, Japan)	
pH	pH was measured using Laqua Horiba (model D-200-2, Japan)	Daily
Total organic carbon (TOC)	TOC was analyzed using TOC-L Series analyzer (Shimadzu, Japan).	Daily

4.2.5 Mass balance calculation

4.2.5.1 Solid mass

In this study, the solid mass balance during biodrying is determined by tracking the (1) initial solid input, (2) microbial biomass generation, (3) organic solid degradation, and (4) the quantity of solid mass retained at the end of the biodrying process. In this section, the calculation of the solid mass balance within the biodrying system under greenhouse conditions is described in a step-by-step manner.

The calculation of initial solid input ($M_{S,0}$, kg) was based on the initial wet mass (M_i, kg) and the percentage of total solids ($\%TS$) measured at the beginning of the experiment.

$$M_{S,0} = M_i \times \%TS \qquad \text{Eq. 4- 1}$$

Microbial biomass growth in this study was determined based on the aerobic biomass growth was modeled using a Monod-type model, incorporating explicit dependencies on waste temperature, moisture content (MC), oxygen concentration, and the availability of biodegradable substrates. The calculation approach developed by Kaneko et al. [19] and Ngamket et al. [20] were adopted and appropriately adjusted the set of equations based on the observed results from this experiment. Eq. 4-2 represents the amount of microbial biomass growth rate.

$$R_{MG} = \mu_s \cdot exp\left[\left(\frac{-E_A}{R}\right) \cdot \left(\frac{1}{T_{SW}+273.15} - \frac{1}{323.15}\right)\right] \cdot f(MC) \cdot \left(\frac{O_2}{K_O+O_2}\right) \cdot \left(\frac{X \cdot S}{(K_C \cdot X)+S}\right) \qquad \text{Eq. 4- 2}$$

Where R_{MG} is microbial growth rate (kg/h), μ_s is specific maximum growth rate constant (h^{-1}), E_A refers to activation energy in Arrhenius' equation (29,000 J/mol), R is gas constant (8.314 J/mol.K), T_{SW} is the average solid waste temperature (°C), O_2 denotes the oxygen concentration (%vol.), K_O is Monod's constant (6%), X and S stands for biodegradable substrate (kg) and microbial biomass (kg), respectively. The determination of biodegradable substrate relies on the properties of each material and its biodegradation fraction, and the details are provided in the supplementary data. K_c is Contois' constant (24, dimensionless). Meanwhile, $f(MC)$, as a function of MC affecting microbial growth, can be determined by Eq. 4-3, as shown below.

$$f(MC)\begin{cases}\frac{(a_w-a_{w0})}{(1-a_{w0})} & ; if\ 30\% < MC \leq 60\% \\ \frac{(a_w-a_{w0})}{(1-a_{w0})}\cdot\frac{(w_H-MC)}{(w_H-w_M)} & ; if\ 60\% < MC \leq 80\% \\ 0 & ; if\ MC \leq 30\%\ or\ MC > 80\%\end{cases} \quad \text{Eq. 4- 3}$$

From Eq. 4-3, a_w is water activity value, estimated by Eq. 4-4. a_{w0} refers to minimum water activity for microbial growth (0.91, dimensionless). This is because the minimum water activity (a_w) required for the growth of spoilage bacteria in highly perishable fresh foods is 0.91[21], which corresponds to approximately 30% MC. In this study, the optimal moisture content (w_M) for microbial growth was set at 60%, with an upper limit (w_H) of 80% MC and a lower limit of 30% MC.

$$a_w = \frac{MC}{((1-K_a)\times MC)+K_a} \quad \text{Eq. 4- 4}$$

Where K_a is constant value to convert a_w and water content (0.04, dimensionless).

Therefore, from Eq. 4-2, the total amount of aerobic biomass growth (M_{MG}, kg) during the biodrying process can be quantified by Eq. 4-5. It is noted that n = 349 represents the total number of monitoring hours during the biodrying experiment.

$$M_{MG} = \sum_{i=1}^{n=349} R_{MG,i} \quad \text{Eq. 4- 5}$$

Organic solid degradation was estimated, regarding microbial growth. The rate of organic substrate degradation (R_{OS}, kg/h) and the total amount of organic degradation (M_{OS}: kg) are described as follows:

$$R_{OS} = \frac{R_{MG}}{Y_{X/S}} \quad \text{Eq. 4- 6}$$

$M_{OS} = \sum_{i=1}^{n=349} R_{S,i}$ Eq. 4- 7

Where $Y_{X/S}$ is microbial yield (0.2 $kg_{substrate}/kg_{microbial\ mass}$) from the study by Kaneko et al. [19]. The total quantity of solid mass retained at the end of the biodrying process ($M_{S,f}$, kg) is calculated using Eq. 4-8.

$M_{S,f} = M_{S,0} + M_{MG} - M_{OS}$ Eq. 4- 8

4.2.5.2 Water mass

For the water balance calculation, this study considered changes in water mass by tracing (1) the initial water content, (2) metabolic water, (3) moisture from inlet air, and water loss in both (4) vapor and (5) liquid forms. In case of the liquid form, water loss may occur as (5a) leachate or (5b) condensate, depending on the specific operational conditions.

(1) The initial water content ($M_{W,0}$: kg) in the synthetic waste was quantified by the initial wet mass and the percentage of MC measured at the beginning of the experiment.

$M_{W,0} = M_i \times \%MC$ Eq. 4- 9

(2) The amount of water produced from aerobic microbial activity was estimated based on the stoichiometric reaction of food waste undergoing aerobic degradation. The reason for this assumption is based on the biodegradation behavior of various organic wastes. Food waste is predominantly composed of fruit and vegetable residues, which typically degrade within 5 to 30 days or more than that, depending on the waste characteristics and the types of biodegradation system [22]. Moreover, the moisture content and biodegradable fraction of the mixture were dependent on banana, cabbage, and white bread. Hence, in this study, the organic substrate as food waste was assumed to have the chemical composition $C_{18}H_{26}O_{10}N$, with a molecular weight of 416, as proposed by Haug [23]. This reaction is shown in Eq. 10. Using this approach, the total quantity of generated metabolic water (M_{MW}: kg) can be calculated using Eq. 4-11.

$4C_{18}H_{26}O_{10}N + 75O_2 = 72CO_2 + 46H_2O + 4NH_3$ Eq. 4- 10

$M_{MW} = M_{OS} \times \left(\frac{4}{72}\right) \times \left(\frac{416}{1000}\right)$ Eq. 4- 11

(3) Moisture input via inlet air ($M_{W,in}$: kg) and (4) moisture output as water vapor (M_V: kg) via outlet air were quantified using airflow rates and observed relative humidity (%RH) values from both the interior and exterior of the reactors. Since three aeration patterns were

performed (including positive aeration, negative aeration, and passive aeration), the calculation methods differed for each condition. Table 4. 3 outlines the specific calculation approaches corresponding to each operational aeration pattern. Furthermore, in the case of passive aeration pattern, the buoyancy-driven airflow was applied to estimate the volume of air movement through the waste pile. In general, the buoyancy-driven airflow, commonly referred to as the normal stack effect or chimney effect, occurs when the indoor air temperature is slightly higher than that of the outdoors, resulting in upward air movement within a building [24, 25]. In contrast, when outdoor temperatures exceed indoor levels, a downward airflow can be observed, known as the reverse stack effect [25]. Accordingly, the estimation of inlet and outlet air volumes in the passive aeration pattern was based on the computational approaches described by Andersen [24] and Zhang et al. [25].

Table 4.3 Calculation Approaches Corresponding to Each Operational Aeration Pattern

Moisture inputs via inlet air ($M_{W,in}$)	
Positive aeration	$AH_{in} = 217 \times \left(\frac{6.1078 \times 10^{\frac{7.5 \times T_{inlet}}{T_{inlet}+237.3}}}{T_{inlet}+273.15} \right) \times \left(\frac{\%RH_{in}}{100} \right)$ Eq. 4- 12 $M_{W,in} = \sum_{i=1}^{n=349} \frac{AH_{in,i} \times q_{in}}{1000}$ Eq. 4- 13 Where: AH_{in} is absolute humidity of inlet air at the bottom part of the reactor (g/m^3) T_{inlet} is temperature of inlet air (°C) $\%RH_{in}$ is relative humidity of inlet air (%) q_{in} is the volume of inlet air (m^3/h). q_{in} is 0.24 m^3/h for P4, and 0.48 m^3/h for P8, respectively
Negative aeration	$AH_{in} = 217 \times \left(\frac{6.1078 \times 10^{\frac{7.5 \times T_{HS}}{T_{HS}+237.3}}}{T_{HS}+273.15} \right) \times \left(\frac{\%RH_{HS}}{100} \right)$ Eq. 4- 14 Where: T_{HS} is headspace temperature (°C) $\%RH_{HS}$ is relative humidity of headspace (%) After that, the quantity of moisture from inlet air entering the waste ($M_{W,in}$) is calculated by Eq. 4-13. q_{in} is 0.48 m^3/h for N8, and 0.90 m^3/h for N15, respectively
Passive aeration	$q_{in} \begin{cases} 3600 \cdot C_d \cdot A_v \left(\frac{2gH_2 \cdot (T_{OR} - T_{HS})}{T_{OR}} \right)^{\frac{1}{2}} ; if\ T_{HS} < T_{OR}\ (reverse\ stack\ effect) \\ q_{out,n} \times \frac{T_{OR} + 273.15}{T_{HS} + 273.15} ; if\ T_{HS} > T_{OR}\ (normal\ stack\ effect) \end{cases}$ Eq. 4- 15 $AH_{in} = 217 \times \left(\frac{6.1078 \times 10^{\frac{7.5 \times T_{OR}}{T_{OR}+237.3}}}{T_{OR}+273.15} \right) \times \left(\frac{\%RH_{in}}{100} \right)$ Eq. 4- 16 In this case, q_{in} can be quantified by two conditions (normal and reverse stack effects) Where: C_d is the discharge coefficient (0.02, dimensionless) A_v is cross sectional area of ventilation channel (0.00196 m^2) T_{OR} is temperature outside a reactor (°C) g is gravity acceleration (9.81 m/s^2) H_2 refers to vertical distance from neutral plane to ventilation channel (m)

	$q_{out,n}$ is the volume of outlet air by normal stack effects (m^3/h) (see also Eq.4-23) Thereafter, the moisture from the inlet air ($M_{W,in}$) is determined based on Eq. 4-13.
Water vapor from outlet air (M_V: kg)	
Positive aeration	$q_{out} = q_{in} \times \frac{T_{HS}+273.15}{T_{inlet}+273.15}$ Eq. 4- 17 $AH_{out} = 217 \times \left(\frac{6.1078 \times 10^{\frac{7.5 \times T_{HS}}{T_{HS}+237.3}}}{T_{HS}+273.15} \right) \times \left(\frac{\%RH_{HS}}{100} \right)$ Eq. 4- 18 $M_V = \sum_{i=1}^{n=349} \frac{AH_{out,i} \times q_{out}}{1000}$ Eq. 4- 19 Where: q_{out} is the volume of outlet air (m^3/h) AH_{out} denotes the absolute humidity of outlet air (g/m^3)
Negative aeration	$q_{out} = q_{in} \times \frac{T_B+273.15}{T_{HS}+273.15}$ Eq. 4- 20 $AH_{sat} = 217 \times \left(\frac{6.1078 \times 10^{\frac{7.5 \times T_B}{T_B+237.3}}}{T_B+273.15} \right) \times \left(\frac{\%RH_{sat}}{100} \right)$ Eq. 4- 21 $M_V = \sum_{i=1}^{n=349} \frac{AH_{sat,i} \times q_{out}}{1000}$ Eq. 4- 22 Where: T_B is the temperature (°C) at the bottom part of the reactor operating under negative aeration. AH_{sat} is absolute humidity of saturated air (g/m^3) $\%RH_{sat}$ is saturated relative humidity (%)
Passive aeration	$q_{out,n} = 3600 \cdot C_d \cdot A_v \left(\frac{2gH_2 \cdot (T_{HS}-T_{OR})}{T_{OR}} \right)^{\frac{1}{2}}; if\ T_{HS} > T_{OR}$ Eq. 4- 23 $M_V = \sum_{i=1}^{n=349} \frac{AH_{out,i} \times q_{out,n}}{1000}$ Eq. 4- 24 if $T_{HS} < T_{OR}$, the outlet air flowed downward (reverse stack effect) and the humid air accumulated in the leachate. To calculate AH_{out} in this case, Eq. 4-18 can be used.

(5) The amount of water lost as (5a) leachate (M_L: kg) and (5b) condensate (M_C: kg) was tracked by the data collection from the experiment.

Thus, the total quantity of water mass retained at the end of the biodrying process in each aeration pattern ($M_{W,f}$: kg) is calculated using Eq. 4-25.

$$M_{W,f} = M_{W,0} + M_{MW} + M_{W,in} - M_V - M_L - M_C \quad \text{Eq. 4- 25}$$

4.2.6 Statistical analysis

Statistical analysis was conducted to examine whether temperature differences among waste layers were statistically significant. As the temperature data did not conform to a normal distribution, the Kruskal–Wallis test was applied in this case. This non-parametric test is appropriate for comparing multiple groups without assuming normality. Subsequently, Dunn's post hoc test was used to further investigate which pairs of waste layers differed significantly (e.g., bottom & middle layers of the waste matrix). The analyses and interpretations were carried out using Statistic Kingdom platform [26] as a reference and calculation tool.

4.3. Results and Discussion

4.3.1 Temperature Profiles

Aeration patterns and environmental factors influenced both the evolution and vertical distribution of temperature across the bottom, middle, and top layers of the waste matrix. This section discusses how aeration patterns, airflow rates, and experimental periods (in relation with external environmental factors) affect the temperature profile under each condition.

Beginning with the effect of aeration patterns, its role in shaping temperature gradients within the waste matrix was explored (see also Figure 4.2 (A)–(C)). In the positive aeration pattern (P8,ex1), a distinct upward temperature gradient was observed, with typical waste temperatures increasing from 9.6 °C at the bottom layer to 13.7 °C in the middle and reaching 16.7 °C at the top, and all layer comparisons were statistically significant ($p < 0.01$), reflecting a strong vertical temperature gradient, where heat accumulation was most intense in the upper layer of the waste. The upward direction of airflow facilitated the movement of heat toward the top of the waste, causing the uppermost section to retain more heat. Additionally, this heat retention was further supported by direct solar radiation in this zone.

Meanwhile, the negative aeration (N8) showed typical waste temperatures in the bottom and middle layers were relatively similar, measured at 23.6 °C and 24.3 °C, respectively, while the top layer was slightly warmer at 20.6 °C. There was no significant difference between the bottom and middle layers ($p = 0.43$), suggesting that heat was more evenly distributed in the lower section of the reactor, due to the downward air movement. However, significant differences ($p < 0.01$) were still observed in the middle and top layers, indicating that some degree of thermal stratification had remained.

For passive aeration (P0), the middle layer exhibited the highest waste temperature at 18.0 °C in the middle layer, compared to 15.5 °C at the bottom and 16.3 °C at the top. There was not statistically significant ($p = 0.08$) between bottom and top layers. This result indicated that, in passive aeration, heat tended to build up in the center of the waste pile, due to limited convective movement and insulation from both the top and bottom.

The airflow rate plays a significant role in influencing the temperature change and distribution within the waste layers during the biodrying process within the greenhouse-type reactor. According to Figure 4.2 (D) and (E), the waste temperature under positive aeration at a lower rate of 4 L/min or 0.45 m^3/kg waste/day (P4) was consistently higher compared to that of 8 L/min or 0.9 m^3/kg waste/day (P8,ex2), with averages of 26.65 °C at the bottom, 29.50 °C at the middle, and 27.50 °C at the top. Also, statistical analysis (post-hoc Dunn's test) indicated no significant difference between the bottom and top layers ($p = 0.39$), and it was remarkable that the temperature evolution pattern observed in P4 resembled that of P0. This result indicated that a lower airflow rate could reduce excessive convective heat loss, allowing more accumulation of metabolic and solar energy within the system. In contrast, the higher airflow rate (P8,ex2) led to greater heat loss, especially in the bottom layer, while simultaneously facilitating the removal of a larger volume of moist air, which will be discussed in the next section.

On the other hand, negative aeration at 15 L/min or 1.7 m^3/kg waste/day (N15) resulted in higher temperatures, averaging 33.5 °C in the bottom layer and 34.8 °C in the middle layer, with a non-significant difference between layers ($p = 0.10$), compared to the lower negative aeration rate of 8 L/min or 0.9 m^3/kg waste/day (N8), which exhibited lower temperatures. This result indicated that the increased downward airflow enhanced heat retention in the waste pile, likely due to the movement of moist and warm air from the headspace of the reactor, which helped to limit heat loss. Remarkably, increasing the airflow rate under negative aeration led to a different temperature profile compared to positive aeration. Nevertheless, it was noted that N8 and N15 were conducted in different months; therefore, environmental factors such as solar radiation intensity and surrounding air temperature were different, contributing concurrently to the variation in waste temperature evolution. The effects of different environmental factors will be discussed in the following section.

The different temperature profiles, observed between the two experimental periods in December 2024 (P8,ex1; Figure 4.2 (A)) and January 2025 (P8,ex2; Figure 4.2 (D)), were primarily attributed to variations in ambient air temperature and solar radiation intensity, which directly influenced the surrounding air temperature within the experimental site. Figures 4.3 and 4.4 illustrate the comparison of typical solar radiation intensity in the experimental site and ambient temperature between all experiments, respectively. In January 2025, solar radiation intensity was higher compared to December 2024, leading to more heat being absorbed by the greenhouse-type reactor. Higher solar radiation resulted in higher temperatures within the waste pile, especially in the middle and top layers, as the greenhouse trapped more thermal energy. Additionally, the surrounding air temperature (the air outside the reactors) in January 2025 was notably higher (an average of 9.29 °C) compared to December 2024 (21.43 °C). The higher surrounding air temperature in January reduced the temperature gradient between the horticulture building and the outside environment, thereby decreasing convective heat loss during biodrying process. As expected, the waste temperature in P8,ex2 was higher, owing to the higher heat content carried by the warmer inlet air. This highlighted the significant role of environmental factors, such as ambient temperature and solar radiation, in affecting the temperature profiles within the waste pile and biodrying process, which will be discussed in the next section. A clear differentiation in the temperature profiles was also observed when comparing P8,ex1 with P8,ex3, and P8,ex2 with P8,ex3.

For P8,ex3, temperature stratification was observed. The bottom layer remained cooler (34.80 °C), while the middle and top layers reached higher temperatures (38.80 and 39.40 °C, respectively). Pairwise comparisons confirmed significant temperature differences between the bottom–middle and bottom–top layers (both $p < 0.01$), whereas middle–top showed no significant difference ($p = 0.7367$). This suggests that although air was forced upward, heat accumulation converged in the upper layers during summer, creating thermal homogeneity between the middle and top regions. This differs from typical results in other seasonal conditions where positive aeration commonly causes three-layer stratification in the waste pile. The reduction in thermal gradient between the middle and top layers is likely due to elevated surrounding air temperatures during summer (an average of 28.20), which may enhance heat retention within the waste pile, ultimately reducing vertical heat loss to the atmosphere.

Meanwhile, inverted aeration (I8) produced a different temperature profile. While overall temperature differences among layers remained significant ($p < 0.01$), Dunn's test indicated that the middle layer was statistically equivalent to the bottom layer ($p = 0.9851$; non-significant difference). Accordingly, temperature distribution remained more different between the bottom and middle layers (33.80 and 37.00 °C), while the top remained relatively cooler (35.30 °C) compared to the middle layer. Remarkably, the temperature profile of I8 exhibited a unique pattern, which can be attributed to the benefit of negative aeration during the initial stage, allowing the waste temperature to reach approximately 60 °C. After day 5, the temperature profile appeared to become similar to the pattern observed under positive aeration trails.

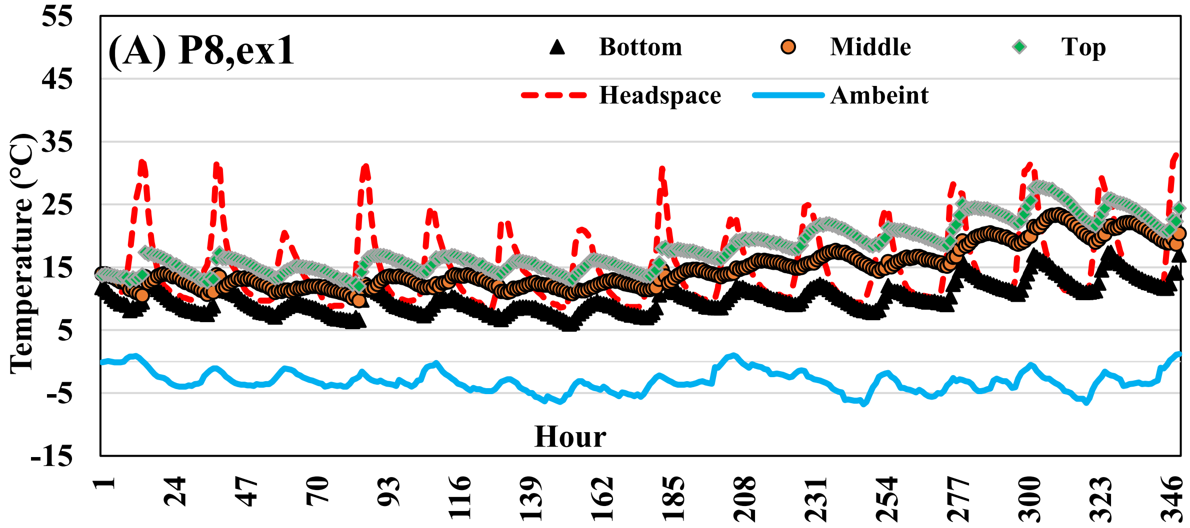

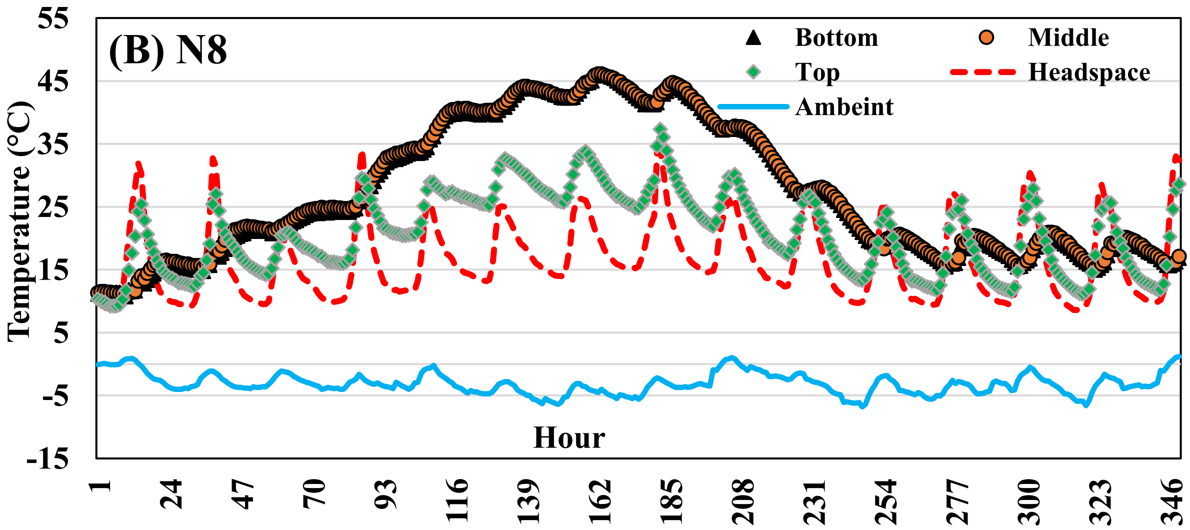

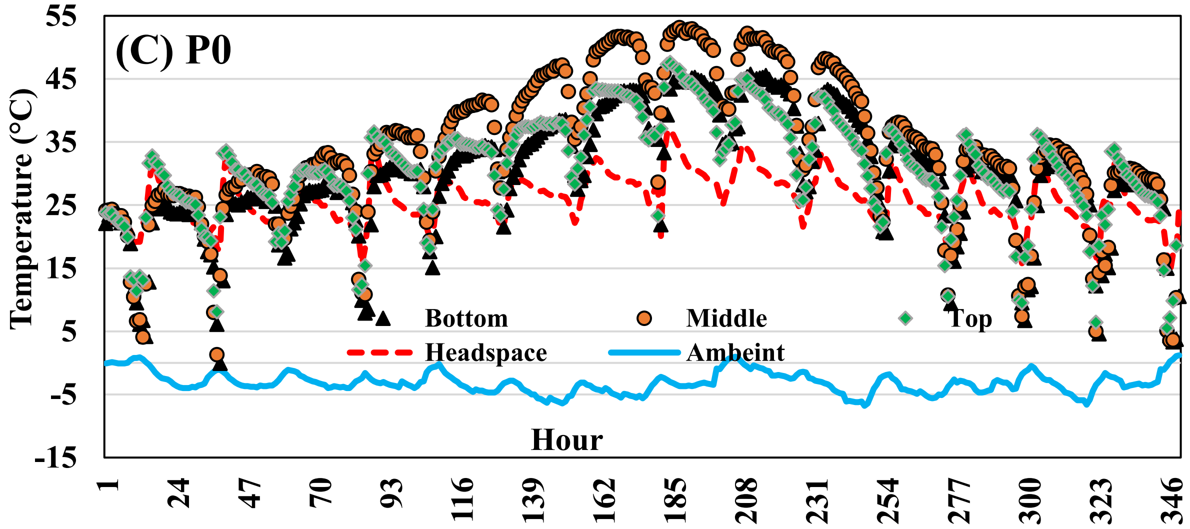
(C) P0
Temperature (°C)
55
45
35
25
15
5
-5
-15
Bottom
Middle
Top
Headspace
Ambeint
Hour
1
24
47
70
93
116
139
162
185
208
231
254
277
300
323
346

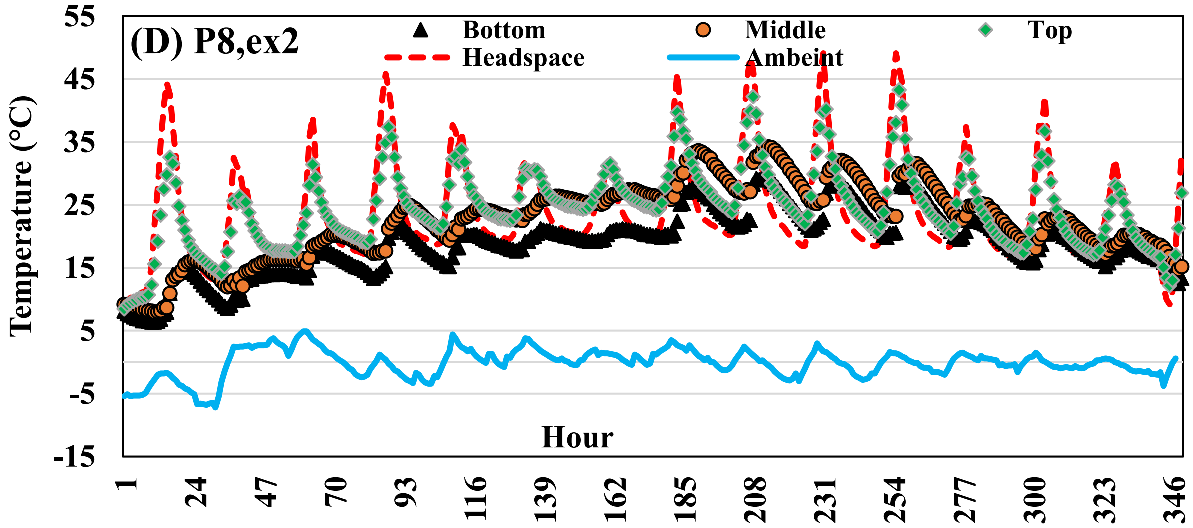
(D) P8,ex2
Temperature (°C)
55
45
35
25
15
5
-5
-15
Bottom
Middle
Top
Headspace
Ambeint
Hour
1
24
47
70
93
116
139
162
185
208
231
254
277
300
323
346

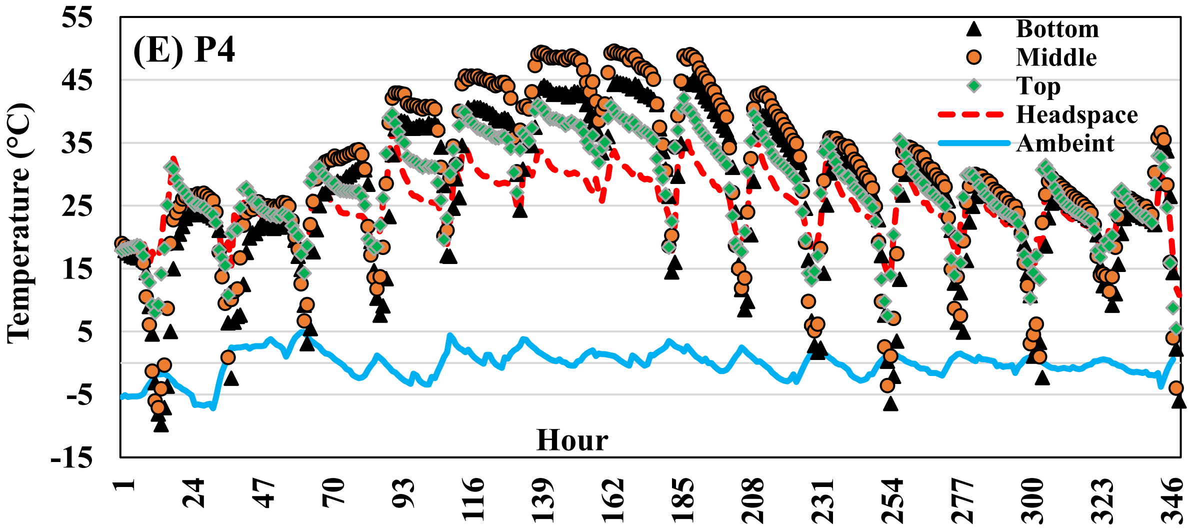
(E) P4
Temperature (°C)
55
45
35
25
15
5
-5
-15
Bottom
Middle
Top
Headspace
Ambeint
Hour
1
24
47
70
93
116
139
162
185
208
231
254
277
300
323
346

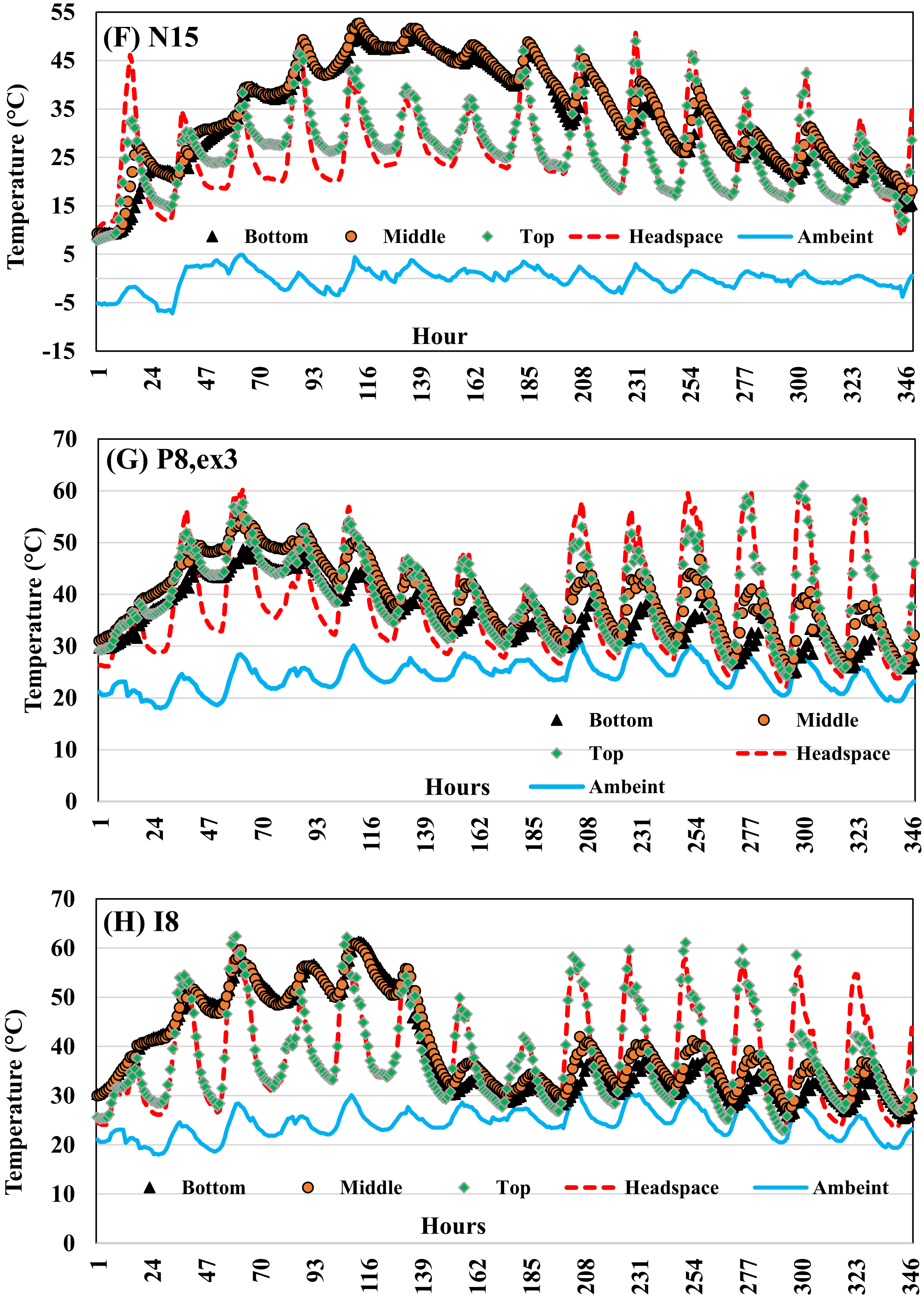

Figure 4.2 Temperature Profiles

Time	Jan	Feb	Mar	Apr	May	Jun	Jul	Aug	Sep	Oct	Nov	Dec
0 - 1	0	0	0	0	0	0	0	0	0	0	0	0
1 - 2	0	0	0	0	0	0	0	0	0	0	0	0
2 - 3	0	0	0	0	0	0	0	0	0	0	0	0
3 - 4	0	0	0	0	0	0	0	0	0	0	0	0
4 - 5	0	0	0	0	21	51	20	0	0	0	0	0
5 - 6	0	0	0	62	146	142	137	100	37	0	0	0
6 - 7	0	5	126	228	222	203	201	210	261	152	13	0
7 - 8	136	203	281	312	285	257	256	270	353	310	186	99
8 - 9	313	327	334	360	343	309	305	326	396	362	263	215
9 - 10	353	365	348	385	371	343	329	334	413	391	277	232
10 - 11	362	395	378	397	392	369	342	355	410	383	282	235
11 - 12	339	367	376	407	397	381	357	350	393	360	275	222
12 - 13	324	347	369	406	388	369	341	341	396	352	271	223
13 - 14	297	317	350	380	367	342	329	324	362	329	246	215
14 - 15	266	288	310	350	337	319	310	309	341	298	223	197
15 - 16	174	260	267	308	299	282	274	276	306	249	121	76
16 - 17	0	86	197	242	241	243	232	234	224	46	0	0
17 - 18	0	0	27	107	164	181	172	140	29	0	0	0
18 - 19	0	0	0	0	24	75	66	8	0	0	0	0
19 - 20	0	0	0	0	0	0	0	0	0	0	0	0
20 - 21	0	0	0	0	0	0	0	0	0	0	0	0
21 - 22	0	0	0	0	0	0	0	0	0	0	0	0
22 - 23	0	0	0	0	0	0	0	0	0	0	0	0
23 - 24	0	0	0	0	0	0	0	0	0	0	0	0

Figure 4.3 Comparison of Typical Solar Radiation Intensity

Map link https://globalsolaratlas.info/map?s=43.078137,141.337967,10

Location Hokkaido University, Kita Ward, Sapporo, Hokkaido Prefecture 060-0808, Japan

Geographical coordinates 43.078137°, 141.337967° (43°04'41", 141°20'17")

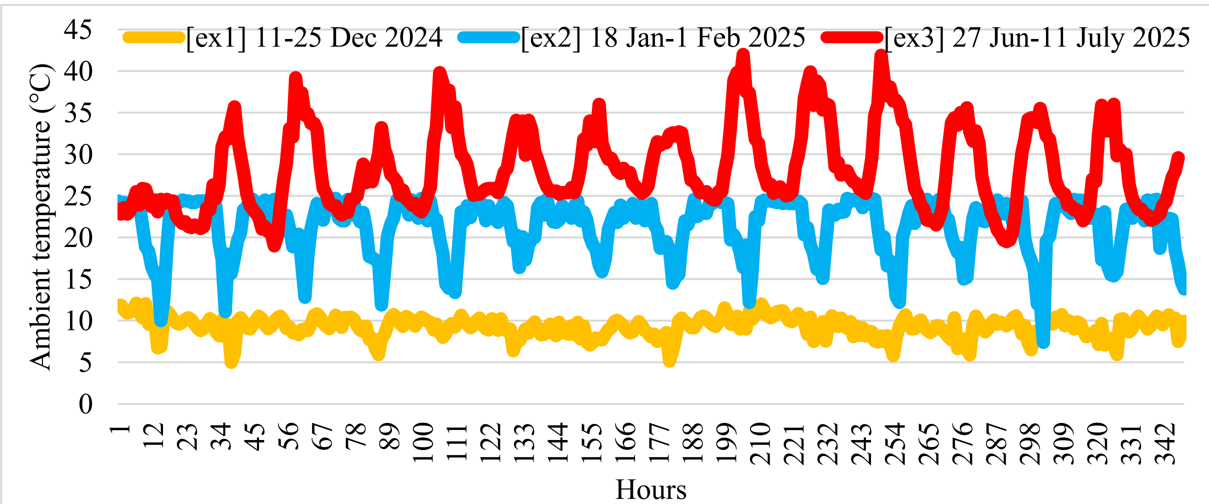

Figure 4.4 Ambient Temperature Between All Experiments

4.3.2 Mass Balance Analysis

The reliability of the mass balance model was assessed by comparing the modeled final mass and %MC with experimental results across trials. The overall prediction error for final mass was within ±2.3%, indicating strong agreement between the model and observed data. Additionally, the predicted %MC values consistently fell within the range of experimental measurements across different waste layers (except the case of I8). These findings confirm that the mass balance model offers a reliable representation of the biodrying process under the greenhouse system. It can be reasonably used to interpret representative mass change behavior within each reactor under different operating conditions in this study. The detailed comparison between the experimental and modeled values of final mass and moisture content is provided in the supplementary data.

This section presents the findings from the mass balance model to understand the effect of different aeration patterns, as illustrated in Figure 4.5. Positive aeration at 8 L/min or 0.9 m^3/kg waste/day (P8,ex1) showed a clear benefit, as it resulted in no leachate production and complete water loss through evaporation (100% of water loss was in vapor form). In contrast, Negative aeration at 8 L/min or 0.9 m^3/kg waste/day (N8) produced both vapor and liquid losses. A total of 2.89 kg (82%) was lost as vapor, while the remaining 18%, equivalent to 0.63 kg, was leachate and condensate. Interestingly, although N8 emitted a higher amount of vapor than P8,ex1, it also induced moisture uptake from the inlet air (2.05 kg), contributing to an increase in the water content within the waste pile. Solid degradation levels varied significantly across aeration patterns. Under P8,ex1, only a small amount of organic solid was degraded (0.21 kg), suggesting this mode is effective in preserving the solid mass while promoting moisture removal. In contrast, N8 led to a substantially higher degradation of organic solid (1.86 kg), which might be attributed to the higher waste temperatures discussed in the previous section, as well as the additional moisture introduced through the inlet air. Considering passive aeration (P0), it exhibited moderate organic solid degradation (1.44 kg), but it performed the lowest total water loss among the three aeration patterns. Water loss in P0 occurred through both vapor (0.87 kg, 80% of water loss) and leachate (0.22 kg, 20% of water loss).

The results of this study differed from those of other research conducted on biodrying without a greenhouse system, where positive aeration was associated with greater organic solid loss compared to negative aeration [16]. Also, these results suggest that positive aeration is more suitable for applications prioritizing solid mass retention and moisture reduction without leachate generation. On the other hand, both negative and passive aeration patterns may enhance biodegradation, but this contributed to increased leachate production and greater solid loss.

The effect of airflow rate on mass change was also examined through P4 and P8,ex2 for positive aeration, while negative aeration is presented in N8 and N15. In the case of positive aeration, the condition operated at a higher aeration rate of 8 L/min or 0.9 m^3/kg waste/day

(P8,ex2) removed a greater amount of moisture in the form of vapor, totaling 3.91 kg, compared to 2.07 kg under the airflow rate at 4 L/min or 0.45 m^3/kg waste/day (P4). This difference can be explained by the increased volume of air intake, which facilitated more efficient moisture removal through the outlet air. In P4, only 0.08 kg of leachate were generated, accounting for 4% of the total water loss, and 2.07 kg or 96 % of the water was removed as vapor. These results are consistent with previous findings that highlight the importance of aeration volume in improving biodrying performance by promoting water evaporation within the waste pile [27, 28]. Remarkedly, the lower airflow rate in P4 led to a greater degree of organic solid degradation. This observation was in agreement with previous results associated with the temperature profile, showing that P4 maintained higher waste temperatures, which might be more suitable for microbial growth and biological activity.

For the effect of airflow rate in the negative aeration pattern, a similar pattern was observed. At an airflow rate of 15 L/min or 1.7 m^3/kg waste/day (N15), vapor emission reached 8.29 kg, representing 89 % of the total water loss. Leachate and condensate discharge accounted for 1.02 kg or 11% of the total water loss. Although N15 removed more moisture than N8, it also introduced more external moisture into the waste by the inlet air. This might have contributed to an increase in heat capacity inside the waste pile, while simultaneously reducing the available space for oxygen transfer, which is essential for aerobic microbial activity. It is important to note that N8 and N15 were conducted during different experimental times, and the initial waste properties, including MC and VS, were different. Therefore, the comparison between these two conditions should be interpreted with caution, and further investigation conducted within the same period is recommended to confirm the specific effects and underlying assumptions related to airflow rate in the case of negative aeration.

The effect of experimental period (in relation to external environmental factors) on mass change was considered, based on the comparison among P8,ex1 conducted in December 2024, P8,ex2 conducted in January 2025 and P8,ex conducted in June-July 2025. This comparison aimed to explore how external environmental conditions, such as surrounding temperature and solar radiation intensity influence the biodrying process under the greenhouse system. The results showed that P8,ex2 and P8,ex3 released a significantly greater amount of vapor, approximately 1.75 and 3.65 times more than P8,ex1. This increase can be attributed to higher levels of solar radiation and ambient temperature (associated with the surrounding air as the air outside the reactors) during January, June and July, which enhanced system warming and improved the moisture-holding capacity of air within the reactor. Additionally, P8,ex2 and P8,ex3 also exhibited a higher degree of organic solid degradation, with 1.60 and 3.76 times greater than that observed in P8,ex1. This finding suggests that the different ambient temperature and solar radiation intensity affected the degree of organic degradation and it might have supported more suitable thermal condition within the system for microbial activity, contributing to enhance biodegradation.

Notably, all trials with positive aeration at 8 L/min or 0.9 m^3/kg waste/day demonstrated zero leachate emission during the biodrying process under the greenhouse system. This finding highlighted a practical advantage of using positive aeration with greenhouse structures, offering effective moisture removal while preventing leachate emission despite ambient temperature variation.

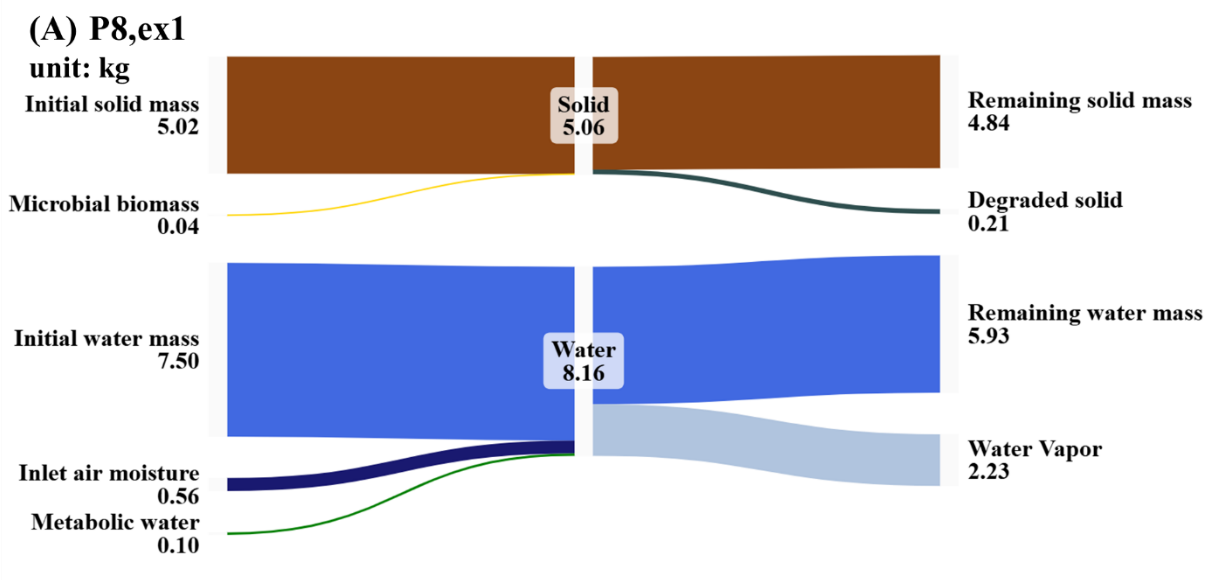

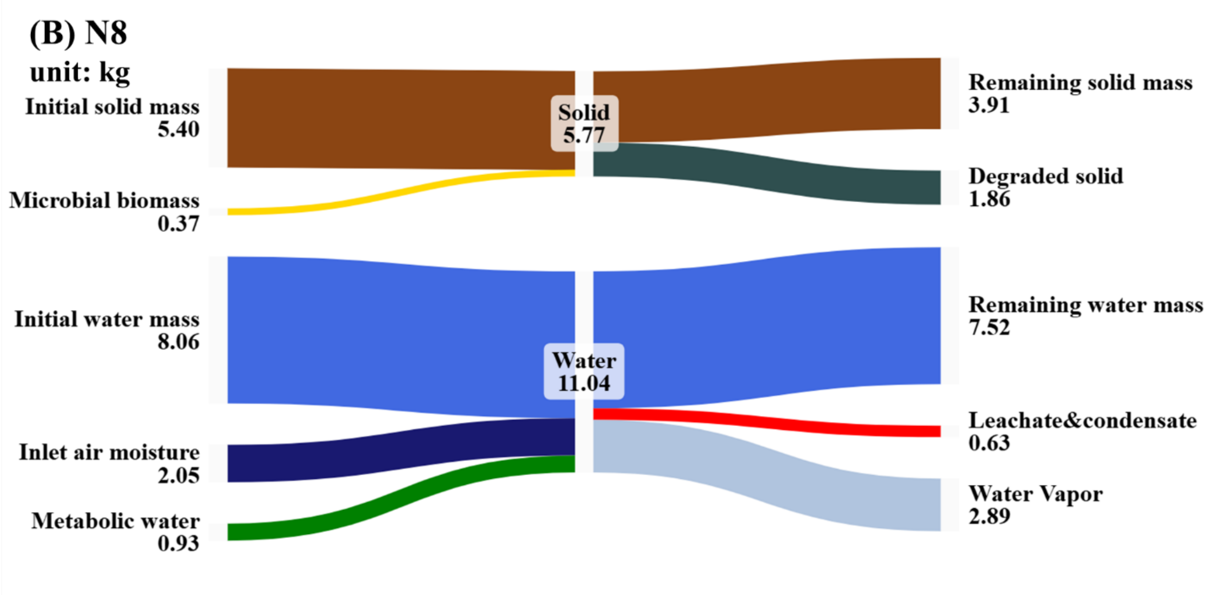

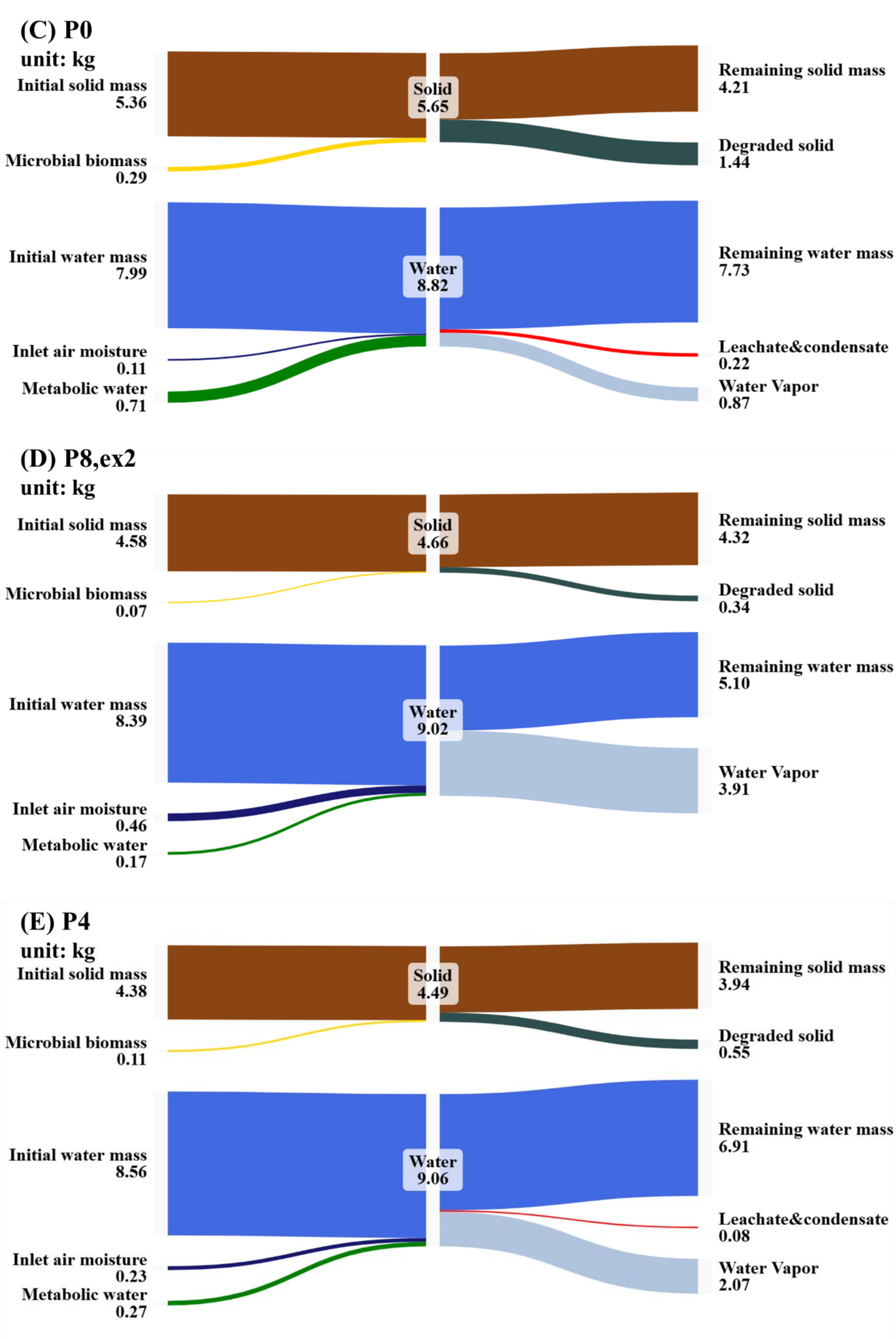
(C) P0
unit: kg
Initial solid mass
5.36
Microbial biomass
0.29
Solid
5.65
Remaining solid mass
4.21
Degraded solid
1.44
Initial water mass
7.99
Inlet air moisture
0.11
Metabolic water
0.71
Water
8.82
Remaining water mass
7.73
Leachate&condensate
0.22
Water Vapor
0.87
(D) P8,ex2
unit: kg
Initial solid mass
4.58
Microbial biomass
0.07
Solid
4.66
Remaining solid mass
4.32
Degraded solid
0.34
Initial water mass
8.39
Inlet air moisture
0.46
Metabolic water
0.17
Water
9.02
Remaining water mass
5.10
Water Vapor
3.91
(E) P4
unit: kg
Initial solid mass
4.38
Microbial biomass
0.11
Solid
4.49
Remaining solid mass
3.94
Degraded solid
0.55
Initial water mass
8.56
Inlet air moisture
0.23
Metabolic water
0.27
Water
9.06
Remaining water mass
6.91
Leachate&condensate
0.08
Water Vapor
2.07

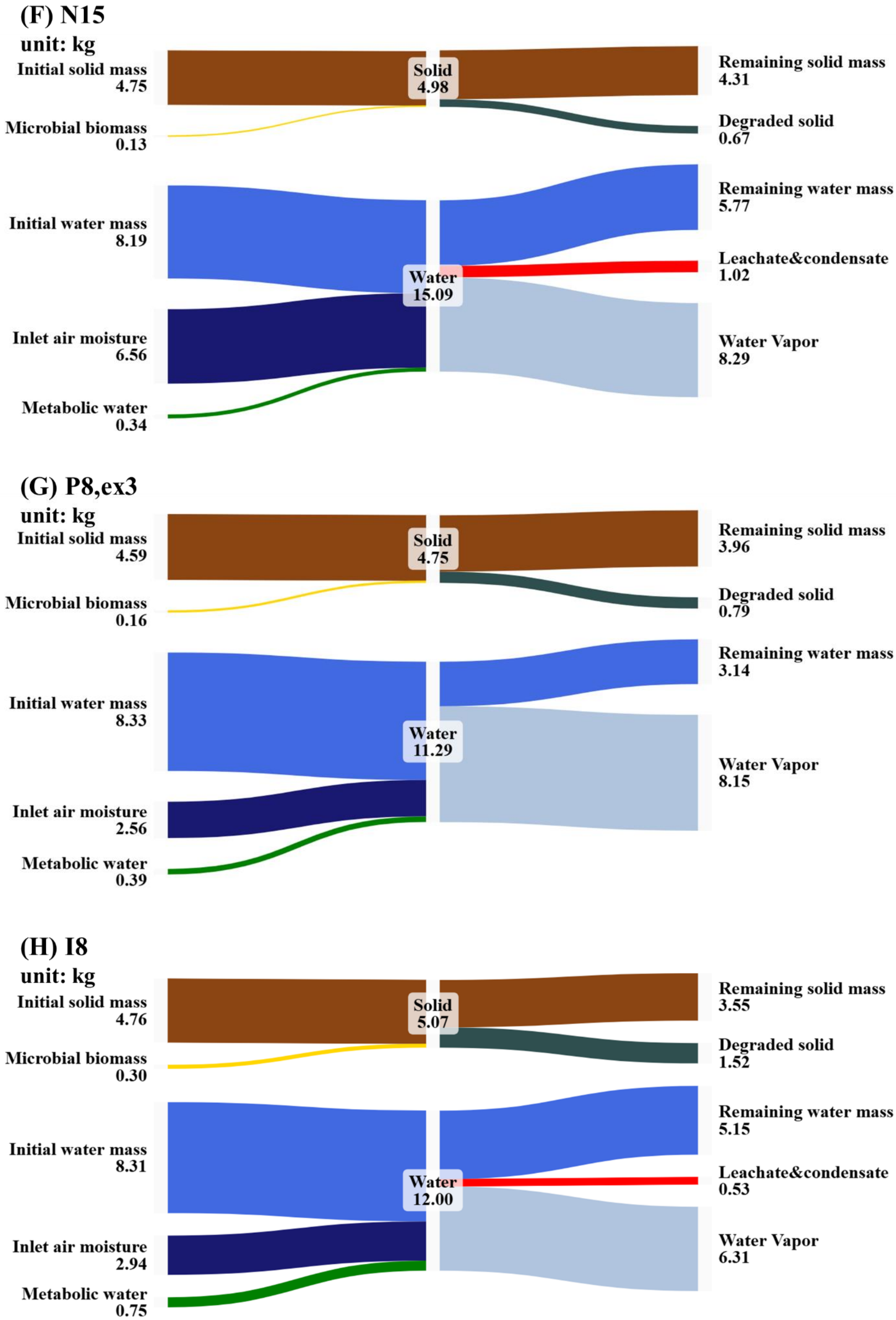

Figure 4.5 Mass Balance Analysis Among Different Trials

4.3.3 Leachate Quantity and Quality

Leachate characteristics under different aeration patterns revealed differences in both organic content and pH value, indicating the influence of aeration patterns on waste biodegradation and leachate production within the solar greenhouse biodrying system. The total organic carbon (TOC) concentration in leachate exhibited substantial temporal variation, with the passive aeration pattern (P0) showing the highest peak of 3,664 mg/L on day 9, followed by the positive aeration pattern (P4) with 1,156 mg/L. In contrast, both negative aeration conditions (N8 and N15) produced comparatively lower TOC levels, remaining mostly below 1,500 mg/L. The leachate pH evolution further supported these observations. During the early biodrying phase (days 3–6), acidic conditions (pH 3.8–5.0) were observed, particularly under negative aeration at high airflow rate (N15), indicating initial acidogenic activity from rapid decomposition of easily degradable organic matter. After that, pH gradually increased to neutral and slightly alkaline values (7.5–8.5) across all aeration patterns, reflecting the transition from active biodegradation to drying process. For the case of I8, leachate production increased steadily during negative aeration (Day 1–5), reaching a maximum of 175 mL on Day 6. This indicates that downward airflow promoted moisture migration to the base and contributed to liquid-phase discharge. During this phase, TOC concentrations were very high (up to 1,657.67 mg/L) and pH continuously decreased to 3.45. No leachate was recorded from Day 7 onward, indicating that positive aeration redirected moisture removal from leaching to evaporation through warm upward airflow. Among all conditions, N8 showed the most stable pH progression with minimal fluctuations, consistent with moderate leachate production (34.96 mL/kg waste input) and lower TOC levels. Overall, these results demonstrate that aeration pattern strongly affects leachate generation, organic load, and pH stability, which together indicate both microbial dynamics and process maturity within the solar greenhouse biodrying system.

According to the EU Council Decision Annex 2003/33/EC, the leachate from stable (non-reactive) waste should exhibit a pH value above 6. In this study, both negative and passive aeration patterns were able to maintain pH values above this threshold, indicating improved stability of the biodried material. Although the TOC concentrations in all conditions remained higher than the typical wastewater discharge limits (15–50 mg/L) [29], the total leachate volume generation was relatively low when compared to the amount of waste input. Regarding these results, negative aeration demonstrated promising potential as an operational setting for waste pretreatment aimed at enhancing waste stabilization. Table 4. 4 presents the TOC concentration and the amount of leachate generated per unit of waste input, while Figure 4.6 illustrates the variations in leachate quantity and pH values under each operational condition.

Table 4.4 TOC Concentration and the Amount of Leachate Per Unit of Waste Input

Day	TOC mg/l				
	N8	P0	P4	N15	I8
1	-	-	-	-	-
2	-	-	-	-	785.25
3	-	-	-	134.21	1,591.12
4	-	-	-	327.21	1,657.67
5	-	-	-	1,481.40	991.04
6	141.06	-	-	709.21	1,018.42
7	186.81	-	378.49	336.29	-
8	184.01	1,622.54	324.22	112.03	-
9	86.60	3,664.28	1,156.06	35.81	-
10	22.22	582.60	-	34.74	-
11	24.14	179.16	-	33.87	-
12	31.78	78.56	-	107.97	-
13	49.57	68.72	-	74.07	-
14	107.45	70.43	-	185.55	-
15	90.31	104.59	-	-	-
Leachate production (ml) per waste input (kg)	34.96	16.44	6.18	70.02	38.79

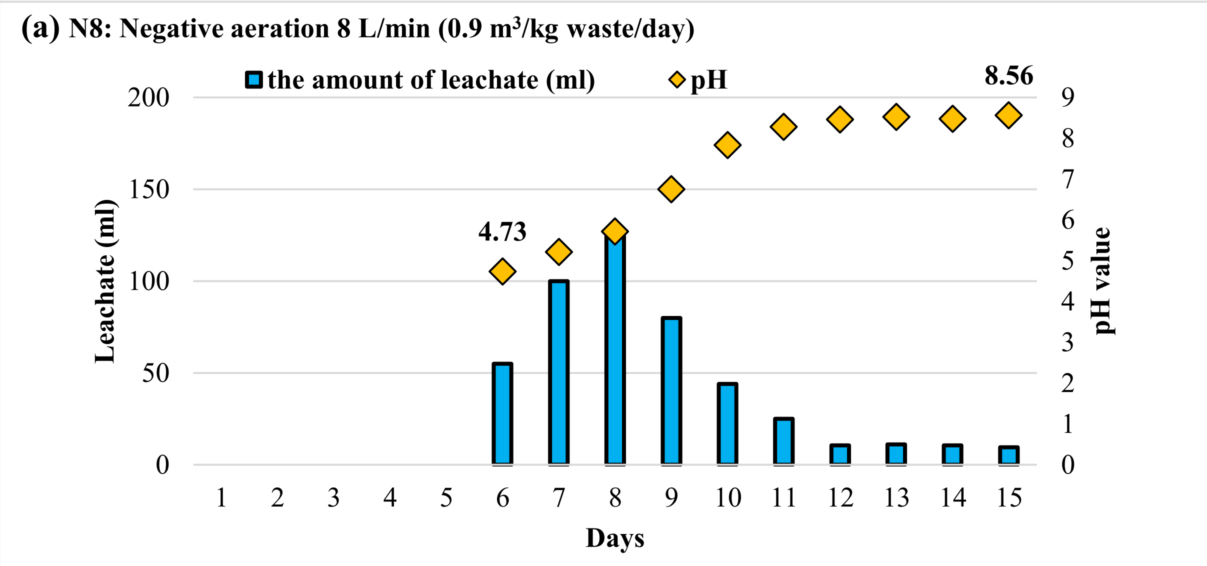

(b) P0: Passive aeration

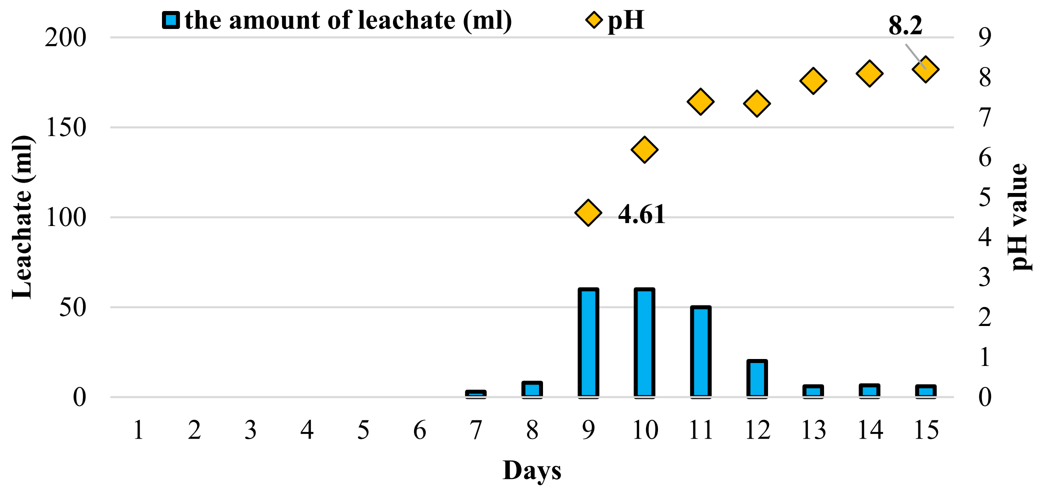

(c) P4: Positive aeration 4 L/min (0.45 m^3/kg waste/day)

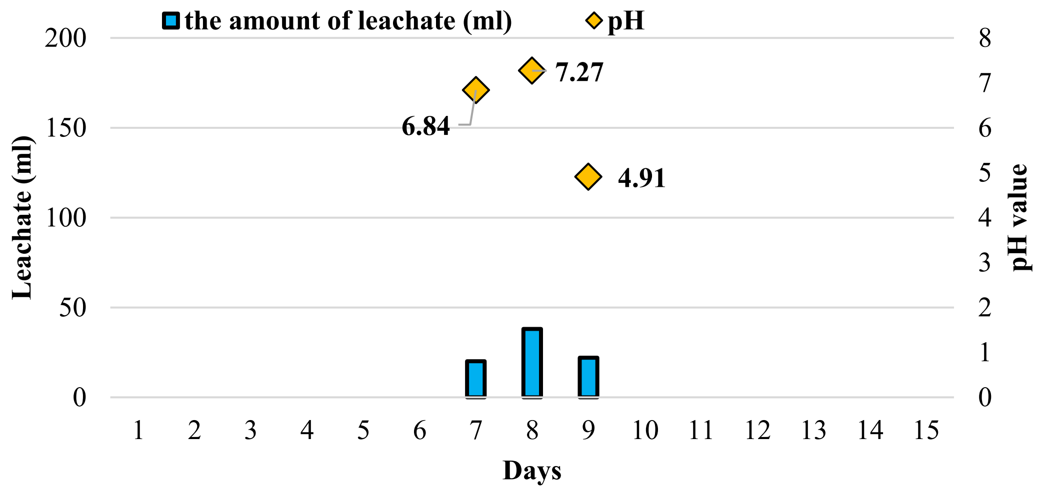

(d) N15: Negative aeration 15 L/min (1.7 m^3/kg waste/day)

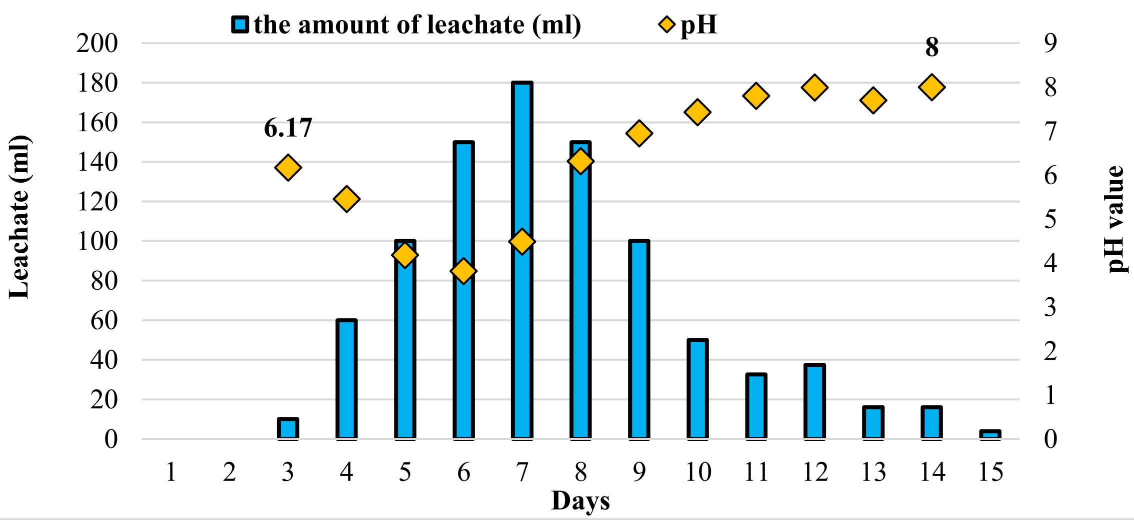

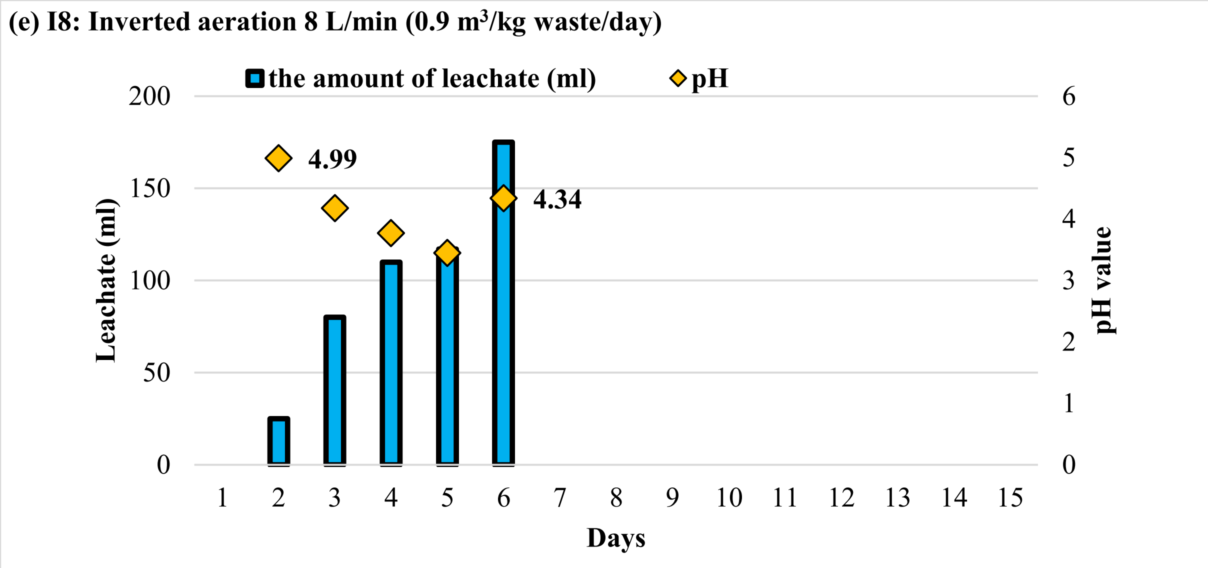

Figure 4.6 The Variations in Leachate Quantity and pH Values under Each Operational Condition

4.4 Conclusion

This study examined the influence of aeration patterns on the biodrying process within the solar greenhouse system, with particular focus on the resulting temperature dynamics, mass changes, and leachate quality. By addressing three key research questions, the findings provide valuable insights into the optimization of biodrying systems for solid waste pretreatment aimed at reducing MC.

First, the study investigated how varying aeration patterns affect the temperature profiles and mass changes within the waste materials during biodrying. The results demonstrated that aeration pattern and airflow rate exerted a strong influence on the thermal evolution and vertical temperature gradients within the waste materials. Positive aeration tended to drive heat upward, leading to higher temperatures in the upper layers, whereas negative aeration facilitated even heat distribution across the bottom and middle layers. Passive aeration, in contrast, promoted heat accumulation in the central portion of the waste pile. Moreover, airflow rate further influenced these waste temperature profiles, with lower positive aeration at 4 L/min (0.45 m^3/kg waste/day) retaining more heat by reducing convective loss, while higher positive aeration at 8 L/min (0.9 m^3/kg waste/day) had more heat dissipation but improved moisture removal. Higher negative aeration at 15 L/min (1.7 m^3/kg waste/day) enhanced heat retention by driving warm-moist air downward. Different mass change behaviors were observed, with positive aeration favoring water removal with minimal organic solid degradation, while negative and passive aeration induced greater biodegradation and leachate generation.

Second, the results from this chapter clearly indicate that higher solar radiation and surrounding air temperature during summer substantially enhanced heat accumulation, moisture content reduction. The results showed that P8,ex2 and P8,ex3 released substantially more vapor, approximately 1.75 and 3.65 times higher than P8,ex1. Similarly, organic solid degradation in P8,ex2 and P8,ex3 was 1.60 and 3.76 times higher than in P8,ex1. This suggests that variations in ambient temperature and solar radiation affected the degree of organic degradation, likely creating more favorable thermal conditions for microbial activity thereby enhancing biodegradation. The suitable thermal condition in summer (P8,ex3) resulted in more effective moisture removal in the biodrying in the greenhouse reactor. The average moisture content of P8,ex3 decreased from 64.49 % to 33.69 % (on average), whereas in winter (P8,ex2) it only reduced from 64.65 % to 47.81 % (on average).

Lastly, the study identified the most suitable operational conditions for biodrying as a pretreatment method for RDF production. The results suggest that positive aeration, particularly at an airflow rate of 8 L/min (0.9 m^3/kg waste/day) in a greenhouse system. This operational setting ensured efficient water removal, minimized organic matter degradation, and provided zero leachate discharge, thereby producing stabilized waste materials with reduced moisture content suitable for RDF processing. Furthermore, the greenhouse headspace part enhanced heat capture from solar radiation, supporting biodrying even under variable ambient conditions.

Overall, this comprehensive comparison contributes novel insights into the interplay of aeration pattern, airflow rate, and environmental factors, especially in the solar greenhouse biodrying system. This study shows that aeration strategies can be adjusted to balance drying efficiency and solid mass preservation, helping to improve understanding of biodrying and providing evidence to guide the development of optimal systems for solid waste pretreatment methods. Beyond academic contributions, the findings of this study also guide practical implications. For instance, an inverted aeration strategy (combining negative and positive aeration) could be applied during the winter season to increase waste temperature at the initial stage, followed by positive aeration in the later stage to accelerate drying in the solar greenhouse biodrying system.

References

[1] Siddiqua A, Hahladakis JN, Al-Attiya WAKA (2022) An overview of the environmental pollution and health effects associated with waste landfilling and open dumping. Environmental Science and Pollution Research 29:58514–58536. https://doi.org/10.1007/s11356-022-21578-z

[2] Kaza S, Yao LC, Bhada-Tata P, Van Woerden F (2018) What a waste 2.0: A global snapshot of solid waste management to 2050. Washington, DC

[3] Tun MM, Juchelková D (2018) Drying methods for municipal solid waste quality improvement in the developed and developing countries: A review. Environmental Engineering Research 24:529–542. https://doi.org/10.4491/eer.2018.327

[4] Febijanto I, Steven S, Nadirah N, et al (2024) Municipal Solid Waste (MSW) Reduction through Incineration for Electricity Purposes and Its Environmental Performance: A Case Study in Bantargebang, West Java, Indonesia. Evergreen 11:32–45. https://doi.org/10.5109/7172186

[5] Edo-Alcón N, Gallardo A, Colomer-Mendoza FJ, Lobo A (2024) Efficiency of biological and mechanical-biological treatment plants for MSW: The case of Spain. Heliyon 10:e26353. https://doi.org/10.1016/j.heliyon.2024.e26353

[6] National Institute for Environmental Studies (NIES) (2020) Mechanical Biological Treatment (MBT) guideline. Tsukuba

[7] Velis CA, Longhurst PJ, Drew GH, et al (2009) Biodrying for mechanical–biological treatment of wastes: A review of process science and engineering. Bioresour Technol 100:2747–2761. https://doi.org/10.1016/j.biortech.2008.12.026

[8] Jalil NA, Ahmad IK, Basri H, et al (2022) Biodrying of Municipal Solid Waste: A Case Study in Malaysia. Springer, pp 375–434

[9] Robles-Martínez F, Silva-Rodríguez EM, Espinosa-Solares T, et al (2012) Biodrying under Greenhouse Conditions as Pretreatment for Horticultural Waste. J Environ Prot (Irvine, Calif) 03:298–303. https://doi.org/10.4236/jep.2012.34038

[10] Colomer-Mendoza FJ, Robles-Martinez F, Herrera-Prats L, et al (2012) Biodrying as a biological process to diminish moisture in gardening and harvest wastes. Environ Dev Sustain 14:1013–1026. https://doi.org/10.1007/s10668-012-9369-1

[11] Contreras-Cisneros RM, Orozco-Álvarez C, Piña-Guzmán AB, et al (2021) The Relationship of Moisture and Temperature to the Concentration of O2 and CO2 during Biodrying in Semi-Static Piles. Processes 9:520. https://doi.org/10.3390/pr9030520

[12] Ngamket K, Wangyao K, Patumsawad S, et al (2021) Quality improvement of mixed MSW drying using a pilot-scale solar greenhouse biodrying system. J Mater Cycles Waste Manag 23:436–448. https://doi.org/10.1007/s10163-020-01152-w

[13] Xu M, Wang Q, Wang X, et al (2024) Sustainable solutions: Bio-drying for organic solid waste management. Ind Crops Prod 222:119606.

https://doi.org/10.1016/j.indcrop.2024.119606
[14] Payomthip P, Towprayoon S, Chiemchaisri C, et al (2022) Optimization of Aeration for Accelerating Municipal Solid Waste Biodrying. International Journal of Renewable Energy Development 11:878–888. https://doi.org/10.14710/ijred.2022.45143
[15] Widyarsana IMW, Sevina R (2024) Study on the Quality Improvement of Mixed Municipal Solid Waste by Greenhouse Blackout Tarp with Biodrying System. Journal of Ecological Engineering 25:200–209. https://doi.org/10.12911/22998993/192673
[16] Shao L-M, He X, Yang N, et al (2012) Biodrying of municipal solid waste under different ventilation modes: drying efficiency and aqueous pollution. Waste Management & Research: The Journal for a Sustainable Circular Economy 30:1272–1280. https://doi.org/10.1177/0734242X12462278
[17] Tom AP, Pawels R, Haridas A (2016) Biodrying process: A sustainable technology for treatment of municipal solid waste with high moisture content. Waste Management 49:64–72. https://doi.org/10.1016/j.wasman.2016.01.004
[18] Michael PR, Johnston DE, Moreno W (2020) A conversion guide: Solar irradiance and lux illuminance. Journal of Measurements in Engineering 8:153–166. https://doi.org/10.21595/jme.2020.21667
[19] Kaneko H, Hirayama K, Fujita K (2001) Simulation of composting reaction. Japan Society of Waste Management Research 12:122–130
[20] Ngamket K, Ishii K, Fujimoto S, et al (2025) Advantages of solar greenhouse biodrying through the lens of heat balance analysis and simulation comparison under tropical climate conditions. Results in Engineering 26:105494. https://doi.org/10.1016/J.RINENG.2025.105494
[21] Majumdar A, Pradhan N, Sadasivan J, et al (2018) Food Degradation and Foodborne Diseases: A Microbial Approach. In: Microbial Contamination and Food Degradation. Elsevier, pp 109–148
[22] Roy P, Mohanty AK, Dick P, Misra M (2023) A Review on the Challenges and Choices for Food Waste Valorization: Environmental and Economic Impacts. ACS Environmental Au 3:58–75
[23] Haug RT (1993) The practical handbook of compost engineering. Routledge
[24] Andersen KT (2003) Theory for natural ventilation by thermal buoyancy in one zone with uniform temperature. Build Environ 38:1281–1289. https://doi.org/10.1016/S0360-1323(03)00132-X
[25] Zhang JY, Lu WZ, Huo R, Feng R (2008) A new model for determining neutral-plane position in shaft space of a building under fire situation. Build Environ 43:1101–1108. https://doi.org/10.1016/j.buildenv.2007.02.004
[26] Statistics Kingdom (2017) Kruskal Wallis Test Calculator. https://www.statskingdom.com/kruskal-wallis-calculator.html. Accessed 23 May 2025
[27] Kristanto GA, Hanany I (2017) Effect of air-flow on biodrying method of municipal

solid waste in Indonesia. p 040007
[28] Yuan J, Zhang D, Li Y, et al (2018) Effects of the aeration pattern, aeration rate, and turning frequency on municipal solid waste biodrying performance. J Environ Manage 218:416–424. https://doi.org/10.1016/j.jenvman.2018.04.089
[29] Park JW, Kim SY, Noh JH, et al (2022) A shift from chemical oxygen demand to total organic carbon for stringent industrial wastewater regulations: Utilization of organic matter characteristics. J Environ Manage 305:114412. https://doi.org/10.1016/j.jenvman.2021.114412

Chapter 5

Performance Evaluation and Heat Balance Model Application in the Solar Greenhouse Biodrying System

Graphical Abstract for Chapter 5

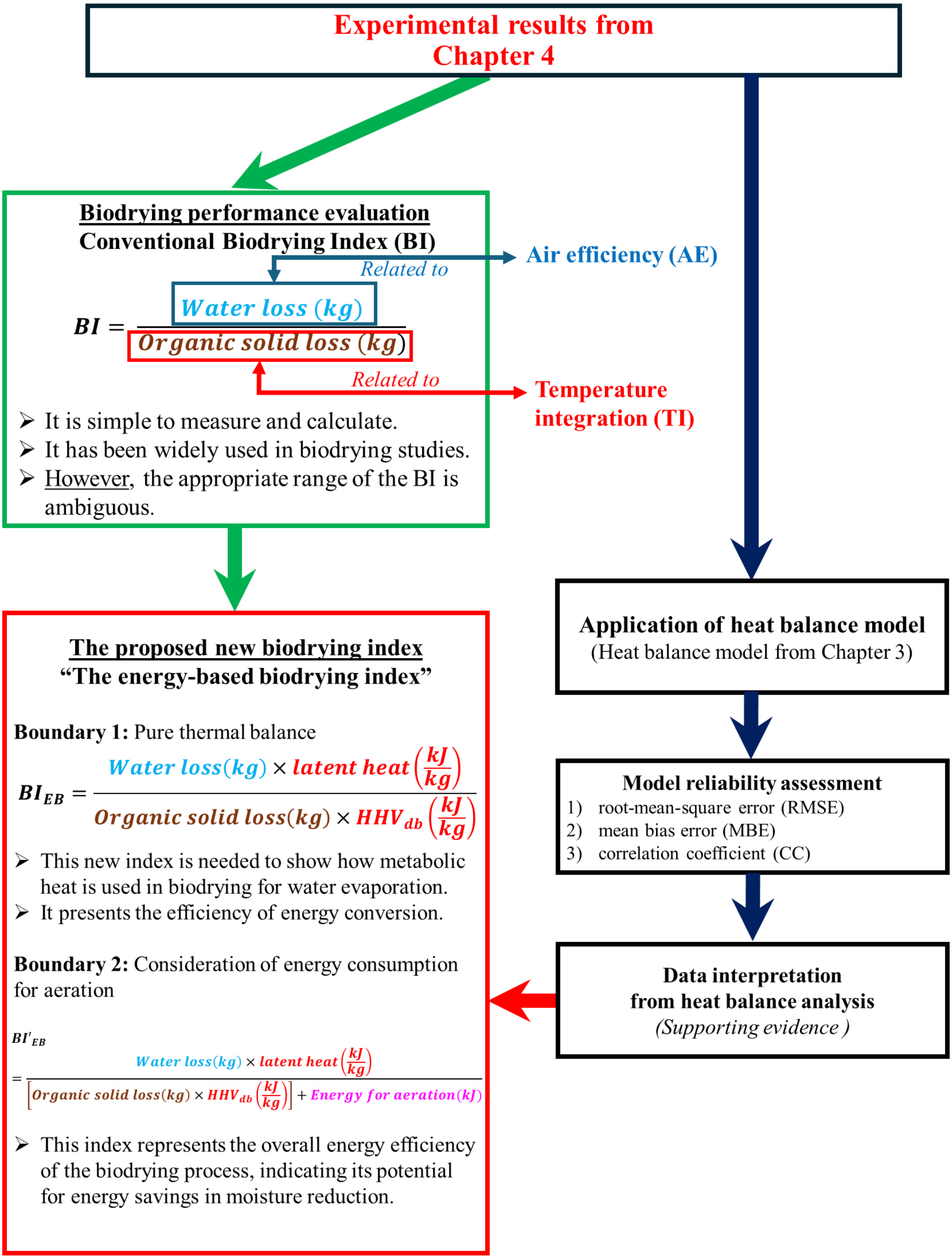

5.1 Introduction

Biodrying is an aerobic decomposition used within mechanical-biological treatment (MBT) system to dry and partially stabilize residual municipal solid waste (MSW) [1]. The key points about biodrying are: 1) It aims to dry the waste and preserve the biomass content, rather than fully stabilize it (like in composting). 2) The thermal energy released during aerobic biodegradation of readily degradable organic matter is combined with excess aeration to dry the waste. From previous chapters, Solar greenhouse biodrying systems or the biodrying process under greenhouse system offer several advantages. First, solar radiation transmitted through the greenhouse cover increases heat input during the daytime, enhancing water evaporation. Second, the greenhouse cover reduces heat loss by limiting wind-driven convection and thermal radiation from waste surface, allowing higher internal temperatures to be maintained. Third, it protects the waste from rainwater, preventing remoisturization. According to comparative simulation of biodrying process, moisture reduction in the solar greenhouse biodrying system occurs more rapidly, enabling the system to reach the target moisture content (<30%) in about 7 days, that is faster than conventional outdoor biodrying. In addition, the aeration pattern plays a highly influential role in the biodrying process within the greenhouse system. It significantly affects the temperature profile as well as the changes in both solid and water mass in the waste.

Given these advantages and the strong influence of aeration patterns on this biodrying system, a comprehensive assessment of biodrying performance is essential to understand how operational conditions affect biodrying process efficiency. Therefore, evaluating biodrying performance through key indicators, such as biodrying index (BI), temperature integration (TI), and air efficiency (AE), provides valuable insights into the system's effectiveness. Practitioners in waste management plants can use these indicators to guide operational settings in accordance with waste characteristics and weather conditions. Conventionally, biodrying performance is evaluated using the mass-based biodrying index (or the mass-based BI), which simply calculates the ratio of water loss to organic matter loss. However, this traditional metric fails to capture the thermodynamic dynamics of the system. To provide a more precise evaluation, the study in this chapter proposes a novel energy-based biodrying index (BI_{EB}). Unlike the mass-based calculation approach, this new indicator measures efficiency by comparing the latent heat utilized for evaporation against the heat generated by metabolic heat. This energy-based biodrying index represents pure thermal balance within the solar greenhouse biodrying system (defined as Boundary 1). Moreover, this chapter proposes an alternative approach for calculating BI_{EB} (defined as Boundary 2), which incorporates the energy requirement of the aeration system into the index calculation. Consequently, this index represents the overall energy efficiency of the biodrying process, indicating its potential for energy savings in moisture reduction.

Furthermore, to interpret the heat transfer mechanisms occurring in the solar greenhouse biodrying system in positive and negative aeration patterns, the application of heat balance model is required. By refining the heat balance model from Chapter 3, the contributions of solar radiation, microbial heat generation, forced aeration, and heat losses can be quantified, serving as a tool for understanding and optimizing the solar greenhouse biodrying system under various conditions. Importantly, the results from the heat balance model can serve as supporting evidence for the newly proposed biodrying index. Therefore, the primary objective of this chapter is to provide a comprehensive evaluation of biodrying performance and to apply the heat balance model under both positive and negative aeration patterns, in order to support a better understanding and optimized design of the solar greenhouse biodrying system. The results presented in this chapter also potentially highlight challenges and directions for further research aimed at the development of the solar greenhouse biodrying system.

5.2 Materials and Methods

5.2.1 Biodrying Performance Evaluation

The experimental results and the results from the mass balance analysis were used to conduct a comprehensive evaluation of biodrying performance. Three biodrying performance indicators were selected to evaluate the biodrying process under different aeration patterns across seasons.

The biodrying index (BI) was used to evaluate the efficiency of biodrying by indicating how much water is removed for every kilogram of organic matter consumed. Several studies have applied this index, with reported BI values typically ranging from 1.75 to 20.51, as documented in previous literature [2–7]. The BI value implies that lower values may signal inadequate oxygen availability during biodrying, while excess values are linked to greater physical dryness [6]. The BI, expressed as kg of water loss per kg of organic solid loss, can be calculated according to the formula provided in Eq. 5-1.

$$BI(kg_{water}/kg_{organic\,solid}) = \frac{WL}{OL} \qquad \text{Eq. 5- 1}$$

Where *WL* represents water loss (kg), and *OL* is the reduction in organic solid mass (kg).

Temperature is another key parameter influencing both water evaporation and biodegradation during the biodrying process. To assess temperature differences between treatments, the temperature integration (TI) index was applied. TI is defined as the cumulative daily difference between waste and surrounding air temperature. The TI value is useful for understanding the thermal behavior of waste during biodrying. A higher TI indicates stronger self-heating capacity, which results in improved heat retention and reduced heat loss [8].

Additionally, higher TI values are associated with enhanced organic matter degradation [9]. This study adopted the TI calculation method from Yuan et al. [6] and Zhang et al. [9], and the TI value can be calculated using Eq. 5-2.

$$TI\ (°C) = \sum_{i=1}^{d}(T_{wt,i} - T_{s,i}) \qquad \text{Eq. 5- 2}$$

Where $T_{wt,i}$ is the average waste pile temperature on day i, and $T_{s,i}$ is the surrounding air

Air supply plays a crucial role in the biodrying process, and the air efficiency (AE) was used as an important indicator for evaluating the system's effectiveness in removing moisture through given aeration system. High AE value signifies a greater capacity for moisture removal under a given airflow rate, indicating better biodrying performance by achieving higher moisture reduction with the same level of aeration energy input [11]. AE can be calculated using Eq. 5-3.

$$AE\ (g\ water/m^3\ air) = \frac{WL \times 1000}{V_{total}} \qquad \text{Eq. 5- 3}$$

Where V_{total} is total air supply over the entire experimental period (m^3).

To evaluate the performance of the biodrying system, a novel energy-based biodrying index (BI_{EB}) was developed. Unlike traditional mass-based ratios (BI in Eq. 5-1), this indicator assesses the process based on thermodynamic conversion efficiency or effective heat utilization for evaporation. This index is defined as the ratio of the energy utilized for moisture vaporization to the total thermal energy generated by microbial degradation, calculated as follows:

$$BI_{EB}(kJ_{latent\ heat}/kJ_{microbial\ oxidation}) = \frac{WL \times L_w}{OL \times HHV_{db}} \qquad \text{Eq. 5- 4}$$

Where BI_{EB} is the energy-based biodrying index, defined as the latent heat of evaporation (kJ) per unit of bio-heat released from biodegradation (kJ). L_w refers to latent heat of evaporation (kJ/kg water), and HHV_{db} stands for higher heating value on a dry basis of organic substrates in the experiment. A bomb calorimeter was used to measure HHV_{db}, and the value of HHV_{db} in this study was 17,409.34 kJ/kg. The calculation method defined as Boundary 1 accounts only for the pure thermal balance within the solar greenhouse biodrying system.

The calculation method defined as Boundary 2 extends this approach by incorporating the energy consumption of the aeration system into the analysis. The calculation is expressed as follows:

$$BI'_{EB} = \frac{WL \times L_w}{[OL \times HHV_{db}] + E_{aeration}}$$ Eq. 5- 5

Where BI'_{EB} is the energy-based biodrying index, considering the energy consumption for aeration. $E_{aeration}$ refers to the electrical energy consumed by the air pump for aeration (kJ).

5.2.2 Heat Balance Model Application

The mass and heat balance model developed in Chapter 3 was applied in this chapter using the experimental data obtained and presented in Chapter 4. The model formulation provided the theoretical framework for quantifying heat generation, utilization, and losses within the solar greenhouse biodrying system, while the experimental results supplied the necessary input parameters for model application. By integrating the outcomes from both chapters, this study conducted heat balance analysis under positive and negative aeration patterns. As aforementioned, the application of the model in this chapter aimed to enhance the understanding of heat transfer behavior and energy utilization efficiency related to different aeration patterns.

Table 5.1 summarizes the experimental trials and operating conditions used for the application of the heat balance model in this chapter. The trials were conducted under both positive and negative aeration patterns with varying airflow rates and experimental periods to capture seasonal and operational variability. Initial waste mass ranged from 12.52 to 13.46 kg, while the specific airflow rates varied from 0.45 to 1.70 m^3/kg waste/day.

Table 5.1 Summary of Experimental Trials and Operating Conditions Used for Heat Balance Model Application

Trial names	**P8,ex1**	**N8**	**P8,ex2**	**P4**	**N15**	**P8,ex3**
Aeration pattern	Positive	Negative	Positive	Positive	Negative	Positive
Initial mass (kg)	12.52	13.46	12.97	12.94	12.94	12.92
Airflow rate (L/min)	8	8	8	4	15	8
Airflow rate (m^3/kg waste/day)	0.9	0.9	0.9	0.45	1.7	0.9
Experimental periods (date)	11-25 Dec 2024		18 Jan-1 Feb 2025			27 Jun-11 July 2025

The details of the heat balance analysis are presented in Chapter 3; however, there is another heat-related element that needs to be considered. That is the heat loss by leachate drainage, because leachate generation was observed under negative aeration and low-airflow positive aeration conditions. Leachate contributes to heat loss from the pile, as liquid water is warmed by biodegradation and then physically exits the system, thereby transporting thermal energy out of the system. The heat loss by leachate drainage is calculated based on the mass of the leachate, its specific heat capacity, and the difference between the leachate temperature and the reference temperature. The measured waste temperature was used to estimate leachate temperature for this heat loss calculation.

$$Q_{leachate} = M_L \times C_{p,water} \times (T_{waste} - T_{ref}) \quad \text{Eq. 5- 6}$$

Where $Q_{leachate}$ represents the heat loss by leachate drainage (kJ). M_L is leachate mass (kg), and $C_{p,water}$ is specific heat of water (4.184 kJ/kg·°C). Meanwhile, T_{waste} refers to the waste temperature and T_{ref} is the reference temperature for calculation (°C). In the case of negative aeration T_{ref} refers to the headspace temperature (the air inside the greenhouse). For positive aeration, T_{ref} refers to the inlet air temperature.

5.2.3 Model Reliability Assessment

In order to assess the reliability of the model outcomes, the results from the model were compared with the experimental temperature data. Despite the existence of temperature gradients within the waste pile, temperatures were assumed to be homogeneous for the purposes of model calculations. To evaluate the model's accuracy, three statistical indicators were employed, including (1) root-mean-square error (RMSE), (2) mean bias error (MBE), and (3) correlation coefficient (CC). The definitions of these indicators and calculation methods are described below.

RMSE quantifies the average magnitude of the deviation between the modeled and measured temperatures. A lower RMSE value indicates better agreement between the model predictions and experimental data. The RMSE value is calculated as follows.

$$RMSE = \left[\frac{1}{n}\sum_{i=1}^{n}(T_{cal,i} - T_{exp,i})^2\right]^{0.5} \quad \text{Eq. 5- 7}$$

Where $T_{cal,i}$ is the modeled temperature at given time, while $T_{exp,i}$ is the experimental temperature at given time. n represents the number of hours.

MBE provides information on the long-term performance of model [12]. A positive MBE indicates that the model tends to overestimate the measured values, whereas a negative MBE indicates a tendency toward underestimation. However, one limitation of MBE is that overestimation in some observations may be offset by underestimation in others. The MBE value is calculated as follows.

$$MBE = \frac{1}{n}\sum_{i=1}^{n}(T_{cal,i} - T_{exp,i}) \qquad \text{Eq. 5- 8}$$

In general, the correlation coefficient (CC) describes the strength of the linear relationship between modeled and measured data [13]. In this study, CC was used to evaluate the level of consistency between the modeled and experimental waste temperature data. CC values range from −1 to 1, with values closer to 1 indicating a strong positive correlation and better model performance (higher level of data consistency). The CC value is calculated as follows.

$$CC = \frac{\sum_{i=1}^{n}(T_{exp,i} - T_{exp,avr})\cdot(T_{cal,i} - T_{cal,avr})}{n \cdot sd_{exp} \cdot sd_{cal}} \qquad \text{Eq. 5- 9}$$

Where $T_{cal,avr}$ is the average modeled temperature, while $T_{exp,avr}$ is the average experimental temperature. sd_{exp} and sd_{cal} are the standard deviation of the experimental and modeled temperatures, respectively.

5.3 Results and Discussion

5.3.1 Interpretation of Biodrying Performance Evaluation

Biodrying performance indicators were applied to evaluate the water removal capacity across different trials. Figure 5.1 (A) presents a comparison of these indicators within this study. Overall, positive aeration at 8 L/min or 0.9 m^3/kg waste/day (P8,ex1, P8,ex2 and P8,ex3) provided high BI values, indicating greater water removal while retaining more solid mass. In terms of temperature integration, passive aeration exhibited the high TI value, mainly because no forced aeration was applied. However, the N15 and I8 trials also demonstrated relatively high TI values, suggesting stronger heat retention under this condition. In contrast, positive aeration, particularly in P8,ex1, served the lowest TI value, which was attributed to upward airflow combined with the low temperature of inlet air. This finding differs from the results reported by Shao et al. [9], where positive aeration achieved higher TI values compared with negative aeration. Regarding air efficiency, positive aeration in P8,ex2, P8,ex3 and P4 achieved high AE values and was more effective in removing water for the given air supply volume compared with N15, which operated under negative aeration at a higher airflow rate. These results indicate that air movement within the greenhouse reactor significantly influences biodrying performance, and different aeration patterns show unique strengths.

Figure 5.1 (B) illustrates the phenomenon between water and solid mass losses in each trial. The results show that aeration pattern and airflow rate strongly affected biodrying performance. Among the trials, P8,ex2 exhibited the highest BI value of 12.18 kg water/kg solid loss, reflecting the high-water removal relative to minor organic solid loss, followed by P8,ex1

(9.29) and P8,ex3 (8.22), all conducted under positive aeration. These results indicate that positive aeration consistently enhances water evaporation while limiting excessive organic matter degradation. In contrast, negative aeration (N8 and N15) produced lower BI values (0.36 and 4.48, respectively), with higher organic solid losses relative to water loss. Passive aeration (P0) exhibited the lowest BI value (0.23), highlighting the limited drying capacity when forced air aeration is absent. The inverted aeration trial (I8), which combined initial negative aeration followed by positive aeration, achieved moderate performance (BI = 2.60), suggesting that aeration sequencing can influence both moisture removal and organic matter preservation. Notably, ambient temperature also affected performance: P8,ex3 conducted in warmer conditions resulted in the highest water loss (5.19 kg), compared to P8,ex1 in cooler weather conditions (1.57 kg), emphasizing the contribution of environmental conditions to water removal efficiency. Overall, these findings demonstrate that positive aeration, combined with favorable ambient temperature, maximizes water removal while minimizing organic solid loss, whereas negative or passive aeration patterns potentially increase organic solid degradation.

It was remarkable that aeration pattern, airflow rate, and ambient temperature affected both heat capture capacity and drying efficiency within the solar greenhouse biodrying system. When comparing P4 and P8,ex2, an increase in airflow rate from 4 to 8 L/min (from 0.45 to 0.9 m^3/kg waste/day) resulted in a higher BI value but a lower TI value, since the larger inlet air volume enhanced the removal of moist air while simultaneously carrying heat out of the system. In the case of negative aeration, the comparison between N8 and N15 showed that increasing the airflow rate from 8 to 15 L/min (from 0.9 to 1.7 m^3/kg waste/day) led to higher BI and TI values. This can be explained by the greater airflow, which improved water removal and introduced more moist air into the waste matrix, thereby increasing the heat acquisition of the waste pile. Nevertheless, the two trials were conducted during different periods, and environmental factors such as ambient temperature and solar radiation intensity might contribute to the observed difference in TI values.

A comparison between P8,ex1, P8,ex2, and P8,ex 3 (Figure 5.1 (C)) further highlighted the influence of ambient temperature. Although all trials operated under the same aeration rate of 8 L/min (0.9 m^3/kg waste/day), the warmer ambient conditions in P8,ex3 led to simultaneous increases in both TI and AE values. This outcome can be attributed to two main reasons. First, higher solar radiation intensity during June and July 2025 elevated the temperatures of both the headspace and waste matrix, which promoted system warm-up and allowed more moisture to accumulate in the headspace, facilitating greater water removal. Second, the warmer inlet air in P8,ex3 carried higher heat content, which encouraged stronger heat input to the waste pile. As a result, P8,ex3 achieved superior TI values when compared with P8,ex1 and P8,ex2.

Altogether, this study confirms that the interplay of aeration pattern, airflow rate, and ambient temperature can simultaneously affect water removal and heat retention, providing practical guidance for improving performance of the solar greenhouse biodrying system.

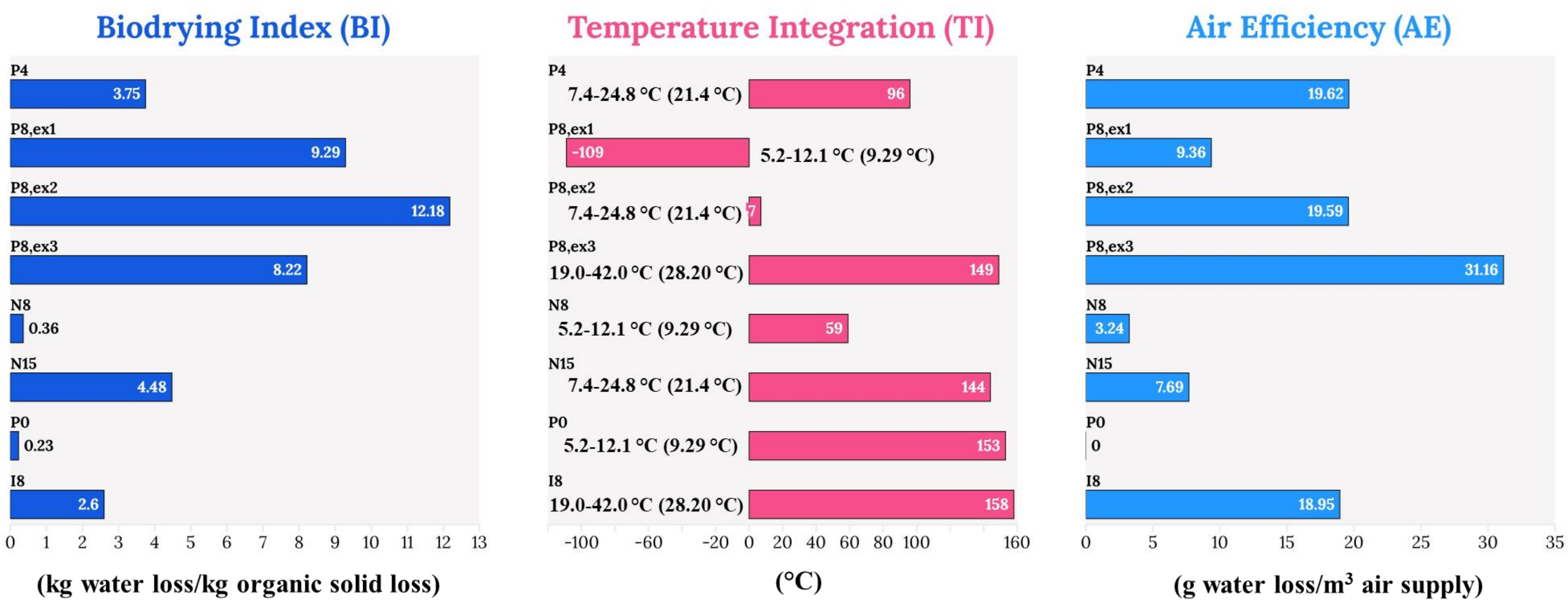

(A)

Noted: The temperatures shown in the temperature integration graph represent the range of air temperatures outside the reactor and the average air temperature outside the reactor, respectively. The values are presented in the format *Min–Max (Average temperature)*.

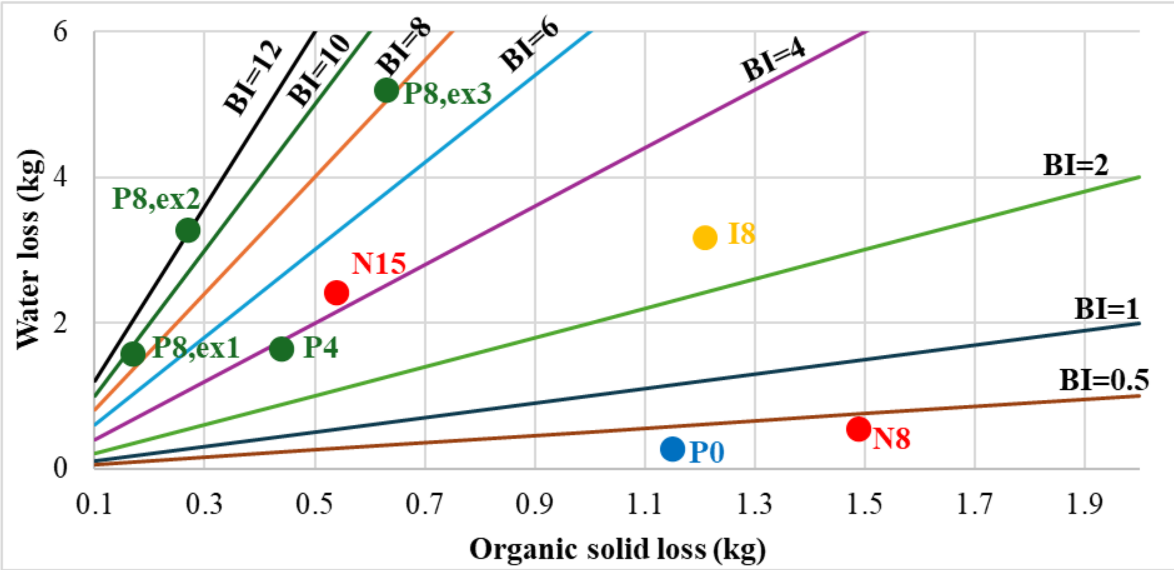

(B)

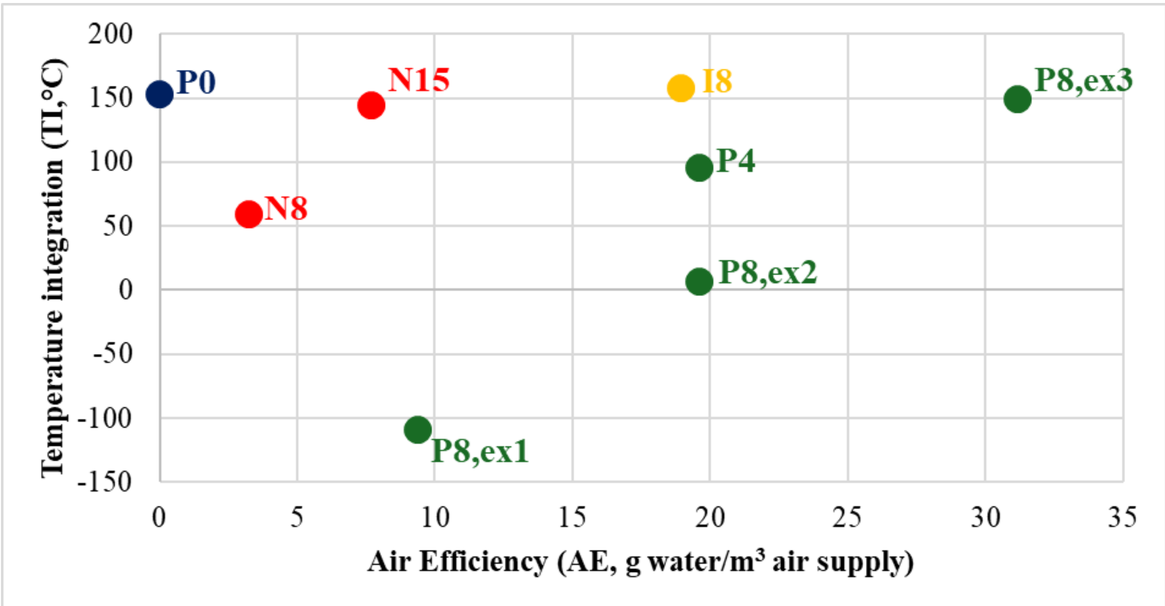

(C)

Figure 5.1 Results of Biodrying Performance Evaluation:
(A) comparison of biodrying performance indicators across trials;
(B) water loss and organic solid loss under different trials;
(C) relationship between TI and AE values among trials.

5.3.2 The Energy-based Biodrying Index

For Boundary 1: Pure thermal balance within the solar greenhouse biodrying system

The calculated energy-based biodrying indices (BI_{EB}) revealed different values across the experimental trials, ranging from a minimum BI_{EB} of 0.03 to a maximum BI_{EB} of 1.57 (see also Figure 5.2). The most significant finding was the superior performance of the positive aeration strategy at 8 L/min or 0.9 m^3/kg waste/day (P8), which consistently yielded the high BI_{EB} value regardless of seasonal variations. The P8 trials achieved indices of 1.20 (Dec 2025), 1.57 (Jan 2025), and 1.07 (Jun-Jul 2026). This result indicates that the latent heat of evaporation in these trials surpassed the heat generated by microbial oxidation.

When comparing between positive and negative aeration, trials with positive aeration demonstrated a vivid advantage over negative aeration in terms of thermodynamic (heat) conversion for evaporation. The negative aeration trial at 8 L/min or 0.9 m^3/kg waste/day (N8) exhibited a critically low index of 0.05. Despite generating the highest amount of metabolic heat among all specific flow rate trials (25,939 MJ), the N8 configuration failed to convert this energy into evaporation, suggesting massive heat accumulation (including sensible heat and other heat transfer to the structure of the reactor) within the system rather than drying. Increasing the negative airflow to 15 L/min or 1.7 m^3/kg waste/day (N15) improved the index to 0.58, which is comparable to the lower-flow positive aeration trial (P4) at 0.48.

Moreover, the passive aeration trial (P0) resulted in the lowest BI_{EB} of 0.03. Although the microbial heat generation was substantial (20,020 MJ), the lack of forced convection prevented effective moisture reduction, resulting in heat entrapment within the system and minimal evaporation (586 MJ). Similarly, the inverted aeration strategy (I8), which combined distinct phases of negative and positive aeration, achieved a modest index of 0.34. While the I8 trial was an improvement for taking advantage between positive and negative aeration patterns, it remained inefficient compared to the continuous positive aeration strategies, indicating that the switching regime may have disrupted the steady-state conditions required for the solar greenhouse biodrying. However, inverted aeration may be applicable under cold weather conditions and could influence the resulting BI_{EB} values. Therefore, further investigation of inverted aeration is required.

Overall, the energy-based biodrying index indicates that the positive aeration rate of 8 L/min or 0.9 m^3/kg waste/day (P8) is the optimal operating condition for RDF production. The consistently high index values above 1.0 observed in the P8 trials demonstrate that this condition effectively utilizes metabolic heat and solar radiation to support the drying process, thereby reducing the reliance on metabolic heat from organic degradation and preserving the energy content of the waste. In contrast, low index values obtained in the N8 and P0 trials indicate a heat accumulation effect, in which microbial activity consumes organic matter without achieving sufficient moisture removal. This result was consistent with TI values in the previous section. Thus, positive aeration at 0.9 m^3/kg waste/day is recommended as the most effective strategy for maximizing drying efficiency and energy recovery in the solar greenhouse biodrying system.

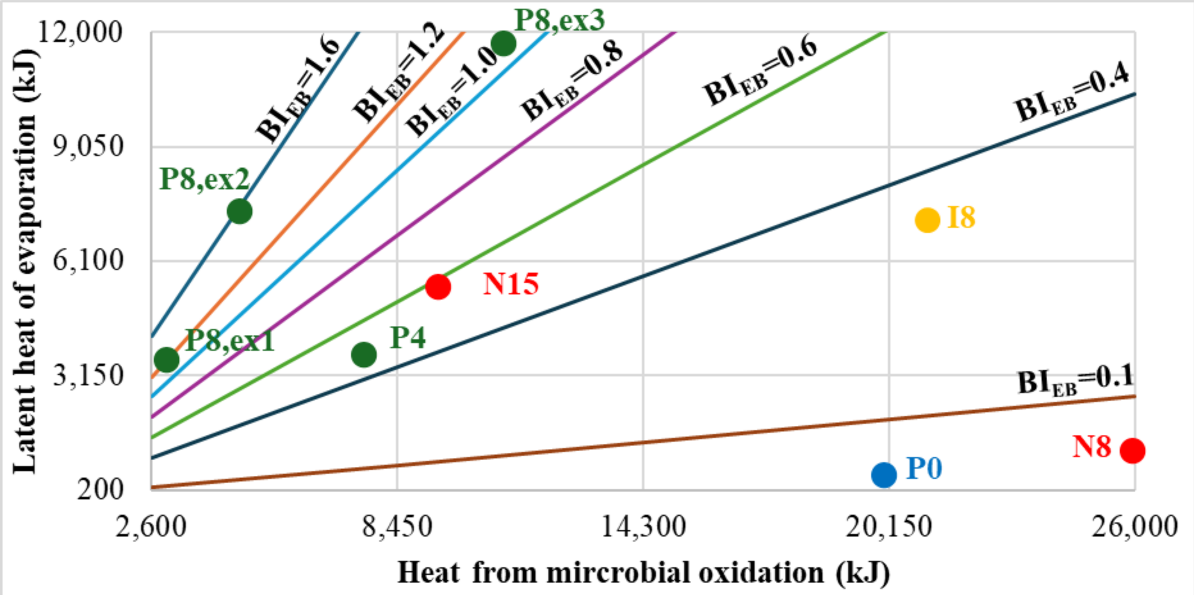

Figure 5.2 The Energy-based Biodrying Index (BI_{EB}, boundary 1) across Trials

<u>For Boundary 2: Consideration of energy consumption for aeration</u>

The energy-based biodrying index measures the process efficiency at Boundary 2 (BI'_{EB}), which accounts for both the metabolic heat and the electrical energy used for aeration. This index serves as a key indicator of the system's overall performance by showing how effectively the total energy input (both metabolic and electrical energy for aeration) is converted into the latent heat required for water evaporation. Essentially, it represents the overall energy efficiency of the biodrying process within the greenhouse system, indicating the potential for energy savings in moisture reduction. Basically, a higher BI'_{EB} value indicates a more efficient biodrying process where more water is removed relative to the energy consumed. Figure 5.3 exhibits The Energy-based Biodrying Index (BI'_{EB}, boundary 2) across Trials.

The results reveal significant variability in BI'_{EB} values based on the aeration patterns and seasonal timing associated with the external environmental factors. Trials with positive aeration generally demonstrated superior efficiency compared to negative or passive aeration patterns. For instance, Trial P8 (ex3), conducted during the summer (June-July 2025), achieved the highest index of 0.38, benefiting from a high latent heat of evaporation (11,711.24 kJ/kg) relative to the total energy for aeration and metabolic heat. In contrast, passive aeration (P0) and negative aeration at 8 L/min (or 0.9 m^3/kg waste/day) (N8), both yielded the lowest BI'_{EB} of 0.03.

Seasonality in relation to external environmental factors also played an important role in determining energy performance, as seen in the varying results in comparison of the same positive aeration rate of 8 L/min (Trials P8,ex1, P8,ex2, and P8,ex3). The BI'_{EB} value increased from 0.16 (in December 2024) to 0.30 (in January 2025), finally peaking at 0.38 during the summer period (June-July 2025). This trend indicates that higher air temperatures and solar radiation intensity likely assist the biological process as biodrying in driving out moisture more efficiently for the same amount of energy for aeration. Conversely, negative aeration trials such as N15 showed moderate efficiency (BI'_{EB} = 0.16), while inverted aeration (I8), which switches from negative to positive aeration, achieved a mid-range BI'_{EB} value of 0.17.

Moreover, these results were compared to ideal and physical drying reference. An ideal BI'_{EB} value of 0.60 was established based on the assumption of maximized water loss from the experiment combined with minimal organic degradation. Additionally, a physical drying reference using a low-temperature heat pump sludge drying system with energy-saving capabilities, and specific power consumption (SPC) was 0.97 kWh/kg water loss [14]. The reference BI'_{EB} value, representing physical drying, was found to achieve a BI'_{EB} value of 0.65. The findings of BI'_{EB} value demonstrate that the energy efficiency of the solar greenhouse biodrying system is highly dependent on the aeration pattern and environmental conditions. In this study, positive aeration was the most effective aeration pattern, particularly during warmer months (June-July) at 8 L/min (0.9 m^3/kg waste/day) when the system achieved its peak BI'_{EB} value of 0.38. While the current values of this study remain lower than the ideal BI'_{EB} value of 0.60, they highlight the significant potential of metabolic heat for moisture reduction as well as energy efficiency for aeration. Future optimization should focus on refining aeration timing and improving heat retention by suitable reactor design to narrow the efficiency gap near the ideal BI'_{EB} value

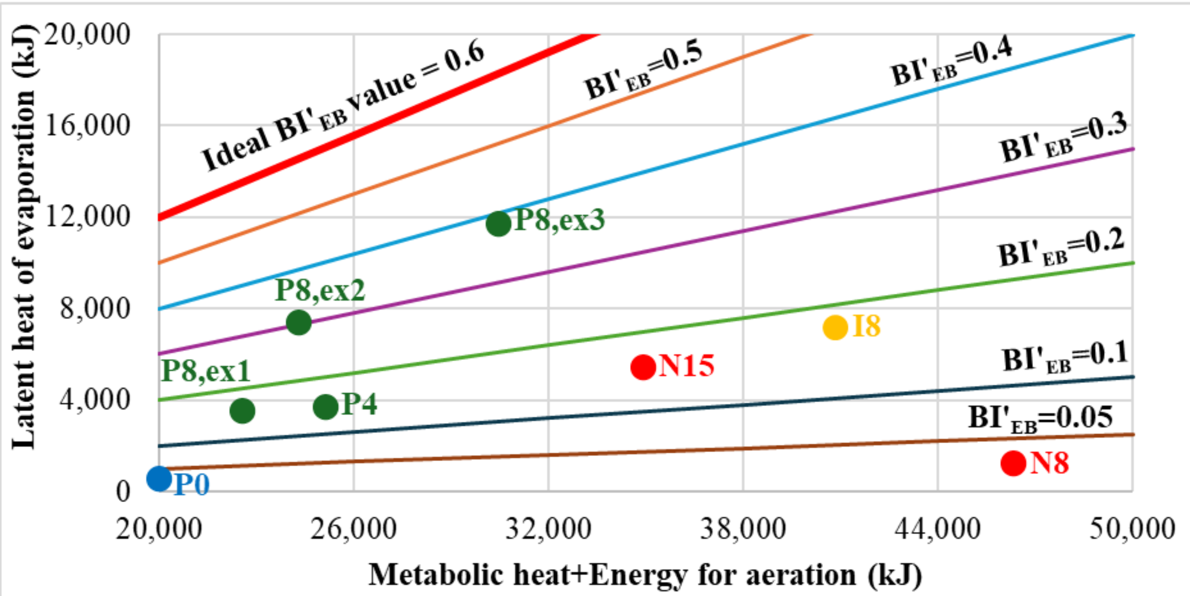

Figure 5.3 The Energy-based Biodrying Index (BI'_{EB}, boundary 2) across Trials

5.3.3 Model Reliability

The results of the model reliability assessment showed different performances between the positive and negative aeration patterns. In the positive aeration trials, the model demonstrated varying degrees of accuracy depending on operating conditions. The P4 trial (4 L/min or 0.45 m^3/kg waste/day) resulted in an MBE of 2.13 and an RMSE of 9.57, with a moderate correlation coefficient (CC) of 0.49. The P8 trials (8 L/min or 0.9 m^3/kg waste/day) showed seasonal variations, with the trial in December (P8,ex1) achieving a CC of 0.61 and the trial in January (P8,ex2) reaching a CC of 0.64, while the summer trial in June–July (P8,ex3) exhibited a lower CC of 0.21 alongside a higher MBE of 6.25. Conversely, the negative aeration trials displayed significantly higher consistency despite larger error magnitudes. The N8 trial (8 L/min or 0.9 m^3/kg waste/day) yielded a high CC of 0.82 with an MBE of 11.72, and the N15 trial (15 L/min or 1.7 m^3/kg waste/day) achieved the highest consistency with a CC of 0.92, together with an MBE of 9.19 and RMSE of 12.71, respectively. Figure 5.4 presents a comparison between the modeled and experimental waste temperatures across the different trials.

The mentioned result of the model application confirmed that both positive and negative aeration patterns were feasible for simulation, though with different strengths. Regarding the mass balance model in Chapter 4, positive aeration resulted in a percentage error of less than 2.3% compared to the final experimental mass (specifically less than 1% for the P8 trials), while negative aeration consistently maintained an error margin of less than 1%. For the heat balance model, the positive aeration pattern was characterized by lower error differentials (MBE 2.13–6.25 °C) but low to moderate consistency levels between modeled and experimental waste temperatures (CC 0.21–0.64), particularly when waste temperature fluctuations were high. Moreover, the negative aeration pattern demonstrated high consistency (CC 0.54–0.80), suggesting a strong linear relationship with experimental data, although it was associated with higher error values between modeled and experimental waste temperatures.

This result indicated that while absolute temperature predictions may deviate, the model successfully captures the thermal trends. With the statistical results of the heat and mass balance models, it is necessary to analyze the implications of these simulation results. The next section will discuss the results from the heat balance model to further investigate the solar greenhouse biodrying system.

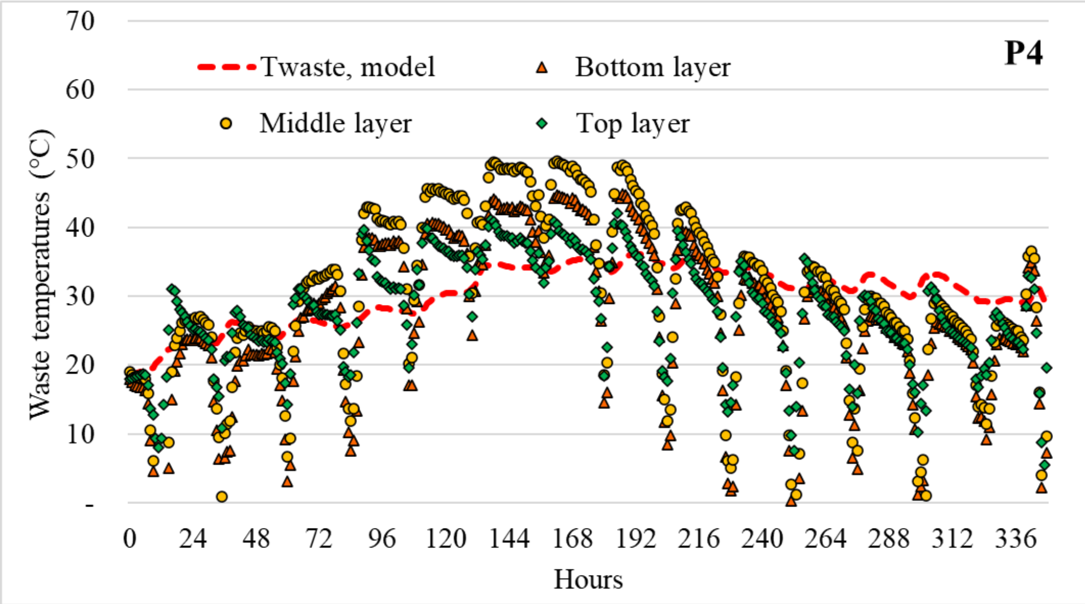

(A) P4: Positive aeration at 4 L/min (0.45 m^3/kg waste/day)

MBE = 2.13 °C, RMSE = 9.57 °C, CC = 0.49

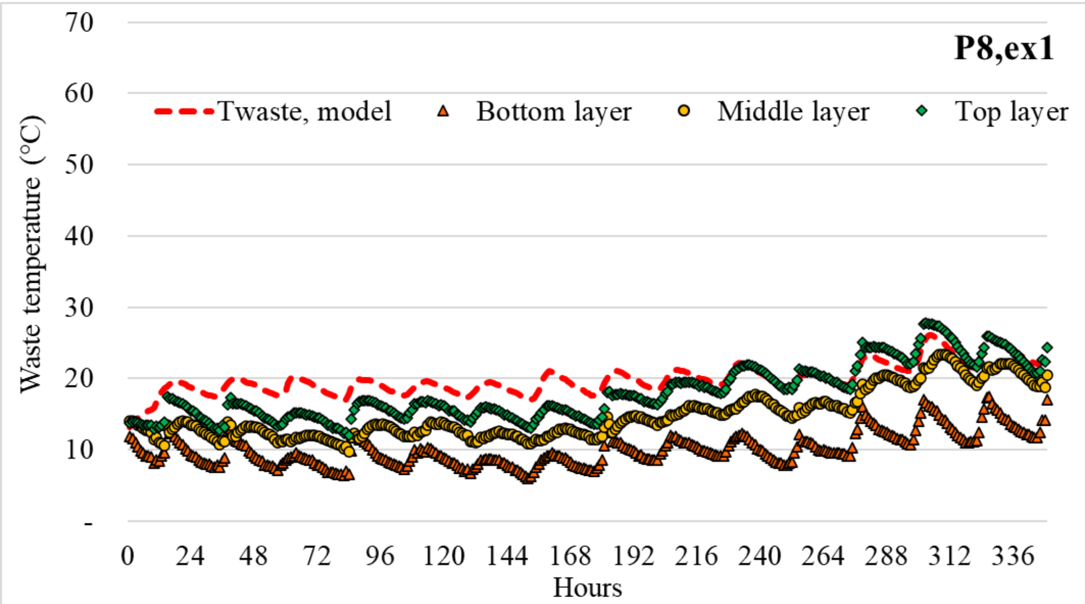

(B) P8,ex1: Positive aeration at 8 L/min (0.9 m^3/kg waste/day)

MBE = 5.59 °C, RMSE = 5.77 °C, CC = 0.61

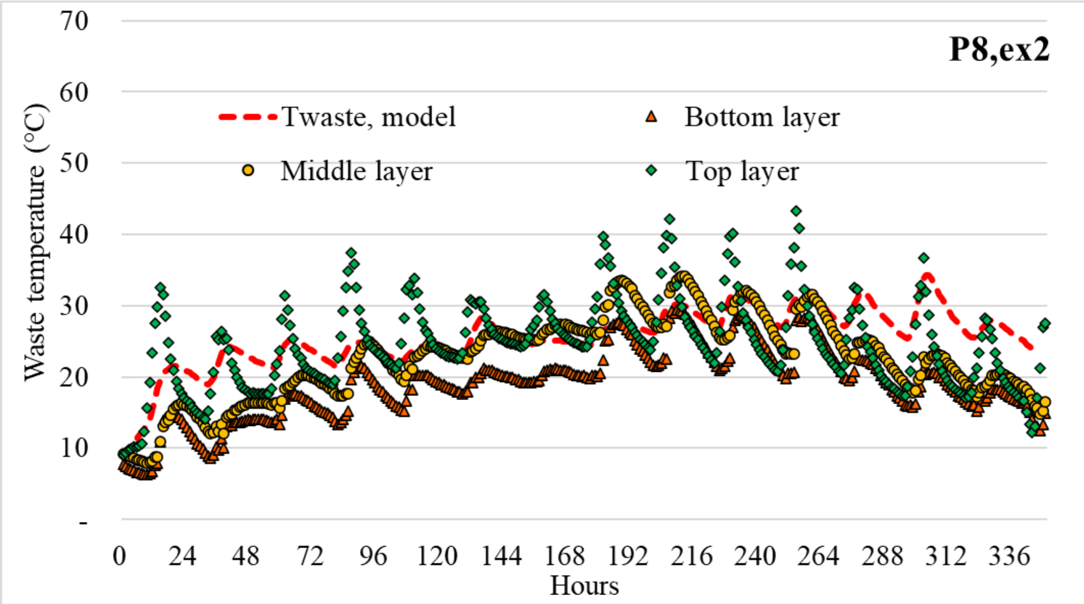

(C) P8,ex2: Positive aeration at 8 L/min (0.9 m^3/kg waste/day)

MBE = 3.46 °C, RMSE = 4.78 °C, CC = 0.64

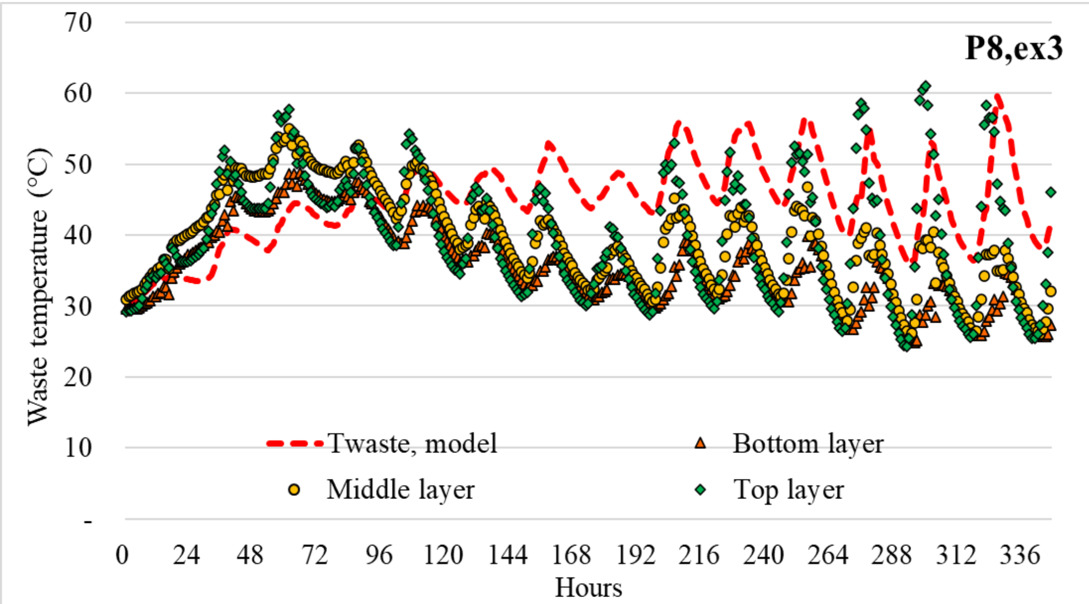

(D) P8,ex3: Positive aeration at 8 L/min (0.9 m^3/kg waste/day)

MBE = 6.25 °C, RMSE = 9.91 °C, CC = 0.21*

*CC=0.33 when compared to experimental waste temperature at top layer

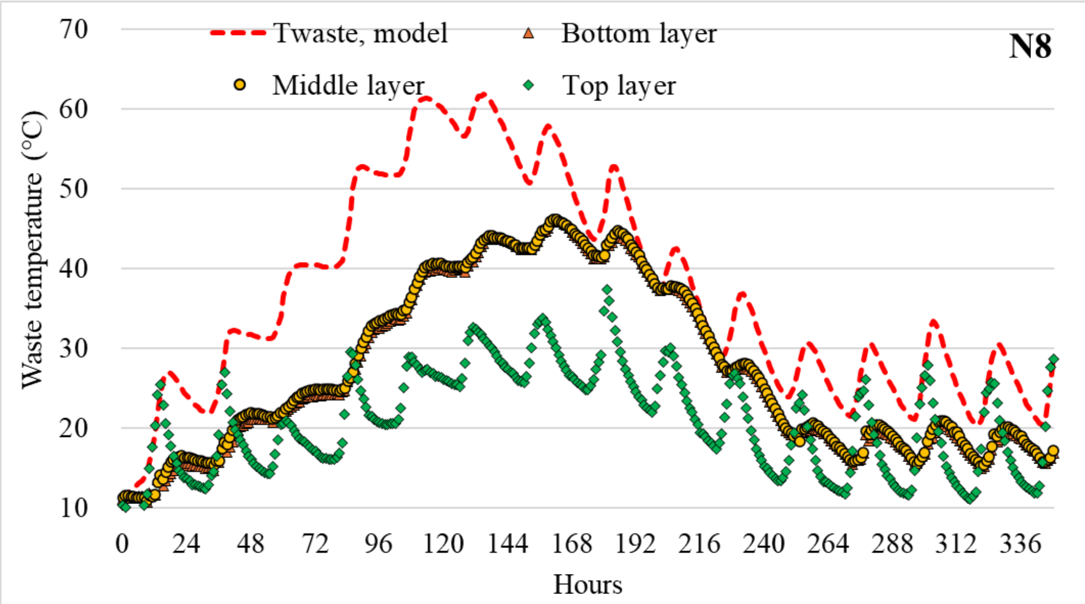

(E) N8: Negative aeration at 8 L/min (0.9 m^3/kg waste/day)

MBE = 11.72 °C, RMSE = 13.34 °C, CC = 0.82

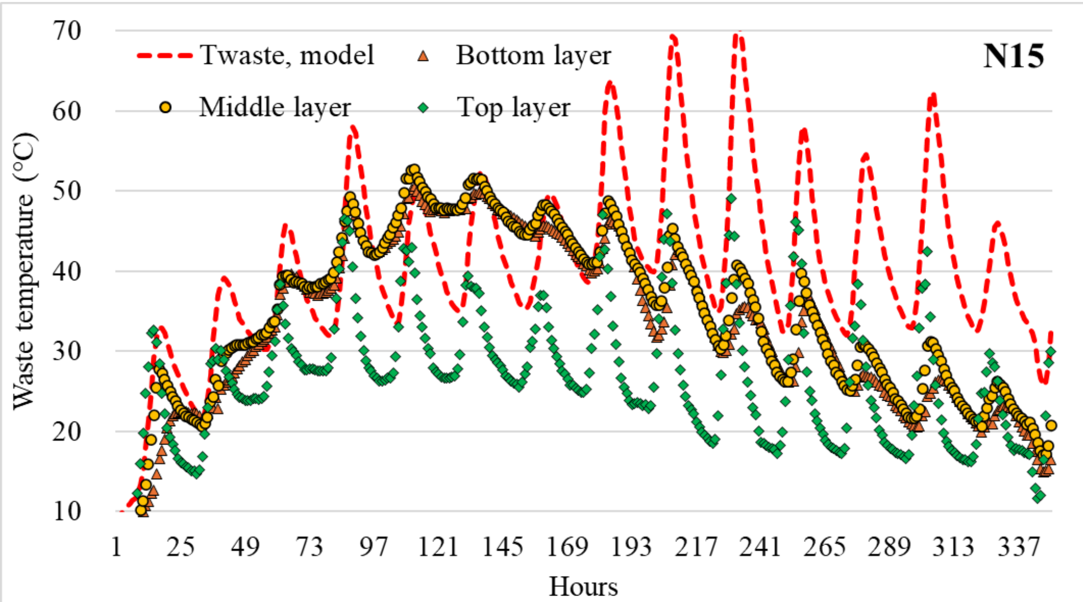

(E) N15: Negative aeration at 15 L/min (0.9 m^3/kg waste/day)

MBE = 9.19 °C, RMSE = 12.71 °C, CC = 0.54

Figure 5.4 Comparison between the Modeled and Experimental Waste Temperatures across the Different Trials

5.3.4 Interpretation of Model Results

The heat balance analysis provides a detailed breakdown of the heat inputs and outputs with the solar greenhouse biodrying system under different aeration patterns. The heat balance results, summarized in Table 5.2, highlight different thermodynamic behaviors between positive and negative aeration patterns, particularly regarding how energy is utilized for moisture removal versus how it is lost to the systems.

In the positive aeration trials (P4, P8ex1, P8ex2, and P8ex3), the heat balance analysis revealed that the system's thermal behavior was influenced by the airflow rate and weather conditions. Regarding heat inputs, metabolic heat generated from biodegradation was the dominant energy source at the lower airflow rate of 4L/min or 0.45 m^3/kg waste/day, contributing 56.15% of the total heat input. However, at the higher airflow rate of 8 L/min or 0.9 m^3/kg waste/day, the contribution of metabolic heat varied (28.19%–38.65%), while the enthalpy of inlet air became more significant, particularly in trial P8ex1 where it accounted for 54.45% of the total input. Solar energy consistently provided a supplementary heat source, ranging from roughly 17% to 24% across these trials. The analysis of heat outputs demonstrated the high efficiency of the positive aeration pattern for biodrying. The latent heat of evaporation, which represents the energy utilized to remove moisture within the waste pile, constituted the largest portion of heat loss (heat utilization) in most positive aeration trials. It had high proportion in trial P8ex2 at 65.30% and remained high in P8ex3 at 49.74% of total heat utilization. This indicates that forcing air upward through the waste pile effectively promotes both biological and physical heat to drive water evaporation.

In contrast to the positive aeration pattern, the negative aeration trials (N8 and N15) exhibited a different heat distribution profile. For heat inputs, the N8 trial (8 L/min or 0.9 m^3/kg waste/day) was heavily dominated by metabolic heat, which accounted for 73.51% of the total energy input, and this trial had the highest proportion observed across all experiments. However, as airflow increased to 15 L/min or 1.7 m^3/kg waste/day (N15 trial), the proportion of heat input was different, and the enthalpy of inlet air became the primary input at 64.44%. Notably, the contribution of solar energy was low in these trials (5.13–9.17%) compared to the positive aeration cases. Regarding heat outputs, the negative aeration pattern demonstrated poor thermal efficiency for drying. The latent heat of evaporation was minimal, representing only 5.62% and 11.59% of the total heat output for N8 and N15, respectively. Instead of driving evaporation, a substantial portion of the energy was dissipated through radiative heat losses to the greenhouse structure. Specifically, radiative heat transfer from the waste to the upper wall, top acrylic, and headspace collectively accounted for approximately 69% of the output in the N8 trial and nearly 55% in the N15 trial. This indicates that pulling air downwards (air movement from top to bottom) leads to significant heat accumulation in the structural components rather than effective moisture removal from the waste pile. A comparison between positive and negative aeration patterns (P8,ex1 and N8) is illustrated in Figure 5.5, highlighting the distinct differences in their respective heat balances.

Table 5.2 Heat Balance Results within the Waste Pile across Different Trials

Heat Elements	P4		P8,ex1		P8,ex2		P8,ex3		N8		N15	
	kJ	%	kJ	%	kJ	%	kJ	%	kJ	%	kJ	%
Metabolic heat	7,723	56.15%	2,975	28.19%	4,741	35.11%	11,111	38.65%	26,261	73.51%	9,488	26.39%
Enthalpy of inlet air	2,733	19.87%	5,747	54.45%	5,465	40.47%	10,915	37.97%	7,631	21.36%	23,173	64.44%
Solar energy	3,297	23.98%	1,832	17.36%	3,297	24.42%	6,721	23.38%	1,832	5.13%	3,297	9.17%
Sum of heat input	**13,752**	**100%**	**10,553**	**100%**	**13,503**	**100%**	**28,747**	**100%**	**35,724**	**100%**	**35,959**	**100%**
Sensible heat of the air	- 17	-0.13%	1,113	10.55%	1,269	9.40%	1,102	3.83%	4,273	11.96%	6,167	17.15%
Latent heat of evaporation	5,120	37.23%	4,334	41.07%	8,818	65.30%	14,298	49.74%	2,009	5.62%	4,167	11.59%
Radiative heat from the waste to the upper wall	3,155	22.94%	2,800	26.54%	675	5.00%	4,640	16.14%	14,238	39.85%	11,191	31.12%
Radiative heat from waste to the top acrylic	1,705	12.40%	1,272	12.06%	707	5.24%	2,333	8.12%	5,208	14.58%	4,360	12.12%
Radiative heat from waste to the headspace	1,202	8.74%	1,060	10.04%	292	2.16%	1,723	5.99%	5,236	14.66%	4,121	11.46%
Conductive heat through the side wall	2,139	15.56%	- 441	-4.18%	994	7.36%	4,002	13.92%	3,701	10.36%	4,692	13.05%
Heat loss by leachate	4	0.03%							58	0.16%	61	0.17%
Sum of heat output	**13,309**	**97%**	**10,138**	**96%**	**12,755**	**94%**	**28,099**	**98%**	**34,723**	**97%**	**34,760**	**97%**

Noted: the percentages (%) represent the proportion of each heat element relative to the total heat input in the biodrying process.

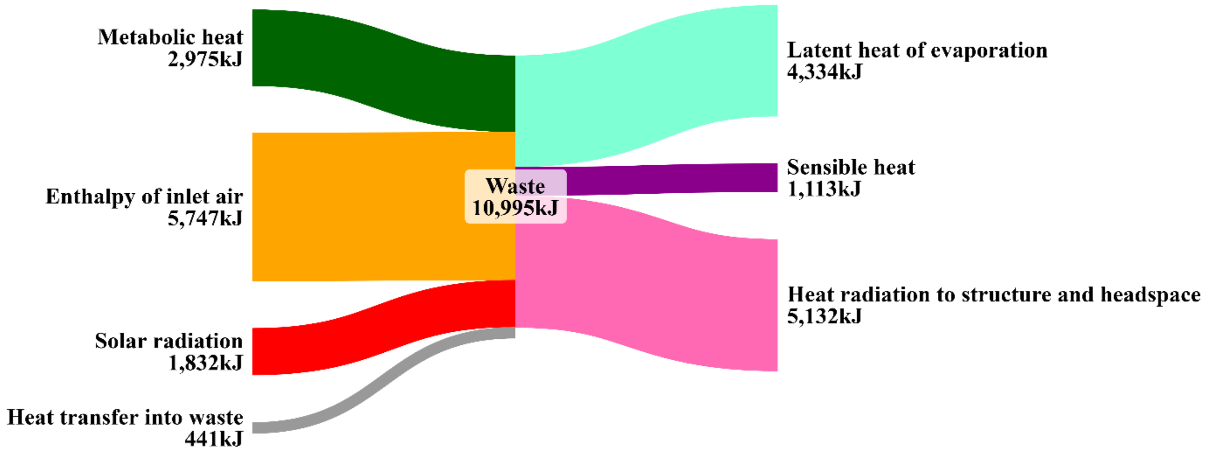

(A) Heat balance in the waste under positive aeration 8 L/min (0.9 m^3/kg waste/day) [P8,ex1]

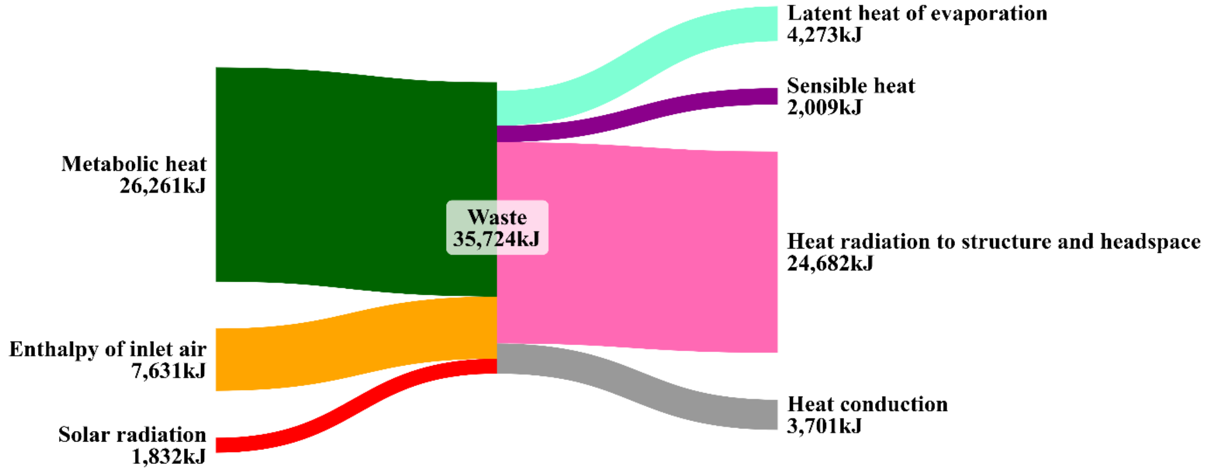

(B) Heat balance in the waste under negative aeration 8 L/min (0.9 m^3/kg waste/day) [N8]

Figure 5.5 Comparison of Heat Balance between Positive and Negative Aeration Patterns

5.4 Conclusion

This chapter provided a comprehensive evaluation of the solar greenhouse biodrying system by analyzing key performance indicators and applying the heat balance model (as the supporting evidence) under positive and negative aeration patterns. The comparative analysis of the Biodrying Index (BI), Temperature Integration (TI), and Air Efficiency (AE) demonstrated that positive aeration is the most effective aeration strategy for this system. Specifically, the trials operating at an airflow rate of 8 L/min (0.9 m^3/kg waste/day) consistently achieved the highest water removal efficiency while successfully retaining organic solid mass. In contrast, the negative and passive aeration patterns resulted in lower drying capabilities and higher organic matter degradation, making them less suitable to produce RDF, where preserving biomass content is crucial.

To gain more understanding of the thermodynamic efficiency and energy efficiency of this system, this study introduced novel Energy-based Biodrying Index (BI_{EB} and BI'_{EB}). The results from this new index highlighted the advantage of the positive aeration pattern, which consistently yielded BI_{EB} values greater than 1.0 (ranging from 1.07 to 1.57). A value above 1.0 indicates that the energy utilized for water evaporation exceeded the heat generated solely by microbial oxidation, proving that the system successfully utilized external energy sources, such as solar radiation and the enthalpy of inlet air, to drive the drying process. Conversely, negative aeration trials exhibited low indices (as low as 0.05), suggesting that despite high metabolic heat generation, the system failed to convert this energy into effective evaporation, leading to heat accumulation within the system. Furthermore, by accounting for both metabolic energy and electrical energy for aeration, the BI'_{EB} value identified positive aeration as the most effective pattern for maximizing water loss with high energy efficiency. The disparity between the highest BI'_{EB} value (0.38) and the reference value of physical drying (BI'_{EB} = 0.65) provides a quantitative baseline for the current system's performance. Moving forward, achieving the ideal value of 0.60 will require a dual focus on minimizing organic solid loss while maximizing water evaporation through improved reactor design and effective aeration control.

The application of the heat balance model provided more explanation for these performance differences by quantifying how heat was distributed and lost within the reactor. For positive aeration, the heat balance analysis revealed that the latent heat of evaporation was the dominant heat output, accounting for up to 65% of the total heat utilization, which confirms that energy was efficiently directed toward removing moisture. However, the negative aeration pattern demonstrated low thermal efficiency; instead of using heat for evaporation, a substantial portion of the energy (approximately 55% to 69%) was dissipated through radiative heat losses to the reactor structure. This finding clarifies that pulling air downward through the waste pile results in significant heat loss to the structural components rather than effective drying.

To sum up, the integration of performance indicators and heat balance modeling identified positive aeration at the airflow rate of 0.9 m^3/kg waste/day as the optimal operating condition in the case of the solar greenhouse biodrying system. The findings also emphasized that external environmental conditions, particularly solar radiation and air temperature, play a supportive role in enhancing the system's performance, providing practical guidance for the optimized design and operation of future solar greenhouse biodrying system.

References

[1] Velis CA, Longhurst PJ, Drew GH, et al (2009) Biodrying for mechanical–biological treatment of wastes: A review of process science and engineering. Bioresour Technol 100:2747–2761. https://doi.org/10.1016/j.biortech.2008.12.026

[2] Huiliñir C, Villegas M (2015) Simultaneous effect of initial moisture content and airflow rate on biodrying of sewage sludge. Water Res 82:118–128. https://doi.org/10.1016/j.watres.2015.04.046

[3] Yang B, Zhang L, Jahng D (2014) Importance of Initial Moisture Content and Bulking Agent for Biodrying Sewage Sludge. Drying Technology 32:135–144. https://doi.org/10.1080/07373937.2013.795586

[4] Sen R, Annachhatre AP (2015) Effect of air flow rate and residence time on biodrying of cassava peel waste. International Journal of Environmental Technology and Management 18:9. https://doi.org/10.1504/IJETM.2015.068414

[5] Mohammed M, Ozbay I, Karademir A, Isleyen M (2017) Pre-treatment and utilization of food waste as energy source by bio-drying process. Energy Procedia 128:100–107. https://doi.org/10.1016/j.egypro.2017.09.021

[6] Payomthip P, Towprayoon S, Chiemchaisri C, et al (2022) Optimization of Aeration for Accelerating Municipal Solid Waste Biodrying. International Journal of Renewable Energy Development 11:878–888. https://doi.org/10.14710/ijred.2022.45143

[7] Yuan J, Zhang D, Li Y, et al (2017) Effects of adding bulking agents on biostabilization and drying of municipal solid waste. Waste Management 62:52–60. https://doi.org/10.1016/j.wasman.2017.02.027

[8] Yuan J, Zhang D, Li Y, et al (2018) Effects of the aeration pattern, aeration rate, and turning frequency on municipal solid waste biodrying performance. J Environ Manage 218:416–424. https://doi.org/10.1016/j.jenvman.2018.04.089

[9] Shao L-M, He X, Yang N, et al (2012) Biodrying of municipal solid waste under different ventilation modes: drying efficiency and aqueous pollution. Waste Management & Research: The Journal for a Sustainable Circular Economy 30:1272–1280. https://doi.org/10.1177/0734242X12462278

[10] Zhang DQ, He PJ, Jin TF, Shao LM (2008) Bio-drying of municipal solid waste with high water content by aeration procedures regulation and inoculation. Bioresour Technol 99:8796–8802. https://doi.org/10.1016/j.biortech.2008.04.046

[11] Li J, Ju T, Lin L, et al (2022) Biodrying with the hot-air aeration system for kitchen food waste. J Environ Manage 319:115656. https://doi.org/10.1016/j.jenvman.2022.115656

[12] Khalil SA, Shaffie AM (2013) A comparative study of total, direct and diffuse solar irradiance by using different models on horizontal and inclined surfaces for Cairo, Egypt. Renewable and Sustainable Energy Reviews 27:853–863. https://doi.org/10.1016/j.rser.2013.06.038

[13] Schober P, Boer C, Schwarte LA (2018) Correlation Coefficients: Appropriate Use and Interpretation. Anesth Analg 126:1763–1768. https://doi.org/10.1213/ANE.0000000000002864

[14] Zhang, T., & Zhu, Q. Z. (2018). Experimental Study on a Low-Temperature Heat Pump Sludge Drying System. IOP Conference Series: Earth and Environmental Science, 168, 012011. https://doi.org/10.1088/1755-1315/168/1/012011

Chapter 6
Conclusion

This study involves with the solar greenhouse biodrying system for solid waste pre-treatment. The system is designed to improve moisture reduction and enhance waste quality, supporting its potential use for energy recovery. Biodrying is an aerobic biological process that uses microbial activity to generate metabolic heat, effectively lowering waste moisture while maintaining its organic solid content. By incorporating a solar greenhouse, the system utilizes solar energy to create a more favorable thermal condition, thereby improving drying efficiency and overall process performance. This thesis systematically examines thermal behavior within the system, as well as effects of aeration strategies and seasonal variations to provide a comprehensive understanding of this system. The findings contribute to both the scientific knowledge of heat generation, transfer, and process optimization. The storyline of this thesis is summarized as follows:

Chapter 1 presented the background and highlights the challenges associated with handling high moisture content in municipal solid waste (MSW). This chapter included the significance of biodrying technology and identification of existing research gaps, particularly in the context of the solar greenhouse biodrying system. These research gaps formed the basis for defining the main objective of this study.

Chapter 2 provided a comprehensive review of biodrying technology within Mechanical-Biological Treatment (MBT) systems. This chapter compared biodrying against thermal and solar-assisted methods, and categorized operational configurations into thin-layer, windrow, and bunker types through global case studies. Through a systematic analysis of existing research, this chapter provided the foundation for the subsequent biodrying simulation and experimental studies.

For **Chapter 3**, This chapter developed mass and heat balance models to quantify the thermodynamic behavior of the solar greenhouse biodrying system. Validated against pilot-scale experimental data, the model demonstrated high reliability with a Relative Root Mean Square Error (rRMSE) of 11.82% for waste temperature (acceptable threshold = 10–20%). Heat balance analysis revealed that while metabolic heat (66%) was the primary energy input, the greenhouse structure contributed significantly by capturing solar radiation (14% of heat input during daytime) and minimizing convective heat losses. Comparative simulations confirmed the solar greenhouse biodrying system superiority over outdoor biodrying scenarios, and it successfully achieved the target moisture content (<30%) within 7 days by preventing re-moisturization from rainfall. Consequently, the solar greenhouse biodrying system produced a Refuse-Derived Fuel (RDF) with a superior Lower Heating Value (LHV) of 7,133 kcal/kg, compared to only 1,321kcal/kg in conventional outdoor biodrying.

In **Chapter 4**, the effects of positive, negative, and passive aeration patterns at airflow rates of 4–15 L/min (0.45–1.7 m^3/kg waste/day) on laboratory-scale solar greenhouse biodrying were investigated. Aeration direction significantly influenced heat distribution within the waste pile. Positive aeration transferred heat to the upper layers, negative aeration distributed heat more uniformly, and passive aeration caused heat accumulation in the middle layer. Positive aeration mainly enhanced moisture removal with minimal organic matter loss, especially at 8 L/min (0.9 m^3/kg waste/day). In contrast, negative and passive aeration resulted in greater organic degradation and leachate generation. Notably, no leachate was observed under positive aeration at 8 L/min (0.9 m^3/kg waste/day), indicating that upward airflow enhanced evaporation as the primary drying mechanism. Negative aeration at 8 L/min (0.9 m^3/kg waste/day), and passive aeration produced 16-70 ml leachate per kg waste input. Moreover, higher solar radiation and ambient temperatures increased evaporation rates by 1.75–3.65 times compared with cooler weather conditions.

Chapter 5 presented a comprehensive performance evaluation of the solar greenhouse biodrying system alongside the application heat balance model to reveal the system's thermal transfer mechanisms. By utilizing the Biodrying Index (BI), Temperature Integration (TI), and Air Efficiency (AE) to compare various aeration patterns, the study demonstrated that positive aeration maximized water removal efficiency and solid content preservation, whereas negative aeration enhanced heat retention but resulted in higher organic solid losses. From the result, positive aeration at 8L/min (0.9 m^3/kg waste/day) was the optimal aeration strategy for RDF production. This finding was confirmed by the novel Energy-based Biodrying Index (BI_{EB}), which consistently yielded values exceeding 1.0 (for all P8 trials), indicating the effective utilization of metabolic heat together with other energy sources, such as solar radiation and inlet air enthalpy, for evaporation. In contrast, heat balance analysis revealed that negative aeration suffered from low thermal efficiency, where substantial energy (55–69%) was dissipated through radiative heat losses to the reactor structure rather than using for moisture removal. Furthermore, by incorporating both metabolic energy and electrical energy for aeration, BI'_{EB} identified positive aeration at 8 L/min (0.9 m^3/kg waste/day) as the most effective pattern for maximizing water loss in this study (BI'_{EB} = 0.38). Achieving the target value of 0.60 will require minimizing organic solid loss while enhancing water evaporation through improved reactor design and optimized aeration control.

Ultimately, this study establishes the novel heat balance model and the energy-based biodrying index, offering a scientific basis for applying the solar greenhouse biodrying system under different operational and environmental conditions. These findings provide an important foundation for future research in this field.

Recommendations in Research

1. Further experimental investigations are necessary to explore microbial communities, specifically the microbial ecosystem within the biodrying process under a greenhouse system.

2. Economic and feasibility evaluations are essential to support the wider adoption of the solar greenhouse biodrying system. Comprehensive economic assessments at full scale are needed to guide investment and operational decision-making, while feasibility and cost–benefit studies can provide policy support and encourage the practical integration of the solar greenhouse biodrying system into waste management systems.

3. Future investigations should compare different airflow rates, particularly for negative aeration, within the same experimental period to eliminate temporal variations in environmental conditions. Conducting these trials simultaneously is essential to confirm the specific impacts of airflow volume on heat capacity and oxygen transfer without the confounding variables present in this study.

4. The application of inverted aeration (sequencing negative aeration to boost initial waste temperatures followed by positive aeration to accelerate drying) requires further optimization. Research should focus on adopting this strategy to enhance the performance of the solar greenhouse biodrying system specifically during the winter season for the retention of internal temperatures within the system.

APPENDIX

Appendix A
Supplementary Information for Chapter 3

A.1 Calculation of Solar Radiation Intensity

Solar radiation heat (Q_{SR}): To calculate the heat from solar radiation entering the MSW pile, the total daily solar radiation was measured using a pyranometer installed at the top of the greenhouse for a period of 10 days. The daily total value was adjusted to hour-scale values by dividing it over a 24-hour period. As the experiment conducted in September, which corresponds to the rainy season, the hourly solar radiation values in the horizontal plane were then converted to total solar radiation in the inclined plane. This allowed for the determination of the amount of solar radiation heat acquisition in hour scale on the experimental days.

Firstly, it was necessary to calculate the position of the sun during the experimental period. The coordinates of the experimental location were set to a latitude of 13.75°N and a longitude of 100.56°E. The experimental period was 7-16 September 2019. The formula for the solar hour angle was derived from the NAOJ's Ephemeris Wiki (National Astronomical Observatory of Japan (NAOJ), n.d.).

$$H = (\vartheta + \lambda - \alpha) \times 24 \qquad \text{Eq. (A. 1)}$$

Where:
H = solar hour angle (h)
ϑ = Greenwich sidereal time (hour:minute:second)
λ = reference time according to longitude (6:42:14 hour:minute:second)
α = right ascension (hour:minute:second)

It was noted that the conversion factor from hour unit to degree unit is 15 °/h. After converting the unit, it was able to calculate the solar altitude angle (h) at each time using H value (From Eq.A.1), where h = 90° represents the zenith (midday at 12.00) by the following equations (Tanaka et al., 2015).

$$\sin h = \sin \varphi \sin \delta + \cos \varphi \cos \delta \cos H \qquad \text{Eq. (A. 2)}$$
$$h = \sin^{-1} h \qquad \text{Eq. (A. 3)}$$

Where:
h = solar altitude angle (°)
φ = latitude of 13.75°N (for Bangkok)
δ = apparent declination (°)

Then, determined the hourly orientation of the sun (Azimuth (A), unit °). In this calculation, the setting values were North = 0°, East = 90°, South = 180, West =° 270°. Pi (π) value is constant with the value of 3.141592654.

$$\cos A = \frac{\sin h \sin \varphi - \sin \delta}{\cos h \cos \varphi} \quad \text{Eq. (A. 4)}$$

$$\sin A = \frac{\cos \delta \sin H}{\cos h} \quad \text{Eq. (A. 5)}$$

$$A = \tan^{-1} A + \pi \quad \text{Eq. (A. 6)}$$

Next, determined the hourly total horizontal solar radiation (J_{th}, unit W/m^2). To do this, first separated the total horizontal solar radiation into direct (J_{dh}) and diffuse (J_{skyh}) solar radiation components using the following equations.

$$J_{th} = J_{dh} + J_{skyh} \quad \text{Eq. (A. 7)}$$
$$J_{dh} = (J_{n0} P^{\csc h}) \times \sin h \quad \text{Eq. (A. 8)}$$
$$J_{skyh} = J_{n0} \times \frac{\sin h}{2} \times \frac{1 - P^{\csc h}}{1 - 1.4 \ln P} \quad \text{Eq. (A. 9)}$$

Where:
J_{n0} = solar constant (1,366 W/m^2)

Since the values of atmospheric transmittance (P) were unknown and it was vital value in order to find J_{dh} and J_{skyh}, so that the P value was adjusted from 0 to 1 with the increment scale of 0.0001. For each adjusted P value, J_{dh} and J_{skyh} were calculated and sum them up. If J_{dh} and J_{skyh} from each adjusted P value closest to the measured solar radiation intensity data (That contributed to the desired value of J_{th} from the calculation with an error less than 0.3% from the measured value.). The calculation was performed using the total J_{th} on the horizontal plane at around noon, close to solar noon for each day. P was determined for each day over experimental period and then calculate J_{dh} and J_{skyh} for each time interval in this calculation.

Table A.1. Atmospheric transmittance (P) values used in the calculation of horizontal solar radiation

Date	P value
7-Sep-19	0.1821
8-Sep-19	0.2361
9-Sep-19	0.1377
10-Sep-19	0.3073
11-Sep-19	0.3679

Date	P value
12-Sep-19	0.3868
13-Sep-19	0.3468
14-Sep-19	0.1755
15-Sep-19	0.4174
16-Sep-19	0.2049

From the previous equations (Eq.A. 7-9), the next step was calculation of the total solar radiation on inclined surface ($J_{t\alpha\theta}$), including the inclined plane direct solar radiation ($J_{d\alpha\theta}$) and the inclined surface diffusion solar radiation ($J_{sky\theta}$). These values refer to the amount of solar radiation that finally reaches the greenhouse system. Here, the following formulas were used.

$$J_{t\alpha\theta} = J_{d\alpha\theta} + J_{sky\theta} \quad \text{Eq. (A. 10)}$$

$$J_{d\alpha\theta} = J_{dh}[\sin h \cos\theta + \cos h \sin\theta \cos(A - a')] \quad \text{Eq. (A. 11)}$$

$$J_{sky\theta} = J_{skyh}\frac{180° - \theta°}{180°} \quad \text{Eq. (A. 12)}$$

Where:
θ = roof angle relative to the horizontal axis (35° and 90°)
a' = the greenhouse orientation (135° for south-west facing and 225° for south-east facing)

From Eq.A.10, $J_{t\alpha\theta}$ values were used for transmitted solar radiation through the acrylic roof ($Q_{SR,ac}$, Eq.21 in the article) and solar radiation through the entire surface of MSW ($Q_{SR,MSW}$, Eq. 3-38 in Chapter 3)

A.2 Temperature Calculation of the Concrete Part Contacted With the Waste Pile (c1)

In this study, the temperatures of the concrete part contacted with the waste pile (c1) were estimated by the overall heat transfer equation, and the method used to estimate both the internal ($T_{c1,in}$) and external ($T_{c1,out}$) sides of the concrete wall was applied from the approach outlined by Baehr et al. (Baehr & Stephan, 2011). Here are equations for $T_{c1,in}$ and $T_{c1,out}$ estimation.

$$T_{c1,in} = T_{MSW,cal} - \left(\frac{K_{tran,c1}}{a_{MSW}}\right) \times (T_{MSW,cal} - T_{am}) \quad \text{Eq. (A. 13)}$$

$$T_{c1,out} = T_{am} + \left(\frac{K_{tran,c1}}{a_o}\right) \times (T_{MSW,cal} - T_{am}) \quad \text{Eq. (A. 14)}$$

Where:
$T_{MSW,cal}$= waste temperature from the heat balance model (°C)
T_{am} = ambient temperature from the experiment (°C)

$K_{tran,c1}$ = overall heat transfer coefficient from MSW to outside through the concrete wall (kJ/m^2·°C)
a_{MSW} = heat transfer coefficient from MSW to reactor wall (33.6 kJ/m^2·°C)
a_o = convective heat coefficient for external surface (kJ/m^2·°C)
It was noted that $K_{tran,c1}$ and a_o were determined using the method described in Chapter 3.

A.3 Temperature calculation of heat balance of concrete contacted with the air inside the greenhouse (c2)

In the case of the concrete, contacted with the air inside the greenhouse (c2), it was possible to also determine the temperature by the heat transfer equation as similar as the temperature determination of c1 in the previous section. The internal ($T_{c2,in}$) and external ($T_{c2,out}$) sides of the concrete wall contacted with the air inside the greenhouse can be estimated using the equation below.

$$T_{c2,in} = T_{GH,mix} - (\frac{K_{cov,GH\rightarrow c2\rightarrow am}}{a_{c2,in}}) \times (T_{GH,mix} - T_{am}) \quad \text{Eq. (A. 15)}$$

$$T_{c2,out} = T_{am} + (\frac{K_{cov,GH\rightarrow c2\rightarrow am}}{a_o}) \times (T_{GH,mix} - T_{am}) \quad \text{Eq. (A. 16)}$$

Where:
$T_{GH,mix}$= headspace temperature estimated from $T_{MSW,cal}$ and $T_{GH,cal}$, representing the stage where air moves through the waste pile and mixes with the greenhouse headspace. (°C)
T_{am} = ambient temperature from the experiment (°C)
$K_{cov,GH\rightarrow c2\rightarrow am}$ = overall thermal transfer coefficient of the concrete wall contacted with the air inside the greenhouse (kJ/m^2·°C)
$a_{c2,in}$ = Interior convective heat transfer coefficient on concrete contacted with the air inside the greenhouse (22.32 kJ/m^2·°C, See also Table 3.2 in Chapter 3)
a_o = convective heat coefficient for external surface (kJ/m^2·°C, See also Table 3.1 in Chapter 3)

A.4 Estimation of Acrylic Surface Temperature

The acrylic temperature was calculated using the overall heat transfer equation. The approach for determining the internal ($T_{ac,,in}$) and external ($T_{ac,out}$) temperatures of the acrylic roof was based on a similar method for concrete temperature determination in the previous section. The equations for estimating $T_{ac,,in}$ and $T_{ac,out}$ are provided below.

$$T_{ac,in} = T_{GH,cal} - \left(\frac{K_{cov,GH\rightarrow ac\rightarrow am}}{a_{ac,in}}\right) \times (T_{GH,mix} - T_{am}) \quad \text{Eq. (A. 17)}$$

$$T_{ac,out} = T_{am} + \left(\frac{K_{cov,GH\rightarrow ac\rightarrow am}}{a_o}\right) \times (T_{GH,mix} - T_{am}) \quad \text{Eq. (A. 18)}$$

Where:

$T_{GH,mix}$= headspace temperature estimated from $T_{MSW,cal}$ and $T_{GH,cal}$, representing the stage where air moves through the waste pile and mixes with the greenhouse headspace. (°C)

T_{am} = ambient temperature from the experiment (°C)

$K_{cov,GH\rightarrow ac\rightarrow am}$ = overall heat transfer (convection) coefficient from greenhouse headspace to ambient via acrylic roof (kJ/kg·°C, see also Table2)

$a_{c2,in}$ = interior convective heat transfer coefficient on c2 (kJ/m^2·°C, see also Table 3.1)

a_o = convective heat coefficient for external surface (kJ/m^2·°C, see also Table 3.1)

A.5 Waste Composition in the Experiment

Table A.2 Initial MSW composition

Waste composition	Initial amount of material sample (kg)	%
Plastic	15.32	20.22
Glass	1.27	1.67
Leather&Rubber	3.28	4.33
Shell&Stone	4.15	5.48
Others	8.60	11.35
Foam	0.27	0.36
Textile	0.68	0.90
Metal	0.27	0.36
Paper	5.00	6.60
Yard Waste	7.75	10.23
Food Waste	11.84	15.64
Organic Matters (non-definable)	17.31	22.86
Total mass (wet basis)	75.74	100 %

A.5 Sensitivity analysis of selected variables

The heat balance model of a pilot-scale solar greenhouse biodrying system was developed, and the observed waste and headspace temperatures were compared with those predicted by the model. Table A.3 presents the results of sensitivity analysis. This sensitivity analysis expresses the effect of a 20% increase in selected variables on the Mean Bias Error (MBE) and Root Mean Square Error (RMSE) of waste and headspace temperatures during the biodrying process under the greenhouse condition. It was noted that reducing both MBE and RMSE simultaneously affected the relative root-mean-square error (rRMSE) at a similar level and led to an increase in the model's correlation coefficient (CC). The results revealed that the relative humidity of air passing through the MSW pile ($\%RH_{MSW \rightarrow GH}$) had the most significant impact. A 20% increase in this variable caused MBE and RMSE of waste temperature to decline by 39.87% and 17.87%, respectively, while the headspace temperature showed a decrease in MBE by 35.94% and RMSE by 5.98%. Meanwhile, the solar radiation absorptivity of the MSW surface (α_{MSW}) enlarged both MBE and RMSE value for waste and headspace temperatures, with increases of 4.69% and 2.38% for waste temperature, and 6.35% and 0.37% for headspace temperature, respectively. The α_{MSW} value was considered the second most influential variable affecting both waste and headspace temperatures.

Considering the absorption coefficient of solar radiation by air inside the greenhouse ($\eta_{SR,air}$), this variable had a relatively small impact on waste temperature, leading to slight increases in waste temperature errors (by 0.52% for MBE and by 0.36% for RMSE). However, it still moderately affected the headspace temperature errors (by 3.18% for MBE and by 0.49% for RMSE) in comparison to the waste temperature.

Table A.3 Sensitivity analysis for the effect of a 20% increase in variables on MBE and RMSE of waste and headspace Temperatures

Variables	%change in waste temperature		%change in headspace temperature	
	MBE	RMSE	MBE	RMSE
Relative humidity of air passing through the MSW pile ($\%RH_{MSW \rightarrow GH}$)	-39.87%	-17.87%	-35.94%	-5.98%
The solar radiation absorptivity of the MSW surface (α_{MSW})	+4.69%	+2.38%	+6.35%	+0.37%
Absorption coefficient of solar radiation by the air inside the greenhouse ($\eta_{SR,air}$)	+0.52%	+0.36%	+3.18%	+0.49%

Noted: A negative value indicates that a 20% increase in the selected variable resulted in a decrease in error, while a positive value indicates that a 20% increase in the selected variable led to an increase in error.

Overall, the sensitivity analysis indicated that $\%RH_{MSW \rightarrow GH}$ was the most influential variable, while the solar absorption coefficient by the air had minimal effects on both temperatures. These results highlight the important role of optimizing relative humidity and solar radiation absorptivity to enhance the accuracy of the heat balance model for the biodrying process within the greenhouse condition in this study.

A.6 Greenhouse Orientation

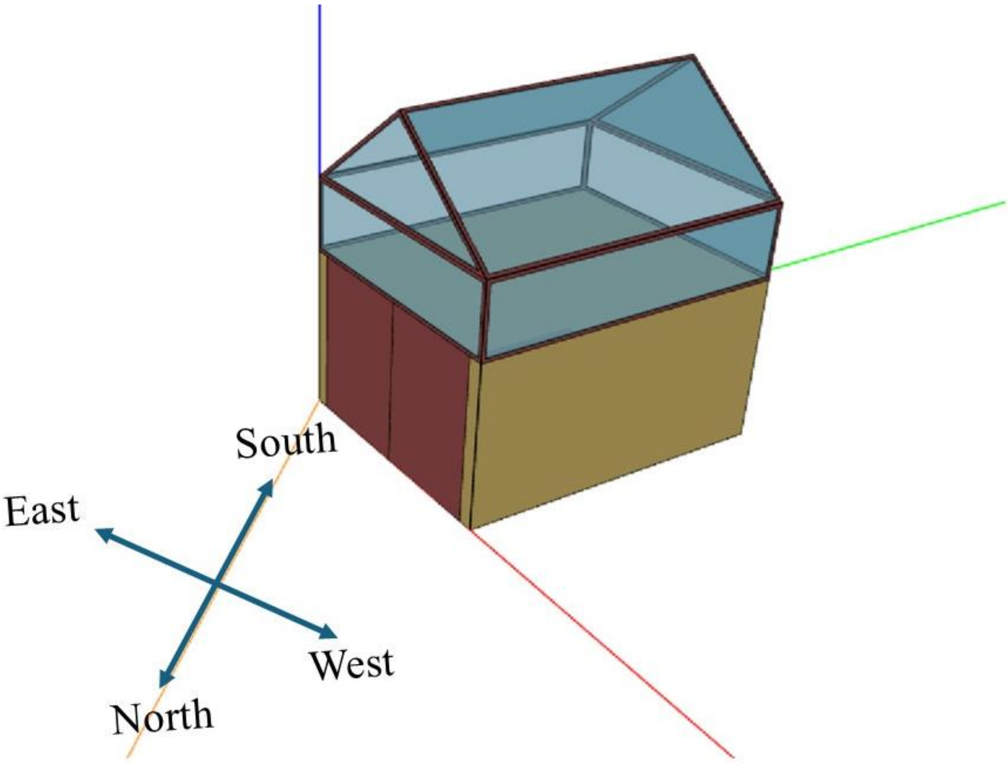

Fig. A.1 Greenhouse orientation

References

[1] Baehr, H. D., & Stephan, K. (2011). *Heat and Mass Transfer* (3rd ed.). Springer Berlin Heidelberg. https://doi.org/10.1007/978-3-642-20021-2

[2] National Astronomical Observatory of Japan (NAOJ). (n.d.). *Calendar Wiki*. National Astronomical Observatory of Japan (NAOJ). Retrieved August 26, 2024, from https://eco.mtk.nao.ac.jp/koyomi/wiki/index.html

[3] Tanaka, S., Takeda, J., Iwata, T., Tsuchiya, T., Terao, M., & Akimoto, T. (2015). *Latest Architectural Environmental Engineering* (4th ed.). Inoue Shoin.

Appendix B
Supplementary Information for Chapter 4

B.1 Waste Material Properties

Table B.1 Each Material Properties and Its Biodegradable Volatile Solid (BVS) Fraction

Waste materials	%MC	%TS	%VS (dry basis)	BVS fraction (values from 0-1)	Note about BVS fraction value
Cabbage	90.44%	9.56%	90.98%	0.430	Haug [1], estimated from lignin content.
White Bread	40.30%	59.70%	81.95%	0.819	[1]
Banana	81.16%	18.84%	75.38%	0.670	[2, 3]
Wood (saw dust)	8.52%	91.48%	75.94%	0.110	Floch et al. [4], estimated from lignin content.
Plastics (polystyrene)	0.12%	99.88%	99.95%	0.000	Polystyrene (PS) is a non-degradable material, and the mass reduction observed from VS analysis is attributed to thermal degradation under high temperatures.
Paper	7.53%	92.47%	91.70%	0.380	Applied method for estimating biodegradable portions by Alvarez et al. [5]

To estimate the biodegradable fraction of volatile solids (VS), the following empirical relationship proposed by Haug [1] can be applied:

$$B = 0.83 - (0.028)X \quad \text{Eq. (B. 1)}$$

where X represents the lignin content expressed as a percentage of VS, and B denotes the biodegradable fraction of VS.

B.2 Optimization Process and Model Reliability

In order to minimize the discrepancy between the final mass from mass balance model and the experimentally observed final mass, an optimization procedure was required. In this study, the specific maximum growth rate constant (μ_s) was optimized for each aeration pattern to achieve the best model fit. Generally, the specific maximum growth rate may vary depending on the operational conditions and system. This section presents the workflow of the optimization process for this parameter. Fig. B.1 presents the procedure applied to optimize the specific maximum growth rate constant.

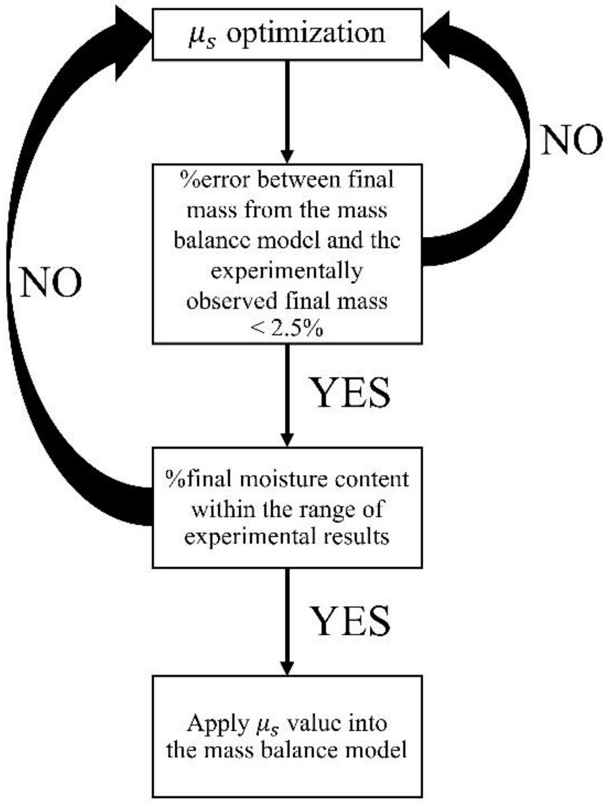

Fig.B.1 Optimization Process of the Specific Maximum Growth Rate Constant Value

Table B. 2 Comparison Between Experimental and Modeled Values for Final Mass and Moisture Content

Trials	**Final mass (kg) from the experiments**	**Final mass (kg) from the mass balance model**	**%Error**	**%Final MC from the experiments**			**%Final MC from the model**
				Bottom	**Middle**	**Top**	
P8,ex1	10.85	10.78	-0.61%	34.27	67.64	58.62	54.97
N8	11.5	11.43	-0.64%	67.99	70.37	65.78	65.78
P0	12.08	11.94	-0.84%	69.55	64.26	66.93	64.75
P8,ex2	9.53	9.42	-1.16%	31.05	58.62	53.75	54.18
P4	10.62	10.86	2.24%	62.07	63.50	65.43	63.67
N15	10.01	9.99	-0.24%	63.83	52.09	48.31	57.82
P8,ex3	7.06	7.10	0.58%	32.66	44.97	23.45	44.27
I8	8.53	8.70	2.01%	48.89	40.14	26.79	59.24*

References

[1] Haug RT (1993) The practical handbook of compost engineering. Routledge

[2] Wohlt D, Kellner V, Kolesnik D, et al (2025) Thermal stabilization of banana peels for the preparation of soluble and insoluble dietary fiber. Future Foods 11:100631. https://doi.org/10.1016/j.fufo.2025.100631

[3] Zaini HM, Saallah S, Roslan J, et al (2023) Banana biomass waste: A prospective nanocellulose source and its potential application in food industry – A review. Heliyon 9:e18734. https://doi.org/10.1016/j.heliyon.2023.e18734

[4] Le Floch A, Jourdes M, Teissedre P-L (2015) Polysaccharides and lignin from oak wood used in cooperage: Composition, interest, assays: A review. Carbohydr Res 417:94–102. https://doi.org/10.1016/j.carres.2015.07.003

[5] Alvarez JVL, Larrucea MA, Bermúdez PA, Chicote BL (2009) Biodegradation of paper waste under controlled composting conditions. Waste Management 29:1514–1519. https://doi.org/10.1016/j.wasman.2008.11.025

Appendix C
Supplementary Information for Chapter 5

C.1 Waste-derived Fuel Productivity Index

The Waste-Derived Fuel Productivity (WFP) Index is another proposed index, used to evaluate the efficiency of the net energy required to improve the heating value of the waste within biodrying process. The heating value of the waste in this context refers to the lower heating value (LHV). The WFP index is calculated by determining the ratio between the energy improved in the waste-derived fuel and the net energy required by the biodrying process (including energy input for aeration, metabolic energy, and solar energy). The calculation method is as follows:

$$WFP = \frac{M_f\ (kg) \times \Delta LHV \left(\frac{kJ}{kg}\right)}{E_{aeration}\ (kJ) - OL\ (kg) \times HHV_{db}\left(\frac{kJ}{kg}\right) - Q_{SR\rightarrow waste}\ (kJ)} \quad \text{Eq. (C. 1)}$$

$$\Delta LHV \left(\frac{kJ}{kg}\right) = LHV_{after} - LHV_{before} \quad \text{Eq. (C. 2)}$$

Where WFP is the Waste-derived Fuel Productivity Index, M_f is the amount of waste-derived fuel (kg) as the final product after biodrying process. ΔLHV refers to the difference between LHV values before and after biodrying process. $E_{aeration}$ is the electrical energy consumed by the air pump for aeration (kJ). *OL* is the reduction in organic solid mass (kg), and HHV_{db} stands for higher heating value on a dry basis of organic substrates (kJ/kg) in the experiment. $Q_{SR\rightarrow Waste}$ is the transmitted solar energy (kJ) to the waste.

The WFP index is introduced as additional performance indicator to assess the productivity by comparing the increase in the LHV value of the waste to the net energy requirement. In the reported results, the WFP index varied significantly across different trials, with the summer trial (P8,ex3) achieving the highest productivity of 2.90, primarily due to a low net energy requirement of 1,799 kJ and a high LHV increase of 5,208 kJ (See also Table C.1). Conversely, winter trials (P8,ex1) and low-airflow positive aeration (P4) exhibited lower productivity indices of 0.11 and 0.10, respectively, while the inverted aeration trial (I8) demonstrated substantial fuel quality improvement (5,104 kJ of LHV increase) despite a mathematically negative WFP of -0.64. In Fig. C.1, trial I8 is shown with a WFP index of -0.64 at the bottom right corner of the graph. This occurs because the net energy requirement becomes negative when metabolic and solar energy are substantially higher than the energy required for aeration.

Therefore, the WFP index requires looking beyond the raw numerical value, as the mathematical structure of the index can make potentially misleading interpretation. A significant limitation of this index occurs when both the numerator (Increased LHV) and the denominator (Net energy requirement) are negative. Table C.1 shows the raw numerical values for the increase in the LHV of waste-derived fuel and the net energy requirement across the trials. From the table, if a trial results in a decreased fuel quality (Negative ΔLHV value) but is achieved with a surplus of energy (Negative net energy requirement, meaning metabolic and solar energy exceeded energy for aeration), the resulting WFP will also be positive (e.g. N8 and P0 trials). Thus, this could misleadingly suggest that N8 and P0 were productive trial; however, in reality, the fuel quality degraded during the biodrying process in both cases (N8 and P0). In this situation, Table C.2 aids in the interpretation of the WFP index.

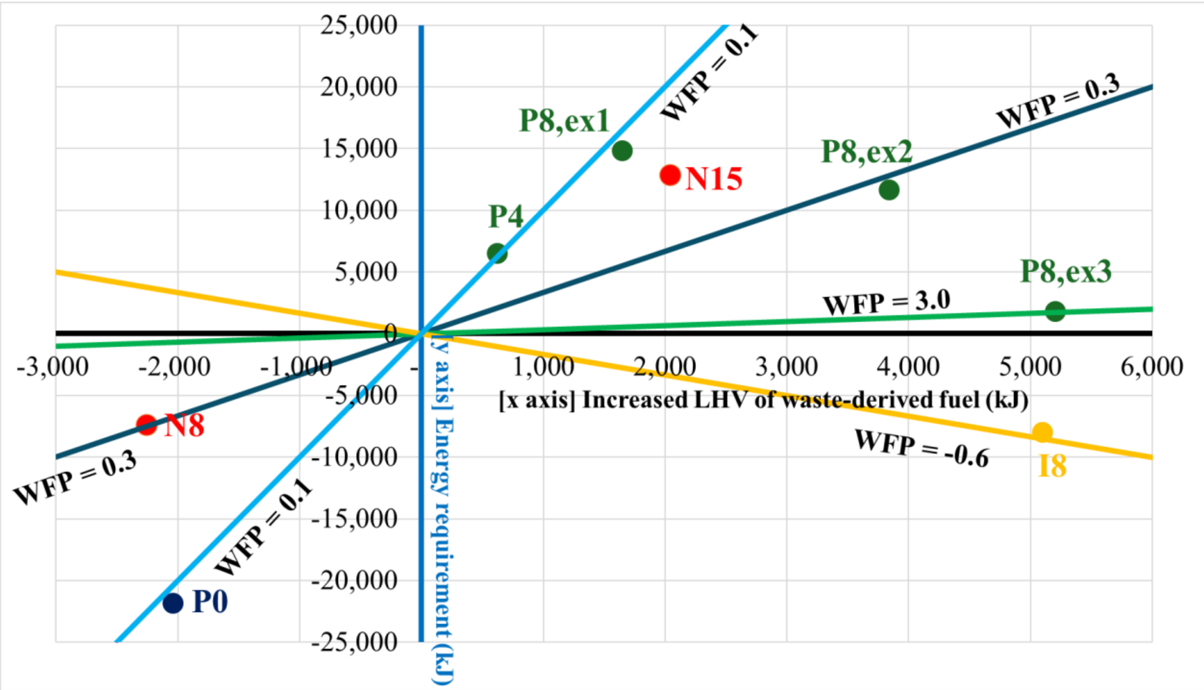

Fig. C.1 WFP Index Values among Trials

Table C.1 Raw Numerical Values for the Increase in the LHV of Waste-derived Fuel and the Net Energy Requirement across the Trials

Trials	Final mass (kg)	ΔLHV (kJ/kg)	Increased LHV of waste-derived fuel (kJ) [M_f*ΔLHV] <X axis>	Energy consumption for aeration (kJ)	Metabolic heat (kJ)	Solar radiation (kJ)	Net energy requirement for improving LHV (kJ) [$E_{aeration}$- OL*HHV_{db} - $Q_{SR \rightarrow Waste}$] <Y axis>	Waste-Derived Fuel Productivity (WFP)
P4	10.62	59.00	**627**	17,464	7,660	3,297	**6,507**	0.10
P8,ex1	10.85	152.32	**1,653**	19,600	2,960	1,832	**14,808**	0.11
P8,ex2	9.53	403.40	**3,844**	19,600	4,701	3,297	**11,602**	0.33
P8,ex3	7.06	737.66	**5,208**	19,488	10,968	6,721	**1,799**	2.90
N8	11.50	-195.83	**-2,252**	20,354	25,940	1,832	**-7,418**	0.30
N15	10.01	204.45	**2,047**	25,505	9,401	3,297	**12,807**	0.16
P0	12.08	-168.69	**-2,038**	0.00	20,021	1,832	**-21,853**	0.09
I8	8.53	598.38	**5,104**	19,773	21,065	6,721	**-8,014**	-0.64

Table C.2 summarizes the interpretations for different combinations of fuel quality (increase in LHV) and net energy requirement. This framework can be used when interpreting the WFP index.

Table C.2 Interpretation of the WFP Index based on Combinations of Fuel Quality Improvement and Net Energy Requirements.

Increased LHV (Numerator)	**Net Energy Requirement** (Denominator)	**WFP Result**	**Interpretation/Implication**
Positive (+)	**Positive (+)**	**Positive (+)**	Efficient LHV improvement in biodrying process, when energy input for aeration was required. Higher value means greater waste-derived fuel productivity (e.g., Trial P8,ex3).
Positive (+)	**Negative (-)**	**Negative (-)**	Fuel quality was improved, and free energy (solar and metabolic energy) exceeded energy input for aeration (e.g., Trial I8).
Negative (-)	**Negative (-)**	**Positive (+)**	This case could make misleading interpretation. Fuel quality has decreased; however, the index appears positive due to a negative denominator, as the free energy (solar and metabolic) exceeded the energy required for aeration. (e.g. Trials N8 and P0)
Negative (-)	**Positive (+)**	**Negative (-)**	Ineffective biodrying process, in which energy input for aeration was spent but fuel quality decreased. This case indicates an unsuitable condition.

Acknowledgments

The completion of this PhD journey marks an important chapter in my life. I would like to express my deepest gratitude to Professor Kazuei Ishii, my supervisor, for his valuable guidance and for fostering a research environment that kept me motivated and happy even during the most challenging periods. His encouragement was the activation that pushed me toward the completion of this thesis, and our discussions always provided a good vibe that sparked my critical thinking.

I am also sincerely grateful to Assistant Professor Geun-Yong Ham for her suggestions and for facilitating the biodrying research project. She has been a role model for my skillful development. My thanks also go to Assistant Professor Satoru Ochiai and Assistant Professor Jumana Al-Mallahi for their constant support and encouragement to keep moving forward in my research.

I would like to extend my appreciation to Associate Professor Sirintornthep Towprayoon and Associate Professor Komsilp Wangyao (from JGSEE-KMUTT) for their academic support and valuable advice. Their warm welcomes whenever I returned to Thailand always made me feel at home.

My heartfelt thanks go to my parents, Mr. Prateep Ngamket and Mrs. Vongdern Ngamket. Because of you, I never felt like I was standing alone, and I always knew you were right there behind me.

To the students of the Laboratory of Sustainable Material Cycle Systems, Mr. Shoki Ida, Mr. Sota Fujimoto, and Mr. Taichi Yagi, thank you for your cooperation. Working with you helped me sharpen my research organization skills. Without your help in data collection, experiments and modeling, this dissertation would not have been possible. I also thank Mr. Shun Otsuka for his help with both my research and navigating life in Japan. To everyone in the laboratory, thank you for making my time as a PhD student so memorable.

I am grateful to the Office of Educational Affairs Royal Thai Embassy in Japan, for their support and for ensuring a smooth journey throughout my PhD study. Additionally, I would like to thank the staff at the E^3 office for their assistance with my many requests, and your kindness made my life much easier.

Finally, I want to thank myself. Thank you for the dedication to secure the scholarship, study abroad, and follow this dream. To my future self, please keep going as far as you can. If you feel exhausted, it is okay to rest and just remember to keep moving forward.
I am handing the relay baton to you for the next chapter of our life.
May The Force Be With You! がんばって!

Katitep Ngamket